

INVESTIGATING THE EFFECTIVENESS OF SCANNING ELECTRON
MICROSCOPY TO IDENTIFY DENSOVIRUS IN *PISASTER OCHRACEUS*
INFECTED WITH SEA STAR WASTING DISEASE

by

Averi A. Azar

A Thesis
Submitted in partial fulfillment
of the requirements for the degree
Master of Environmental Studies
The Evergreen State College
June 2018

© 2018 by Averi A. Azar. All rights reserved.

This Thesis for the Master of Environmental Studies Degree

by

Averi A. Azar

has been approved for

The Evergreen State College

by

Erin Martin, Ph.D.
Member of the Faculty

Date

ABSTRACT

Investigating the effectiveness of Scanning Electron Microscopy to identify densovirus in *Pisaster ochraceus* infected with sea star wasting disease

Averi A. Azar

Sea stars on the Pacific Northwest coast of North America experienced massive sea star wasting disease induced die-offs from 2013 to 2015. Some of the sea stars most affected by wasting disease were the keystone predator, the purple-orange ochre sea star, *Pisaster ochraceus*. In 2014 evidence demonstrated sea star wasting is strongly correlated with presence of the sea star-associated densovirus (SSaDV). Traditional methods for viral identification have involved metagenomics, a highly expensive and technical method. This research aimed to develop a financially accessible method to identify densovirus in *P. ochraceus*. This thesis implemented the use of Scanning Electron Microscopy (SEM), to test its ability to resolve densovirus in *P. ochraceus* and potentially develop a SEM method that could help others with limited expertise and funding contribute to sea star wasting disease literature. This project found viral isolation from *P. ochraceus* tissue to be challenging and difficult to successfully execute. Thus, this project performed whole *P. ochraceus* tissue analysis using traditional SEM sample preparation methods. Through scanning, *P. ochraceus* tissue was resolved under multiple magnifications, covering a range of X to Y. Bacteria were not present in any of the samples. Even at the highest magnification of 300,000X, the SEM was not strong enough to produce a quality image at high resolution and was therefore unsuccessful at identifying densovirus at 20-25 nm in necrotic *P. ochraceus* tissue. The SEM implemented for this research (Model JEOL JSM-6480LV), is not sufficient to identify densovirus in *P. ochraceus*

Table of Contents

List of Figures	vi
Introduction	1
Literature Review	5
<i>Pisaster ochraceus</i>	5
Sea Star Wasting Disease	8
The Densovirus	14
Testing for the Densovirus	19
SEM and Densovirus	20
Scanning Electron Microscopy	23
Components of the SEM	23
SEM Operation	25
Standard SEM Methods	26
Methods	29
Methodological Introduction	29
Tissue Sample Collection	30
Environmental Data Collection	30
Method 1	32
Filtration	32
Filtration Testing	32
Result & Discussion	33
Method 2	35
Vacuum Filtration	35
Result and Discussion	36
Method 3	38
Swinlock Filter Holders & Polycarbonate Membranes	38
Tissue Sample Preparation for SEM	39
Result and Discussion	40
Whole Tissue Sample Preparation	42
Experimental Drying	42
Sputter Coating	43
SEM Calibrations	44
Sample Analysis	44

Densovirus Characteristics _____	45
Results _____	47
Introduction of Results _____	47
Sample 1 _____	47
Sample 2 _____	59
Sample 3 _____	65
Sample 3.5 _____	69
Sample 4 _____	76
Sample 4.5 _____	80
Sample 5 – Healthy Tissue _____	84
Conclusive Results _____	88
Discussion _____	91
Conclusion _____	95
Bibliography _____	97
Appendices _____	105
Appendix A _____	105
Sample 1 _____	105
Sample 3 _____	108
Sample 3.5 _____	110
Sample 4 _____	112
Sample 4.5 _____	116
Sample 5—Healthy Tissue _____	118

List of Figures

Figure 1.	6
Figure 2.	10
Figure 3.	11
Figure 4.	16
Figure 5.	21
Figure 6.	24
Figure 7.	26
Figure 8.	48
Figure 9.	49
Figure 10.	50
Figure 11.	51
Figure 12.	52
Figure 13.	53
Figure 14.	54
Figure 15.	55
Figure 16.	56
Figure 17.	57
Figure 18.	58
Figure 19.	59
Figure 20.	60
Figure 21.	61
Figure 22.	62
Figure 23.	63
Figure 24.	64
Figure 25.	65
Figure 26.	66
Figure 27.	67
Figure 28.	68
Figure 29.	69
Figure 30.	70
Figure 31.	71
Figure 32.	72
Figure 33.	73
Figure 34.	74
Figure 35.	75
Figure 36.	76
Figure 37.	77
Figure 38.	78
Figure 39.	79
Figure 40.	80
Figure 41.	81
Figure 42.	82
Figure 43.	83
Figure 44.	84

Figure 45.	85
Figure 46.	86
Figure 47.	87
Figure 48.	88
Figure 49.	105
Figure 50.	106
Figure 51.	107
Figure 52.	107
Figure 53.	108
Figure 54.	109
Figure 55.	110
Figure 56.	111
Figure 57.	112
Figure 58.	113
Figure 59.	113
Figure 60.	114
Figure 61.	115
Figure 62.	116
Figure 63.	117
Figure 64.	118
Figure 65.	119

Acknowledgements

This project was made possible through the generosity and interest of the Clean Energy Committee and the Master of Environmental Studies Association. In combination, these groups were responsible for fully funding my research and I am so grateful for their contribution. I would like to thank my thesis reader, Erin Martin, for supporting me throughout this journey. I began my work on this project in Spring of 2017 and completed it during the Spring of 2018. Erin was my advisor and reader throughout this process and I'm so grateful for her patience, encouragement and mentorship despite the series of unfortunate events which seemed to plague my project.

I would also like to thank Trisha Towanda, my SIT, for teaching me to use the SEM and supporting my learning through Advanced Microscopy training. Trisha's unyielding confidence in me and my project was essential for my success and I'm so thankful for her tutelage and support. Likewise, Erik Thuesen and Gerardo Chin-Leo often provided critical guidance and advice throughout my SEM analysis which helped informed decisions and results in this thesis.

My success during the thesis process was highly influenced by the professional support of my boss Andrea Martin, Assistant Director of the Master of Environmental Studies program. Andrea has been the best supervisor, mentor and support system during the last year and a half. Her excellent organization and planning abilities have made working in the MES office a true joy and frequently the easiest part of each day. I couldn't have done this without her. Additionally, my coworkers in the MPA program, Jan Hays (whom I've had the distinct privilege of sharing an office with) and Puanani Nihoa, Assistant Director to the MPA Tribal Governance program, have been a constant source of light and happiness. I was always buoyed by their humor and molded by their experience and mentorship, an honor I am so thankful to have experienced during this time in my life.

I would like to thank my family and friends for supporting me throughout my time in graduate school. Thank you for always listening to me when I was stressed or upset about my thesis project and for offering words of wisdom when my project would encounter another challenge. Thank you for also putting up with my physical absence and letting me focus so I can accomplish this monster of a task: write a thesis.

Most of all though, I would like to thank my cohort, the *best* cohort ever! It has been a true joy to work with and get to know all of you. Your experiences and guidance have informed my work and I truly value the influence you all have had on me both personally and professionally. I would like to specifically thank those that have continuously offered me emotional and academic support throughout my thesis work. Nicole George & Leslie Carman—my primary thesis support system—for being my writing buddies, helping me understand the SEM and being totally awesome. My lab group, Amanda Mintz, Morgan Maupin, Stephanie Blair, Max Calloway, Alex Case-Cohen and John Messina for being so helpful and filling the lab with laughter.

Introduction

The Pacific Northwest coast of North America from Juneau, Alaska to Baja, California was plagued with massive sea star die-offs from 2013 to 2015. This mass mortality event was caused by sea star wasting disease (Hewson et al. 2014, Eisenlord et al. 2016, Fuess et al. 2015). A combination of disease outbreak in 2013, followed by warming ocean temperatures in 2014, exacerbated the disease and further enhanced sea star mortality to wasting (Miner et al. 2018). The disease looks as its name suggests, as a form of sea star tissue disintegration and melting in a mass of white lesions; an appearance which has left many on the Northeast Pacific coast alarmed and baffled (Fuess et al. 2015). The mass mortality event is often considered a two-year incident, ending in 2015, due to the collective mass dying which occurred in this period. Post-2015, sea star wasting still plagues the Northeast Pacific coast (Eisenlord et al. 2016). However, populations of sea stars were thrown into such a sharp decrease that presence of wasting disease is not felt as critically with fewer sea stars to be affected.

The strongest correlations to the source of wasting disease have been temperature increases in the Pacific (Miner et al. 2018) and the presence of the sea star-associated densovirus (SSaDV) in diseased individuals (Hewson et al. 2014). Much of our knowledge of sea star wasting causation has only recently been gained in the last couple years with the largest breakthrough occurring in 2014 by Hewson et al. The challenge with studying wasting disease is the deductive reasoning involved in learning about the phenomena. The disease is not only present in infected individuals but appears to persist in the environment and seems to be transmissible from sick to healthy individuals. These observations lead Hewson et al. (2014) to examine the likelihood that sea star wasting

could be caused by a pathogen much smaller than bacteria, parasites or fungi: a virus. This observation proved to be likely with the implementation of viral metagenomics, Hewson et al. (2014) successfully discovered the presence of a densovirus—a member of the Parvoviridae family—in sick sea star tissue. This virus was therefore named, sea star-associated densovirus (SSaDV) for its apparent relationship to the presence of wasting disease and its genetic difference to other known densoviruses (Hewson et al. 2014).

Continued research into the source of sea star wasting disease is imperative as the impact of the disease is still felt on the Pacific coast. In the Pacific Northwest of North America, a species of great importance to the coastal ecosystems is the purple orange ochre sea star, *Pisaster ochraceus* (Paine 1969). *P. ochraceus* are one of the organisms responsible for maintaining species biodiversity in rocky intertidal zones. Their role as a keystone species is felt most intensely in their voracious appetites for mussels, especially the highly prolific California mussels (*Mytilus californianus*) (Paine 1995, Lawrence 2013). Without *P. ochraceus*, many intertidal ecosystems have experienced biodiversity loss from mussels that frequently outcompete other organisms for prime intertidal habitat (Miner et al. 2018). Although *P. ochraceus* populations are attempting to rebound from the 2013-2015 mass die-off, sea star wasting is still present and remains a threat to the future of *P. ochraceus* and subsequently, the health of rocky intertidal habitats (Moritsch & Raimondi 2018).

Questions about the source of wasting disease continue to swirl amongst the confusion and despair about the state of *P. ochraceus*. Sea star wasting disease is not definitively caused by a single source or pathogen (Bucci et al. 2017). Additionally, viruses in marine invertebrates as a whole are highly understudied so our knowledge of

viral-host interactions is murky and undefined (Menge et al. 2016, Suttle 2005). The relationship between densovirus and sea star wasting disease is the strongest pathogen-disease relationship to date. Therefore, a greater understanding of this relationship is necessary to further our knowledge of this viral-host interaction in *P. ochraceus*. While viral metagenomics is the most accurate form of viral identification in sea stars, it is also a highly technical and expensive method, requiring a great deal of genetic expertise and money to execute successfully. As a result, this project aimed to develop a less technical, cost-effective method for identifying densovirus in *P. ochraceus* infected with sea star wasting disease. This would aid in expanding the accessibility of sea star wasting literature to those with limited genetic expertise and restricted funds.

The method implemented to achieve this project's research goals was Scanning Electron Microscopy (SEM). SEM is a fantastic method historically used to visualize anatomical structures in biologic organisms and identify pathogens such as bacteria, fungi, and viruses in organisms and people inundated with disease. The traditional methods for SEM sample preparation are achievable for those with limited research funding. Furthermore, Scanning Electron Microscopes do not require extensive knowledge and lengthy training. Instead, advanced microscopy training is obtainable in a matter of weeks and comprehension of the theory behind SEM functionality is much easier to attain and interpret than metagenomics. Therefore, this thesis focused on investigating if the SEM could be a viable method for identifying densovirus in *P. ochraceus* to assist in developing an accessible and cost-effective method to study sea star wasting disease.

This thesis will begin with an overview of the keystone species central to this project, *Pisaster ochraceus*. The literature review will focus only on those aspects of *P. ochraceus* integral to understanding the nature of sea star wasting disease. These include *P. ochraceus*' relationship to the wasting phenomenon such as physiological responses and will address the impact of reduced *P. ochraceus* populations on the Pacific rocky intertidal zones. Next this thesis will review the literature on sea star wasting disease, placing the greatest focus on research performed since 2014. This was the year Hewson et al. (2014) discovered densovirus in *P. ochraceus* and is responsible for launching sea star wasting disease literature into a new chapter of understanding. Topics discussed within sea star wasting literature are disease characteristics and potential causes and correlations to disease outbreak and spread.

Following sea star wasting disease literature, this literature review will pay particular focus to current knowledge of sea star-associated densovirus and other related densoviruses which similarly affect invertebrates in terrestrial and marine hosts. Next the feasibility of implementing Scanning Electron Microscopy will be examined as a method for identifying SSaDV in *P. ochraceus* tissues. A review of traditional SEM methods and theory will proceed, with care taken to explain its distinction from Transmission Electron Microscopy. The literature review will conclude with an explanation of SEM implementation for this research.

Literature Review

Pisaster ochraceus

One of the organisms' integral to maintaining biodiversity on the rocky intertidal zone is the purple-orange ochre sea star, *Pisaster ochraceus* (Figure 1). *P. ochraceus* are a keystone species, meaning their presence in the rocky intertidal ecosystem is important because of their influence on other species in these environments, particularly mussels (Paine 1969). These are the organisms which inspired Paine in 1969 to propose the concept of a keystone species. A keystone species exists as a highly important member of an ecosystem because of the influence it has on other organisms and their interactions. It is a species that regulates the relationships in an ecosystem, and without them, the composition of the ecosystem would become drastically different or could potentially fail (Paine 1969, Eisenlord et al. 2016, Menge et al. 2016).



Figure 1. A healthy orange *P. ochraceus* in the rocky intertidal zone.

This keystone species concept, has been adopted most especially in conservation biology to explain complex ecosystem relationships and champion species conservation. Contrarily, this concept has also been refuted because it has the potential to oversimplify complex species interactions within ecosystems (Paine 1995). Nevertheless, Paine's observations about the influence *P. ochraceus* have over molluscs and crustaceans such as bay mussels (*Mytilus tossulus*), acorn barnacles (*Balanus glandula*) and the California

mussel (*Mytilus californianus*) are relevant to the Pacific Northwest intertidal ecosystems today (Lawrence 2013). It exists as the basis for continued research exploring *P. ochraceus* and their importance on North American Pacific coastlines.

The sea stars which inhabit the rocky intertidal ecosystem are fascinating organisms in that they have remained relatively static in their physiology and anatomy since the Triassic period, 208-245 million years ago (Lawrence 2013). Through their unchanging characteristics they have been named a “living fossil.” Although it is understood that the class of asteroids (Asteroidea) have remained fairly static through time and evolution, the phylogeny or rather, the genetic origins of the current Class of Asteroidea we see today, come from a single ancestor. This ancestor was most likely able to survive the Permian-Triassic boundary or so called the Great Permian Extinction, responsible for the dinosaur extinction 252 million years ago (Lawrence 2013). From that single surviving ancestor, we see the rise of a clade of asteroids known as the Neoasteroidea. These Neoasteroidea are the sea stars which all currently living Asteroidea derive from (Gale 1987), including *Pisaster ochraceus*.

The North American Pacific coast is where *P. ochraceus* inhabit the dynamic and often harsh environments of the rocky intertidal zones. They range from coasts in Alaska to sunny Baja California. Their bright purple and orange pigmentation are a treasure to the Pacific Northwest. Their presence in the rocky intertidal zone is largely responsible for maintaining species biodiversity in this extreme habitat (Paine 1969). *P. ochraceus* have a highly voracious appetite and they use it to eat the most abundant shellfish on the intertidal zone: mussels (Lawrence 2013, Eisenlord et al. 2016). Mussels are a concern for this ecosystem along the North American Pacific coast because their presence in the

rocky zones can be prohibitive to other organisms seeking prime intertidal habitat (Paine 1969). Often, if left unchecked, mussels rapidly multiply and outcompete other species for space such as sponges, chitons, limpets, crabs, anemones and algae, reducing biodiversity in the intertidal zone (Paine 1969, Eisenlord et al. 2016). This decreases the number of species existing in prime rocky intertidal habitat, altering the species composition of the coastline.

Sea Star Wasting Disease

In the Pacific Northwest *P. ochraceus* have been a perpetual staple to beaches and coastal systems (Paine 1967). However, in recent years this steadiness has been interrupted by a disease which has swept the North American Pacific coastline, decimating populations of sea stars. This disease is called sea star wasting and has been most devastating to *P. ochraceus* since 2013 when the first signs of disease outbreak took hold (Fuess et al. 2015). Since the mass wasting event which lasted into late 2015, populations of *P. ochraceus* have rebounded in many of their usual habitats and recently even began approaching pre-outbreak numbers along the North American Pacific coastline. Although the number of sea star individuals is reaching pre-outbreak levels, sea star population densities have not rebounded in the same way, with populations more spread out along the coast (Moritsch & Raimondi 2018, Eisenlord et al 2016). As a result, mussels are still not experiencing the same level of predation pressure as populations prior to 2013. Sea star recovery is not uniform and the rocky intertidal zone will continue to be altered by the impact of sea star wasting disease in years to come (Moritsch & Raimondi 2018).

Sea star wasting is a disease that most negatively affects sea stars of the Class Asteroidea. When the animals contract the disease, the first sign of infection are white lesions that appear on the top of the body either on the arms or the central disk (Staehli et al. 2009) (Figure 1). As the disease progresses, the lesions grow in size and multiply across the body of the sea star. The animal loses its turgidity so they are no longer plump and full but instead deflated and appear to collapse on themselves (Eisenlord et al. 2016, Fuess et al. 2015). Typically, a sea star will lose the ability to move their tube feet and slowly become immobile. They are unable to hunt and feed, so as the disease spreads, their bodies lose their coloring, turning their tissues into a white mass of lesions (Menge et al. 2016, Hewson et al. 2014, Fuess et al. 2015). Sea stars usually collapse and die within one to two weeks of contracting wasting disease (Eisenlord et al. 2016, Hewson et al. 2014).



Figure 2. Image of a *P. ochraceus* infected with early stages of sea star wasting disease. The sea star was a deflated appearance with white lesions on the top of the central disk and sides of the arms. The left most arm is beginning to curl, a typical response to wasting disease in this organism.

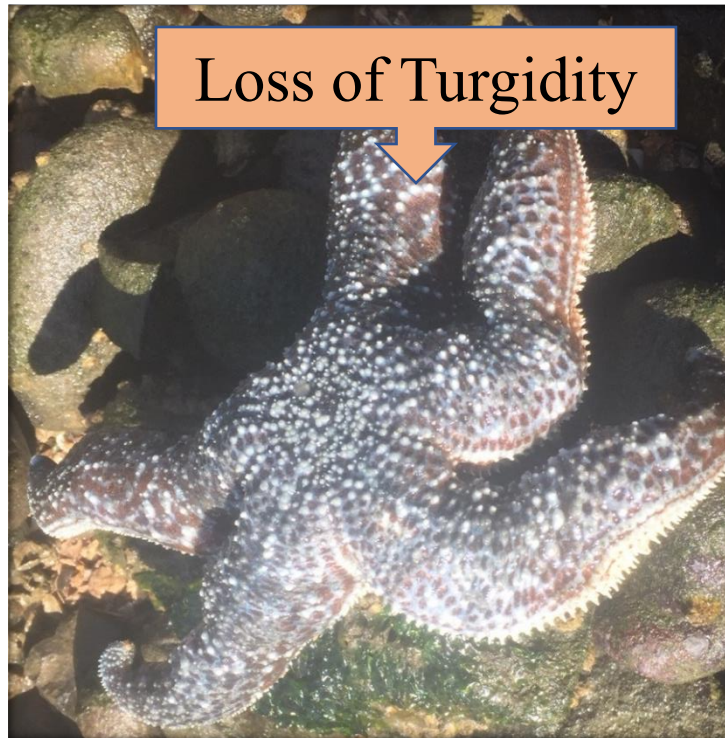


Figure 3. A *P. ochraceus* infected with sea star wasting disease. This organism exhibits signs of turgidity loss with increased sponge-like, hollow qualities in the arms and decreased mobility.

Sea star wasting disease is highly fatal in the majority of sea stars infected such as the sunflower sea star (*Pynapodia helianthoides*), the morning sun star (*Solaster dawsoni*) (Eisenlord et al. 2016), the forbes sea star (*Asterias forbesi*), and the purple/orange ochre sea star (*Pisaster ochraceus*) (Bucci et al. 2017). There is however, a silver lining in that it is not entirely fatal in adults of the species, *P. ochraceus*. The purple/orange ochre sea star implements the unique asteroid anatomy that allows the animal some protection from wasting syndrome. The tissues of *P. ochraceus* are held together by what look like a woven mesh of tissue. *P. ochraceus* has complete control over the fluidity of the tissues and are therefore able to relax their tissues and tear themselves apart (Mothersill & Austin 2000). This act is called autotomy and is

particularly useful in staving off death from sea star wasting disease. When *P. ochraceus* contract a lesion on an arm, they are able to autotomize the limb to save the central nervous system and prevent disease spread throughout the rest of the body. When the infected limb is removed, *P. ochraceus* can heal and regenerate the autotomized limb by growing another in its place (Mothersill & Austin 2000).

Although *P. ochraceus* have the ability to save their bodies from sea star wasting disease through autotomy, this did not save them from experiencing mass die-offs from wasting syndrome from 2013 to 2015. Populations of *P. ochraceus* from Baja California to Juneau Alaska were decimated by sea star wasting disease (Hewson et al 2014, Menge et al. 2016). In Washington State, *P. ochraceus* mortality from sea star wasting was most pronounced in the San Juan region with significant losses incurred on the coast as well as the Puget Sound (Eisenlord et al. 2016) The rapid decline in *P. ochraceus* populations coupled with the length of the population rebound period, has made it difficult for the rocky intertidal zone to maintain species composition on the Pacific coast of North America (Menge et al. 2016, Eisenlord et al 2016, Miner et al. 2018).

Temperature appears to have a significant effect on sea stars and their susceptibility to wasting disease (Kohl et al. 2016, Bonaviri 2017). Often, increases in temperature are implicated with the presence and mortality from wasting in *P. ochraceus* which can be especially rapid for juveniles (Bates et al. 2009, Eisenlord et al 2016, Staehli et al 2009, Bates et al. 2009, Miner et al. 2018). Adults in warmer waters contract sea star wasting disease faster than juveniles. However, juvenile mortality to wasting disease is more dependent on increases in temperature than it is for adults (Eisenlord et al. 2016). The greatest correlation between temperature and wasting events exists in the

relationship between the wasting disease outbreaks in 2009, and then from 2014-2015. In 2009, sea star wasting appeared as a minor blight in the Puget Sound. Bates et al. (2009) found that at the time, minor increases in ocean temperatures had a strong influence on the presence and mortality of wasting disease in sub-tidal zones in Vancouver, Canada.

In 2013 the mass mortality *P. ochraceus* experienced on the coastline began but was then exacerbated in conjunction with warming ocean temperatures in the Pacific (Miner et al. 2018). Wasting continued through 2014 with the increases in water temperatures and then hit a peak in 2015 with ongoing warming in the Puget Sound and San Juan Islands. In the Puget Sound region of Washington state, wasting events spiked especially from Winter to Spring in 2014 (Eisenlord et al. 2016, Miner et al. 2018). *P. ochraceus* populations were immersed in higher temperatures, experienced advanced proportions of infected sea stars. Since adults' contract wasting disease faster than juveniles particularly in warmer waters, the wasting events that occurred during these years severely reduced adult populations by a quarter of their original population size, thus decreasing the number of reproductive individuals on the rocky intertidal zone (Eisenlord et al. 2016).

Although the relationship between temperature and sea star mortality to wasting disease is strong, the prevalence of wasting may be driven by factors which are not exclusively environmental. In 2009, Pankey & Wares identified a genetic mutation present in *P. ochraceus* called EF1A. This gene is overdominant in *P. ochraceus* which means that the gene is phenotypically outside the range of the homozygous parent genes. Those organisms which carry this gene are thus heterozygous (Chandler & Wares 2017). This means that the sea stars with this new gene carry two different sets of alleles for the

same gene, while those sea stars without the mutation carry two of the same sets of alleles. Therefore, unmutated sea stars are homozygous. Overdominance of the EF1A gene is quite possibly a positive contribution to *P. ochraceus* genetic makeup because it is linked to greater disease tolerance (Pankey & Wares 2009). Chandler & Pankey (2017) recently found that individuals with the EF1A mutation carried an increased ability to respond to stresses from increased temperatures. Therefore, heterozygous *P. ochraceus* carrying EF1A may have greater fitness against sea star wasting disease and increased environmental temperatures (Chandler & Pankey 2017).

During the 2014 wasting event, temperature seemed to increase the prevalence of sea star wasting disease on the Pacific Northwest coast of North America. However, later in 2014, Hewson et al. presented evidence that sea star wasting is also strongly correlated with presence of a densovirus, from the *Parvoviridae* family called the sea star associated densovirus (SSaDV) (DelSesto et al. 2015, Eisenlord et al. 2016, Menge et al. 2016). The relationship between SSaDV and sea star wasting disease has been explored in multiple sea star species on both the east and west coasts of North America (Hewson et al. 2014, Bucci et al. 2017). A great deal of evidence exists which implicates the SSaDV in the sea star wasting disease epidemic and sea star mortality as a result. However, the topic of correlation versus causation is challenging because of the nature of pathogen detection and the variability surrounding sea star wasting disease and SSaDV presence.

The Densovirus

A well-known viral family which infects both terrestrial and marine organisms is the Parvoviridae or better known as parvo for short (Cotmore 2014). Parvoviridae viruses

are nonenveloped meaning they do not have the lipid membrane around them that carries viral proteins and often acts as a method for binding to the cells of their host (Yang et al. 2016, Bruemmer et al. 2005). Instead, these viruses must replicate through cell division and have been known to be more lethal in young hosts as a result (Bruemmer et al. 2005).

A genus of the Parvoviridae family is the Densovirinae or rather densoviruses.

Densoviruses are single-stranded DNA viruses that typically infect invertebrates in terrestrial and marine ecosystems such as crustaceans and insects (Jackson et al. 2016, Bruemmer et al. 2005, Bucci et al. 2017, Tijssen et al. 2016). The sea star-associated densovirus (SSaDV) is a circular single-stranded DNA virus suspected of contributing to sea star wasting disease in echinoderms (Fahsbender et al. 2015, Hewson et al. 2014, Bucci et al. 2017).

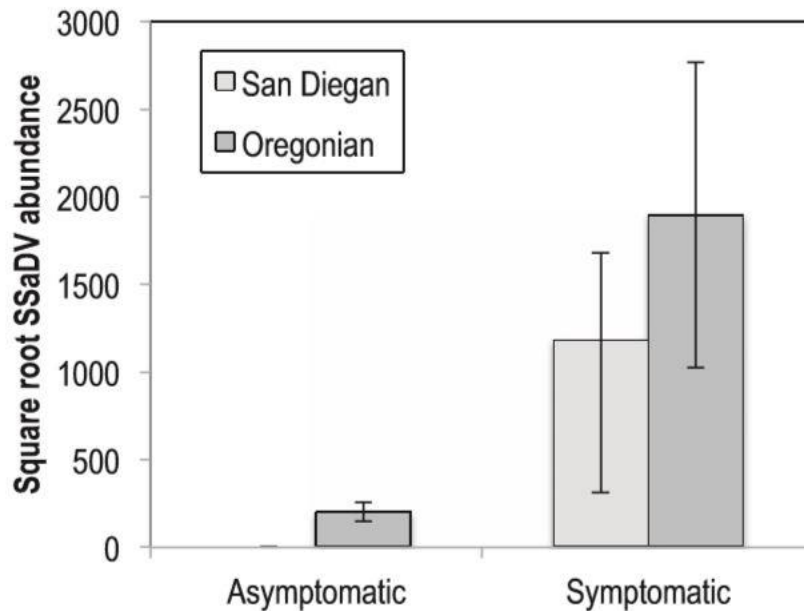


Figure 4. The above figure is a graph from research performed by Hewson et al. (2014). It depicts the relationship between presence of SSaDV and sea star wasting disease in symptomatic individuals. For this analysis 107 sea stars of three species *Pisaster ochraceus*, *Pycnopodia helianthoides*, and *Evasterias troschelii* were tested for presence of SSaDV. Physiological characteristics such as sea star size, and population abundance with SSaDV presence in the organism were statistically analyzed against each other to test for independent variables which may predict sea star wasting disease in these three species of asteroids. Hewson et al. (2014) found that presence of SSaDV was the variable which most effectively predicted the presence of wasting disease in the sea stars tested.

In 2014, the densovirus became the first virus associated with echinoderms in Hawaii and Asteroids in the Northeast Pacific Coast. Previous research on densoviruses demonstrates an expanding host range in marine plants and invertebrates such as the oyster, *Crassostrea ariakensis* (Kang et al. 2017), sea barley (*Hordeum marinum*) (Francois et al. 2014), and three urchin species off the coast of Hawaii; the helmet urchin (*Colobocentrotus atratus*), collector urchin (*Tripneustes gratilla*) and burrowing urchin (*Echinometra mathaei*) (Gudenkauf et al. 2014). Since then, sea star-associated densovirus (SSaDV) has been found in many of the sea stars infected with sea star wasting disease such as the sunflower sea star (*Pynapodia helianthoides*) and over 20

other asteroids in Northeast Pacific coast (Hewson et al. 2014, Smith 2017). Presence of densovirus in sea stars has also been found on the Northeast coast of North America in the forbes sea star (*Asterias forbesi*). Phylogenetically, the densovirus nearest to SSaDV is an *Ambidensovirus* identified in a freshwater crayfish (*Cherax quadricarinatus*) called *Decapod ambidensovirus* variant *Cherax quadricarinatus* densovirus (CqDV) (Bochow et al. 2015). At the time of discovery, the SSaDV had not been genetically identified. Thus, this new densovirus was named for its association to the wasting disease and the organisms most affected, sea stars (Hewson et al. 2014).

Although SSaDV holds the strongest pathogen correlation to sea star wasting disease to date, questions about SSaDV causation of wasting disease are still present. The enigma of this relationship, lies in the fact that SSaDV cannot fulfill the decisive test which determines the relationship between a pathogen and a disease. This test is demonstrated by Henle-Koch Postulates or Koch's postulates as they're more commonly known. These guidelines offer the most secure avenue for demonstrating a pathogen is responsible for causing a disease. The first of these postulates states that "The parasite occurs in every case of the disease in question and under circumstances which can account for the pathological changes and clinical course of the disease" (Evans 1976). This is not true for the relationship between SSaDV and instances of sea star wasting disease as not all animals who have shown symptoms of the disease tested positive for SSaDV presence using viral metagenomics (Hewson et al. 2014, Bucci et al. 2017).

The second postulate states that "It occurs in no other disease as a fortuitous and nonpathogenic parasite" (Evans 1976). At present the sea star-associated densovirus has not been found in any other disease though it is present in sea stars that do not have

symptoms of wasting and has been found in specimens from natural history collections, stored for 70 years, without any symptoms of wasting (Hewson et al. 2014). The third, and most challenging to fulfill, is the postulate which demands that “After being fully isolated from the body and repeatedly grown in pure culture, it can induce the disease anew” (Evans 1976). This third postulate is nearly impossible with our current technology and understanding because no cell lines exist for asteroids (Mothersill & Austin 2000, Bucci et al. 2017). Furthermore, isolating pure densovirus from the host has not yet been achieved and has the potential to be highly improbable to nearly impossible (Bucci et al. 2017). Subsequently, the inability for SSaDV to fulfill Koch’s Postulates to sea star wasting disease is why testing for SSaDV transmissibility in sea stars has largely involved challenge experiments.

Although the relationship between SSaDV and the disease, sea star wasting remains inconclusive based on our current standards for pathogen detection, it is important to continue to study this relationship especially in invertebrates. Viruses in invertebrates are highly understudied since most viral work tends to focus on vertebrates, as the risk of disease spillover to humans is higher in these organisms (Gudenkauf et al. 2014, Jackson et al. 2016, Francois et al. 2016). Therefore, our understanding of viral interactions in echinoderms such as sea stars and urchins is limited (Gudenkauf & Hewson 2016, Jackson et al. 2016). The discovery of the SSaDV in tissues of sick sea stars has sparked further research into viruses that may be associated with echinoderms to better understand the host ranges of viral pathogens in invertebrates.

Prior to 2014 (Gudenkauf et al.) no echinoderm-associated virus had been named. Francois et al. (2016) demonstrated a much larger host range for viruses in the

Parvoviridae family, such as densoviruses, than had been previously thought, including two asteroid orders, *Paxillosida* and *Spinulosida*. Furthermore, viral presence and influence in the aquatic environment is vastly underestimated (Suttle 2005). Gudenkauf et al. (2014) posits viruses may be causing many echinoderm diseases, however, this cannot be confirmed given the current gaps in the echinoderm-viral literature. It is therefore necessary to continue to increase our knowledge of viral interactions in these organisms. This is important not only to understand how viruses may be linked to sea star wasting disease but to increase our knowledge of the influence they may have on trophic cascades in the marine ecosystems (Buck 2017).

Testing for the Densovirus

Viral Metagenomics is the primary method Hewson et al. (2014) used to identify correlations between densovirus presence and sea star wasting disease. Metagenomics has been a breakthrough in sea star wasting research because it does not require sea star cell cultures, a feat which has not been possible since no cell lines exist in marine invertebrates as a whole (Jackson et al 2016, Bucci et al. 2017). Most of *P. ochraceus*'s ability to regenerate derive from their unique tissue and cell structure. Many organisms in the Class Asteroidea are comprised predominantly of tissues with multiple cell types and functions within each tissue (Mothersill & Austin 2000). This has made it challenging to create cell cultures of sea star tissues which, until the use of metagenomics, has greatly hindered research on viruses and diseases in these organisms.

Although metagenomics has allowed for wonderful scientific breakthroughs regarding the study of viruses in echinoderms because of its use of molecular diagnostic assays (Hewson et al. 2014, Jackson et al. 2016), this method is extremely technical and

highly expensive, costing on average \$1000.00 to process one sample for accurate viral identification. Another method used to identify densovirus in sea stars infected with wasting disease is Transmission Electron Microscopy (Hewson et al. 2014). This method uses electrons to penetrate the sample and obtain a microscopic image of the virus's form. It is a proven method for effective identification and although it does not provide the same positive assurances as genetic testing, it can be accomplished without species specific knowledge of protein structures or organism cell cultures.

SEM and Densovirus

In 2014, Hewson et al. successfully captured an image of the SSaDV using Transmission Electron Microscopy. Their image resolved a virus that was 0.020-0.025 microns in diameter. The shape of the virus was icosahedral so that it appears as many equilateral triangles arranged together to create a geometric hexagon shape. Similarly, a Transmission Electron Microscope was also successful at resolving an image of an insect parvovirus, *Junonia coenia* densovirus (JcDENV) captured by Bruemmer et al. (2005), which belongs to the same densovirus genus as the SSaDV. Bruemmer et al. describes the shape of JcDENV as icosahedral which illustrates the shape as a collection of equilateral triangles symmetrically arranged. This description of JcDENV coincides with the SSaDV description by Hewson et al. (2014) using Transmission Electron Microscopy after having performed the metagenomic analysis to understand the physical characteristics of SSaDV.

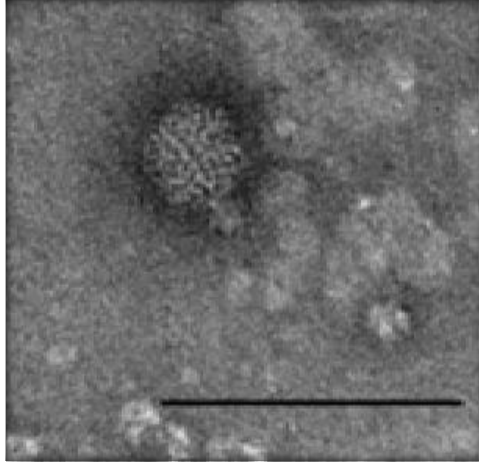


Figure 5. Image of an icosahedral single stranded circular DNA virus captured by Hewson et al. (2014) using Transmission Electron Microscopy. The viral particle is 0.020-0.025 microns in diameter. Hewson et al. (2014) believes this image to be a representation of the structure of the sea star-associated densovirus (SSaDV).

Transmission Electron Microscopy is an important method used most frequently for viral identification because electrons emitted by the electron beam are able to penetrate the sample. For this to occur, the samples themselves must be of a very thin size. The resulting image captured by TEM is two dimensional, therefore the outline of a potential virus is all that is resolvable by the TEM (Kessel & Shih 2012).

Another member of the microscopy family is the Scanning Electron Microscope (SEM). For an SEM to capture images at the microscopic scale, electrons do not need to pass through the sample. Instead the electrons bounce off of the sample and emit smaller, weaker secondary electrons (Scanning Electron Microscope A To Z 2009, Kessel & Shih 2012). These electrons are collected and produce a light image which appears three dimensional. This allows for better topographical visibility at the microscopic level that would not otherwise be seen with the TEM (Kessel & Shih 2012). When it comes to viral identification though, the methods for sample preparation are part of the more

challenging issues associated with successful viral identification with a SEM (Golding et al. 2016).

While Hewson et al. (2014) resolved an image of densovirus, their methods for sample preparation are different than those that are typically implemented for SEM. The nature of TEM which allows electrons to pass through a sample, are beneficial to sample preparation involving aqueous solutions (Golding et al. 2016, Kessel & Shih 2012). Often TEM samples undergo staining so it is easier to discern between background noise and the object itself. This allows for fewer obstructions and more contrast in the sample (Kessel & Shih 2012). Sample preparations for SEM require that the sample be coated in a metal such as gold or aluminum. This ensures that the sample will not experience charging while inside the vacuum chamber. This is also important because the electrons must be able to bounce off of the sample inside the chamber, meaning the sample itself must be conductive. The challenge of resolving an image of a sample as small as a virus, lies in the fact that the metal coating may also coat the virus, preventing successful identification of densovirus (Golding et al. 2016). Nonetheless, this method is important to pursue because if imaging is successful, it will not only provide another method for viral identification, but can also help inform other SEM users about the ideal amount of time sputter coating should occur for viral resolution.

SEM is a method used for quick and cost-effective identification of viruses and bacteria. A SEM can successfully identify viruses in biologic organisms (Kessel & Shih 2012) but has not been attempted for viral identification of densovirus in *P. ochraceus*. Since TEM offers the greatest contrast for viral resolution, work with SEM and viral particles has been less popular. When SEM is implemented for research and is

unsuccessful at resolving images or obtaining the desired result, the trials go unpublished. Consequently, lack of failed research contributes to gaps in SEM knowledge for methods which have worked and those that haven't (Golding et al. 2016). If the SEM is unsuccessful at resolving densovirus in *P. ochraceus*, the method can be eliminated as a source for sea star wasting disease research.

Scanning Electron Microscopy

A Scanning Electron Microscope (SEM) is one type of electron microscope able to resolve images of inorganic and organic matter at microscopic levels (Kessel & Shih 2012). To put it in perspective, a light microscope is able to visualize samples at a maximum of 1000X magnification, while a SEM can scan a sample at a maximum of 300,000X magnification (Wells 1974). This great difference in magnification ability is due to the incredibly small size of the electron (Hayat 1974, Scanning Electron Microscope A To Z 2009). Since the electron is 2.82×10^{-15} meters in diameter, the theoretical size a sample can be visualized is slightly greater than the electron's size (Kessel & Shih 2012). Therefore, the electron's incredibly small size is how the SEM is able to provide a window to the microscopic world.

Components of the SEM

A SEM is comprised of several important parts which allow the machine to scan a sample using electrons, they are the electron gun, microscope column and the sample chamber (Hayat 1974). The electron gun rests at the top of the microscope column, it is where the electrons are separated from the atoms and the electron beam, used to scan

samples, is created (Wells 1974, Scanning Electron Microscope A To Z 2009). The beam is then sent down the second component of the SEM, the microscope column, which focuses the beam of electron energy so that it can be manipulated to scan a sample (Hayat 1974). The beam is sent from the column into the sample chamber, a small box at the end of the column (Kessel & Shih 2012). Inside the chamber are the microscope stage where the beam of electrons is sent out, the sample placed at the base of the chamber, and sensors to detect electrons (Scanning Electron Microscope A To Z 2009, Wells 1974).



Figure 6. Image of The Evergreen State College's Scanning Electron Microscope. Model JEOL JSM-6480LV. To the left is the microscope and to the right is the computer monitor with SEM control panel between them.

SEM Operation

As the beam of electrons comes down the microscope column and into the sample chamber, the electrons are focused onto the sample. When electrons hit a part of the sample, they release weaker negative electrons (Wells 1974). These weaker electrons are collected by the sensor which converts the electron reading into light that is projected onto the computer monitor as an image (Heywood 1971). When electrons hit a part of the sample that is higher up from the sample holder, weaker electrons are released. When the electron beam touches an area lower to the sample holder, few or no electrons are released. The more electrons released when it hits the sample, the greater the light produced by the microscope will be (Scanning Electron Microscope A To Z 2009). Thus, the images produced are in a type of grayscale and the differences in light and dark are actually the differences in topography of the sample.



Figure 7. Image of The Evergreen State College Scanning Electron Microscope sample chamber.

Standard SEM Methods

The priority for this project was to test the ability of the Scanning Electron Microscope to detect and successfully visualize the densovirus in *P. ochraceus* infected with sea star wasting disease. The standard Scanning Electron Microscopy method coats the sample in a metal such as gold or aluminum (Kessel & Shih 2012, Hajibagheri 1999). This is important because samples in the SEM need to be conductive so the electrons can react to the surface of the specimen and produce a light image (Heywood 1971). If the sample is not conductive, the electrons cannot react and bounce off the surface of the specimen and the electrons will refract, making it impossible to obtain an image. Prior to

coating the specimen with a metal, it is important that the tissue is dried in a Critical Point Dryer so that there is no water present in the sample (Hajibagheri 1999). This is due in large part to the fact that the SEM holds the specimens in a vacuum chamber so any organic matter will dry out and shrink. Wet samples are therefore difficult to process in the SEM (and also highly dangerous because a wet sample can combust inside the vacuum chamber). It is necessary to perform critical point drying to remove water from the sample prior to sputter coating (Kessel & Shih 2012, Heywood 1971).

There are several potential issues with these methods in relation to studying viruses and sea star tissue samples. The first is that the drying process will have the negative effect of altering the topography of the tissue sample and thereby reducing the ability of the SEM to detect fine details. The second issue is that sputter coating the sample with metal to create conductivity may obscure fine details making it challenging to see any viruses that may be present in the sample (Golding et al. 2016). However, it is important to try these methods with *P. ochraceus* tissues as they are the standard and have been successful at producing quality images of viruses in other organisms and in people for rapid disease diagnosis (Heywood 1971, Kessel & Shih 2012, Golding et al. 2016)). Thus, this project seeks to understand if standard SEM methods are a viable option for studying densovirus in *P. ochraceus*.

Successful development of a method which implements SEM would provide additional resources to study the phenomena of sea star wasting disease. Furthermore, this method would offer researchers with limited funding, an opportunity to contribute to the sea star wasting literature without the financial burden genetic testing often imposes. With a developed method for successful viral identification in echinoderms using SEM,

there is potential for other students at Universities housing SEMs to participate in larger research discussions and experimentation on sea star wasting disease.

Methods

Methodological Introduction

The primary focus of this project was to explore and develop a method to identify densovirus in *P. ochraceus* infected with sea star wasting disease. This thesis is a methods development thesis and highly experimental in nature. Thus, the process for resolving the viral material was complex and involved a great deal of trial and error with few fruitful results. Consequently, the layout of this methods is arranged in order of experimental trials and results.

These methods begin with an overview of the field collection of *P. ochraceus* tissue samples with a brief explanation of the data collection process using the GIS Collector application. Then the first filtration method, which utilized the pop-top filter head unit, is described. Following Method 1 is a Results & Discussion, elucidating why it was not appropriate for this project. Next the second attempted method, vacuum filtration, is introduced with a proceeding Results & Discussion section. The third method follows the same model as the prior two methods sections but chronicles the final filtration method which implemented the Swinlock filter head unit. A Results & Discussion is then presented for this method to explain why filtration as a whole was unsuccessful, with discussion of what could have been done differently and possibilities for the future in regards to micro-filtration recommendations.

Finally, the fourth method utilized in this project is described. This method involves whole *P. ochraceus* tissue sample preparation for SEM analysis. Following this method, an explanation of how this project intends to identify densovirus is discussed based on current literature with Transmission Electron Microscopy (TEM) images of this

viral genus as reference sources. Finally, the methods reinforce the comparison between SEM and TEM to clarify the difference between the method used for this project and the method used in the literature to resolve densovirus. Finally, these methods discuss the implementation of the GIS Collector application for data collection and explains the usefulness of displaying sea star data through this platform. The Results section, following the full Methods section, will expand on findings from whole *P. ochraceus* tissue sample preparation and analysis.

Tissue Sample Collection

P. ochraceus were collected from the Puget Sound and Pacific Coast in Washington state. Individuals were chosen as samples based on their degree of wasting disease. Sea star tissues decimated with wasting were collected because this is the tissue that carries the largest quantity of densovirus if it is present in the organism (Hewson et al. 2014). Diseased sea star tissues were removed using an 8 mm sterile punch biopsy commonly used in veterinary medicine. The animal tissue was then placed in tin foil and preserved in a cooler with dry ice. The cooler was taken back to The Evergreen State College lab and tissue samples were stored in a deep freezer at -80 degrees Celsius.

Environmental Data Collection

Tissue samples were obtained from Tacoma Narrows, Narrows Marina and Boston Harbor Marina in South Puget Sound, Washington. Each collection site was chosen based on historical presence of *P. ochraceus* with wasting disease as documented in Eisenlord et al. (2016), the Rocky Intertidal Monitoring Group citizen science data

collected during sea star wasting outbreaks from 2013-present. Sites were also selected based on personal observations of historically dense sea star populations in the Puget Sound prior and during the 2013-2015 sea star wasting disease outbreaks. A GIS collector app was created using ArcGIS 10.5 prior to sample collection with all pertinent environmental and physiological attributes that would be recorded in the field. The following information was recorded: GPS coordinates, Total *P. ochraceus* at site, Color (purple/orange), Size (radius in centimeters), Age (juvenile/adult), SSWD presence (yes/no), average water Temperature (celsius), Salinity (ppt), Dissolved oxygen (mg/L), and Conductivity (spc). *P. ochraceus* age was determined according to length of the sea star radius. Juveniles are any sea star unable to reproduce; *P. ochraceus* can reproduce after 75 mm radius (Eisenlord et al. 2015). Therefore, juveniles are any *P. ochraceus* under 75 mm and adults are sea stars with a radius greater than 75 mm.

A picture was captured of each sea star when a tissue sample was removed at every sample location. Measurements were taken of sea star radius size in inches, the color and approximate life stage as well as the degree of wasting disease. Other environmental variables such as salinity, dissolved oxygen, and conductivity were measured on site during the day of tissue collection using a Yellow Springs Institute (YSI) meter. Water quality measurements were taken from 5 separate points in the intertidal zone where wasting was present to capture ancillary environmental data while recognizing the inherent variability of ecological measurements in the intertidal zone.

Method 1

Filtration

To best visualize densovirus under SEM, *P. ochraceus* tissue sample filtration was attempted for this research. This is important to eliminate background noise that would be present in a sample prepared with tissue and other organic matter around the viral material. Viral isolation from tissue was successfully performed by Hewson et al. (2014). This is possible through homogenization and the fact that densovirus can persist in the environment and subsequently, sea water bases.

The filtration method for this project was developed through a combination of methods by Hewson et al. (2014) and Golding et al. (2016). Both sources implemented viral isolation, one for TEM analysis and the other for SEM respectively. Although Hewson et al. (2014) isolated densovirus successfully from sea star tissue, their method, which created a viral pellet suspended in fluid, was not appropriate for SEM sample preparation methods as it would not provide a platform to dry out the viral material to mount on a sample stud. The resulting viral material needed to be mounted on a filter so that ethanol could be passed through the sample to fully dry it out and mount on a 10 mm SEM sample stud. Therefore, sample homogenization and centrifuge were performed following Hewson et al. (2014), while viral filtration using polycarbonate track-etched membrane filters was adapted from Golding et al. (2016).

Filtration Testing

Proper sample filtration and viral isolation was the primary focus of this stage of method development. The first filtration method attempted, utilized procedures published

by Golding et al. (2016). The filters were 13 mm polycarbonate track etched membrane filters with a pore size of 0.015 μm . This filter diameter was chosen in part because it is easily seated on SEM sample studs with diameters of 10 mm and would not require trimming to mount the filters to the studs, post-filtration. The pore size is necessary to capture dengue virus measured by Hewson et al. (2014) at approximately 0.020-0.025 μm . The corresponding filter holders utilized would be compatible with 3 mL Luer-Lok syringes and 13 mm polycarbonate track etched membrane filters. The filter holders implemented were the Whatman Pop-Top Syringe-Type Reusable Membrane Filter Holders, with a 13 mm diameter at dimensions 2.7 cm x 2.7 cm.

Result & Discussion

Initial testing of the Pop-Top filter holder and filter membrane was performed using deionized water to assess the filtration rate without tissue samples. This was important to understand how the filter should behave under normal conditions to recognize how it acts when it clogs. This was a concern because clogging was frequently an issue Golding et al. (2016) experienced with 13 mm polycarbonate track etched filters having a 0.05 μm pore size. While Golding et al. (2016) implemented a Swinnex filter head unit for the 25 mm filter diameter, this filter head was unavailable for this research. Therefore, this project relied on the most compatible filter holder for the 13 mm diameter membrane, the Whatman Pop-Top Syringe Filter Holder.

This Pop-Top Filter Holder is reusable and autoclavable. It seats the filter membrane between the filter head components and the third piece locks them together by snapping the front and back of the unit to seal the washer around the filter membrane. To

test this apparatus, 3 mL of deionized water was filtered through the unit and 13 mm membrane filter. The filter head unit immediately leaked water out the sides of the filter head and no water was able to make it through the tip of the syringe head. This meant that the water wasn't actually able to penetrate the filter because the unit could not create a solid seal between the washer and the membrane. The challenges with this filter unit exist in the fact that the filter head snap was highly variable and wasn't easily seated onto the syringe head. Furthermore, when a solid fit could be achieved, the filter unit lost most of the water out the sides due to inefficiencies in the filter head unit design.

Correspondence with the manufacturing company, Whatman, elucidated a couple issues with this filter set-up. One issue is the diameter of the filter membrane in conjunction with the extremely fine pore size used for this project provides inherent challenges with filtration. The pore size itself is so small, filtration should take a very long time, however, a decent amount of pressure should be placed on the filter to force the water through the membrane. The recommendation was to increase the surface area of the filter membrane in hopes that a larger surface area would evenly disperse the pressure placed on the filter during filtration. Therefore, the filter membrane was increased from 13 mm to 25 mm diameter to attempt this method with Whatman's recommendations.

The other challenge this project experienced with the 13 mm diameter filter membrane is that it was only compatible with one type of filter head unit, the Pop-Top Syringe Type Filter Holder. This unit was unable to withstand the pressure necessary to force water through the membrane. Whatman admitted this filter unit was not their most reliable apparatus for micro filtration. Increasing the filter head diameter to a 25 mm polycarbonate track etched membrane filter would also allow this project to experiment

with another, more reliable filter head unit, the Whatman Swinlock filter holder. Since the Pop-Top Filter Head Unit and the 13 mm diameter were unable to produce an effective filtration result with deionized water, this set up was not pursued as a viable filtration option for this project.

Method 2

Vacuum Filtration

One of the challenges syringe filtration presented is that it only allowed a single sample to be processed at a time. An alternative filtration method which could support filtration of multiple samples and circumvent potential faulty filter head units was vacuum filtration. This method utilizes a vacuum pump with side-arm Erlenmeyer flasks, and a funnel to force a sample through the filter unit. Filtration is achievable because the vacuum decreases the pressure in the chamber of the side-arm Erlenmeyer flask below the funnel. The funnel seats the filter sample and as the pressure decreases, the sample is filtered through the membrane. Multiple side-arm flasks can be connected to a manifold to process up to 10 samples at once.

This method was first tested using deionized water and the Whatman 25 mm polycarbonate track-etched membrane filters with the 0.015 μm pore size. Side-arm 250 mL Erlenmeyer flasks were connected to The Evergreen State College lab's house vacuum. This trial implemented rubber stoppers, to hold the glass towers, with 20 mm diameter glass funnels. Polycarbonate track etched membrane filters were placed in the bottom of the glass filters against the filter base. Deionized water was added to the funnel with the filter seated at the base and the vacuum initiated. Filtration with this method was

unsuccessful as the polycarbonate filter immediately lifted from the base of the glass filter. Thus, this setup was not effective filtration with this filter type.

To prevent filters lifting from the funnel, a filter tower with screw cap and washer, was used as a replacement for the glass funnel because it effectively seats the filter and seals it between the apparatus. The filter was secured inside the filter tower and the side-arm flask was attached to the vacuum, then 20 mL of deionized water was added to the top of the tower. After 2 minutes, the deionized water did not filter through the membrane and the vacuum was shut off. Since the house vacuum was not successful at pulling water through the filter, the Erlenmeyer flask was attached to a standing vacuum because it offered controlled pressure settings and could increase the vacuum power greater than the house vacuum. The standing vacuum was adjusted to pull at maximum pressure and was allowed to sit for 1 minute. The standing vacuum was unsuccessful at pulling deionized water through the filter membrane.

Result and Discussion

None of the vacuum filtration options attempted were able to successfully pull deionized water through the 0.015 μm Whatman polycarbonate track-etched filter membrane. The purpose of this filtration method was to increase the number of samples that could be filtered at one time. Multiple sample filtration was to be accomplished through the use of a filtration manifold. Unfortunately, the pressure needed to pull deionized water through the filter membrane was insufficient with a manifold and not implemented for this project. This is because a manifold distributes the same level of pressure to ten side-arm Erlenmeyer flasks. The same pressure was inadequate at drawing

deionized water down through a single filter unit, thus diluting the pressure through a manifold would be ineffective.

Vacuum filtration with the funnel was unsuccessful for known and unknown reasons. The known issue with this method deals again with the incredible smallness of the pore size. Communication with Whatman indicated that vacuum filtration may not have provided enough differential pressure to filter deionized water through the 0.015 μm pores. The maximum pressure that could have pulled the water down through the membrane was achieved with the standing vacuum. Prolonged vacuum connection beyond the 1 and 2 minute pressure intervals tested would not have increased the pressure in the Erlenmeyer flask or the draw down from the funnel. This is because vacuum filtration pulls the maximum pressure capacity within the first couple minutes and this pressure would not increase with extended exposure to the vacuum. Therefore, the maximum pulling capacity for the house vacuum was achieved and did not result in deionized water filtration through the 0.015 μm polycarbonate track-etched filter membrane. The polycarbonate membranes are hydrophilic so that they are able to maximize their contact with water because of the filter surface's natural attraction to water molecules (Xie et al. 2005). Hence, polycarbonate filters should have no issue filtering water-based solutions as they are the most well-equipped micro filter material for this process. As such, it is curious that the pressure is insufficient at drawing water through the filter membrane, even one as small as 0.015 μm .

Method 3

Swinlock Filter Holders & Polycarbonate Membranes

The final filtration method attempted referred again to the method implemented by Golding et al. (2016) with some modifications based on obstacles encountered in Method 1. Instead of 13 mm polycarbonate track-etched membrane filters, this method used 25 mm diameter polycarbonate track-etched filters and the Whatman Swinlock Filter Holders. Filters in the sizes 5 μm , 2 μm , 0.05 μm and 0.015 μm were initially tested using deionized water similar to the previous methods, to test the flow rate and the firmness of the filter holder seal. These pore sizes were initially used because they were available as free samples through Whatman. Later, filters were chosen by powers of 5 beginning with the filter size goal of 0.015 μm . Filters purchased and implemented by this research were as follows: 0.015 μm , 0.08 μm , 0.4 μm , and 2 μm .

Deionized water filtered easily through 5 μm and 2 μm filters. At 0.05 μm the Luer-Lok syringe required more pressure but 3 mL could be pressed through the filter at a rate of 1 mL per 5 minutes. The most challenging filter pores size was again, the 0.015 μm filter. Deionized water could pass through the filter head but with great care because if the pressure placed on the filter head exceeded 52 psi the Swinlock filter head washer seal would leak water through the sides of filter unit. If a pressure balance was achieved that could both filter sample through the membrane while preventing leaks, then 3 mL of deionized water could filter through the membrane in approximately 25 minutes. Thus, the Swinlock Filter Holder and polycarbonate track-etched membrane filters were utilized for sea star tissue filtration methods development.

Tissue Sample Preparation for SEM

Frozen tissue samples were placed in 10 mL of artificial buffered sea water to prevent contamination from an environmental water sample. The sea water was used to homogenize the samples using a mortar and pestle. After homogenization, samples were centrifuged at 1000 X g for 5 minutes to separate larger tissue material following methods published by Hewson et al. (2014). The liquid material was filtered using a Whatman Swinlock filter holder and Whatman 25 mm polycarbonate nuclepore track-etched membrane filters. Tissue homogenate filtration was attempted using a 3 mL Luer-Lok syringe through descending pore sizes of 2 μm , 0.4 μm , 0.08 μm to the final pore size of 0.015 μm . Unfortunately, tissues homogenized in buffered sea water were unable to pass through even the largest filter pore size of 2 μm . The few remaining 5 μm polycarbonate track-etched membrane filters from the first trials were then used for tissue filtration. The 5 μm was also unsuccessful at passing tissue homogenate through the filter membrane. As a result, tissue homogenates in sea water were too dense to pass through the polycarbonate filter membranes and thus this was not a successful filtration method.

Sea star tissue was therefore homogenized in 10mL of deionized water and centrifuged at 1000 X g for 5 minutes. Sample filtration was tested first on the largest polycarbonate pore size available, the 5 μm filter membrane. Filtration with this homogenate presented its own set of problems because, while some of the sample was able to filter through the membrane, the pressure required to perform this filtration exceeded the 52psi the Swinlock Filter Holder could withstand without leaking. Although some of the sample could be filtered through the membrane, at least half the sample was lost through the sides of the filter holder. Filtration with deionized water was

inconsistent. The sample was repeatedly diluted with increases of 20mL of deionized water to create better filtration without too much pressure but the Swinlock Filter Holder always leaked. Filtration of sea star tissue to separate potential viral particles, even at the larger pore sizes, was unsuccessful at producing the desired filtration result and further filtration decreases were not attempted after these failed trials.

Result and Discussion

This filtration method, though successful with deionized water, proved challenging with samples of sea star tissue. Tissue samples that were homogenized and centrifuged in artificial sea water were first filtered through the 2 μm polycarbonate filter. Continuous, firm pressure was placed on the syringe for 30 minutes but the sample would not filter through the membrane and Swinlock holder. The sample did not carry visible particles but the solution did possess a thick gelatinous quality that potentially clogged the filter. The sample was then removed from the syringe and diluted in more sea water. After dilution, the sample was still resistant to filtration through a 2 μm filter. Therefore, a 5 μm filter was then used to perform sample filtration but a similar result occurred with the 5 μm filter and the solution was unable to pass through the membrane.

It is curious why the samples, with such high dilution, refused to pass through the filters even those with larger pore sizes. Questions about the polycarbonate filter's compatibility with sea water arose but Whatman would not disclose detailed information about its' filter membranes, citing that the information was proprietary. Correspondence with Evergreen faculty, Gerardo Chin-Leo, confirmed the suspicion that the homogenate was in fact too dense with the use of sea water plus tissue. It was recommended that this

project attempt to homogenize sea star tissue in deionized water instead to reduce the density of the sample. This recommendation proved to be true, as deionized sea water created a fluid, less dense homogenate than samples homogenized with buffered sea water which were pretty gelatinous and thick. However, filtration with deionized water presented its own set of challenges, in that the homogenate was more prone to break the Swinlock filter head unit washer tight seal and leaked through the filter head unit with less pressure placed on it than the sea water homogenate. This caused at least half the sample homogenate to be lost and was not an effective filtration solution for this project.

A component this project could not financially support is the implementation of a syringe pump similar to the one used by Golding et al. (2016) to filter their sample homogenates through 0.05 μm filter membranes. Syringe pumps are machines that can accurately control the pressure placed on the filter units and hold continuous pressure for long periods in ways a user cannot. Golding et al. (2016) was able to filter their samples at a rate of 1000 μL per minute through a 0.05 μm filter unit using a syringe pump. Their filters did experience clogging at this pore size and multiple dilutions were necessary for full sample filtration but the syringe pump allowed them to have more control over the filter unit than this project could achieve. Implementing a syringe pump for micro filtration would be a recommendation this project would make for others pursuing a similar methodology. Those with sufficient resources or syringe pump availability in their laboratories should budget for at least one of these machines as filtration variability and lack of pressure control was a primary issue with this methods development.

Whole Tissue Sample Preparation

Since sea star tissue filtration could not be achieved with any of the filtration methods implemented by this project, whole tissue samples were processed and analyzed with the SEM to scan for viral presence. This method was also implemented to examine the difference between wasting and non-wasting sea star tissues at the microscopic level. Tissues were frozen at -80 degrees Celsius then placed in 3% glutaraldehyde solution for 72 hours following methods published by Becker et al. (2004) (Hajibagheri 1999). Six samples removed from wasted *P. ochraceus*, were submerged in increasing ethanol concentrations of 20 mL of 50%, 70%, 90% and three 100% treatments each for 15 minutes per SEM tissue preparation methods from Knox University Faculty, Linda Dybas which are standard methods implemented for soft tissue SEM sample preparation. Although both methods from Dybas and Becker et al. (2004) did not indicate the necessity to also place the samples in 100% acetone, this method was chosen, as acetone acts as a better transition fluid to CO₂ for optimum soft tissue desiccation during CO₂ Critical Point Drying (Thuesen & Towanda, Personal Communication). Therefore, samples were submerged in acetone and then critical point dried in acetone in the CO₂ Critical Point Dryer sample chamber.

Experimental Drying

To compare the difference between tissue dried with ethanol and acetone, and tissue dried in exclusively acetone, a seventh wasted sea star tissue sample was removed from the top of an adult purple *P. ochraceus*. This sample was held frozen at -80 degrees Celsius then placed in 3% glutaraldehyde solution for 72 hours following methods

published by Becker et al. (2004). This sample was then submerged in increasing ethanol concentrations of 20 mL of 50%, 70%, 90% and three 100% treatments for 15 minutes each (Linda Dybas). The sample was then submerged in ethanol in the CO₂ Critical Point Dryer during the final drying process. Upon Critical Point Drying completion, the sample was removed from the sample chamber and found expanded and soaked in ethanol. This indicates that the ethanol was insufficient at completely drying the soft tissue and was unable to fully bleed out as CO₂ was added to the sample chamber. This permanently damaged the sample and so was thrown out.

Sputter Coating

The standard SEM method of sputter coating the sample in gold-palladium was applied to this methodology for *P. ochraceus* tissue sample preparation. Samples were dried in a CO₂ Critical Point Dryer, then mounted on SEM studs, purged with argon and sputter coated in gold-palladium. Standard SEM methods typically sputter coat a sample for 120 seconds, however, the samples were coarse with variable topography so more sputter coating was required to completely coat the sample in gold-palladium. Sample studs, with sample mounts, were laid on their sides and sputter coated on both left and right angles of the samples to ensure full gold-palladium coverage of each sample. Although Golding et al. (2016) found that aluminum was also a viable conductive metal which produced quality viral images in the SEM, The Evergreen State College lab does not have the ability to attempt this method as they exclusively use gold-palladium.

SEM Calibrations

Each sample was mounted on a 10 mm carbon disk and affixed to a 10 mm SEM stud. Samples were then placed in a 32 mm stud holder and inserted in to the SEM. The SEM was initially calibrated with the aperture set to stage 2 and the voltage to 5kV with a spot size of 45 and a working distance of 8 mm for all samples. The capacity of the stud holder was for 3-cylinder studs or for 5-point studs depending on the style of stud the samples were mounted on. The samples were first observed under View and then gradually adjusted to Stage 1 then 2 for finer detail. Auto brightness and contrast were selected first, and then auto focus second, to obtain the best image at each magnification level. Magnifications of 38,000X and 40,000X were used to capture fine detail images of densovirus per methods used by Bruhmmmer et al (2005).

Sample Analysis

A total of 7 wasted sea star tissue samples were collected and prepared for whole tissue SEM analysis. The first sample, removed from the top of an arm of an adult, purple sea star was examined. The second sample was taken from the top of an adult orange sea star. Sample three was removed from the top of an adult purple sea star and a secondary sample was removed from this organisms' underside to examine the tube feet, they are called Sample 3 and Sample 3.5 respectively. This was also performed for the fourth organism collected, so that we have both a Sample 4 representing the top of the organism and Sample 4.5 representing the underside of the same specimen. A fifth sample was collected from an infected sea star; however, this sample was botched due to improper sample preparation in exclusively ethanol. The sample was not completely dried during

CO2 Critical Point drying which cause the tissues to expand. It was no longer usable and was discarded.

To visually compare characteristics in wasted sea star tissue to healthy sea star tissue, an 8th sample was collected from a healthy *P. ochraceus* for whole tissue analysis under SEM. This sample was dried in both ethanol and acetone, since this method was the most successful SEM sample preparation approach. It was analyzed under SEM and used as a “control” sample to compare features and characteristics between wasted and non-wasted sea star tissue. This sample was imaged after Sample 4.5, and will therefore be referred to as Sample 5 to maintain continuity and avoid confusion.

Densovirus Characteristics

Successful identification of viruses in the Paroviridae family inside of *P. ochraceus* tissues was performed with reference to images of an insect parvovirus, *Junonia coenia* densovirus (JcDNV) captured by Bruemmer et al. (2005) using Transmission Electron Microscopy (TEM). JcDNV belongs to the same densovirus genus as the sea star-associated densovirus (SSaDV). Reference for the characteristics and a single image of the SSaDV were taken by Hewson et al. (2014) using TEM (see Figure 5 in Literature Review) after having performed a metagenomic analysis to understand the physical characteristics of SSaDV. Both Hewson et al. (2014) and Bruemmer et al. (2005) were able to describe densoviruses as icosahedral viruses which looks like many equilateral triangles symmetrically placed together. Hewson et al. (2014) successfully captured a TEM image of the densovirus and recorded its size as being between 20 to 25 nm. These size and magnification specifications allowed this thesis to have a reference

for viral image resolvability using the SEM. The images taken by the TEM from both papers were able to provide visual examples of how the densovirus would appear under microscopy if present in the samples.

It is important to note, however, that both reference papers (Hewson et al. 2014 & Bruemmer et al. 2005) implemented the Transmission Electron Microscope to produce their sample images and this research used the Scanning Electron Microscope. Although both technologies are able to see at the microscopic level, the TEM is different in that the electrons emitted by the machine pass through the sample to resolve an image of the object. Since TEM requires that the electrons be able to pass through the object, the sample itself must be very thin so that this process can occur (Kessel & Shih 2012). Subsequently, the image obtained is two dimensional which limits the depth of field for the microscope.

Conversely, The SEM is able to detect material on the surface of a sample, but on a microscopic scale. The SEM scans the topography of an object and is able to resolve differences in topography through light given off by electrons when they touch the surface of an image. The greater the light, the higher the sample is from the sample stage. Therefore, the image obtained is often 3-dimensional, and is able to demonstrate differences in depth of field better than the TEM. The benefit of using the SEM is that the samples do not have to be particularly thin, in fact, whole organisms such as insects and small animals and plants can be desiccated and inspected under the SEM. This provides a better understanding of the cellular structures of organisms while they are intact and can offer a better picture of the assemblages which comprise some of the smallest organisms on earth.

Results

Introduction of Results

The following Results section chronicles images of whole *P. ochraceus* tissue analyzed under the SEM. Samples were individually scanned to observe surface features present within each sample to better understand the nature of *P. ochraceus* tissue infected with wasting disease. The primary goal for this project was to ascertain whether or not the SEM would be a good method for resolving densovirus in *P. ochraceus*. Thus, samples were scanned with the focus of obtaining a quality, high resolution image of densovirus in high magnification. The images shown below are the result of careful sample scanning at multiple scales to increase image resolvability as magnification was increased.

The Results are arranged in order of samples chronologically removed from the field. Each sample is introduced as its own section with a description of the images at the beginning of the sample section. Each sample section begins with a wide-view micrograph of the sample, followed by images taken at multiple magnifications. The final image at the end of each sample section was captured at the highest magnification achievable by The Evergreen State College SEM.

Sample 1

The first image of sample 1 (Figure 8) was captured to observe the characteristics of its full surface area. Sample 1 was removed from the top of an adult, *P. ochraceus* arm infected with sea star wasting disease. The orientation of the tissue on the sample stud is the top of the organism's tissue. On the top right and bottom left of Figure 5 are spines

from the top of the sea star body. The middle of the sample appears to have many cracks and crevices, with rounded characteristics, henceforth referred to as nodes in this Results section.

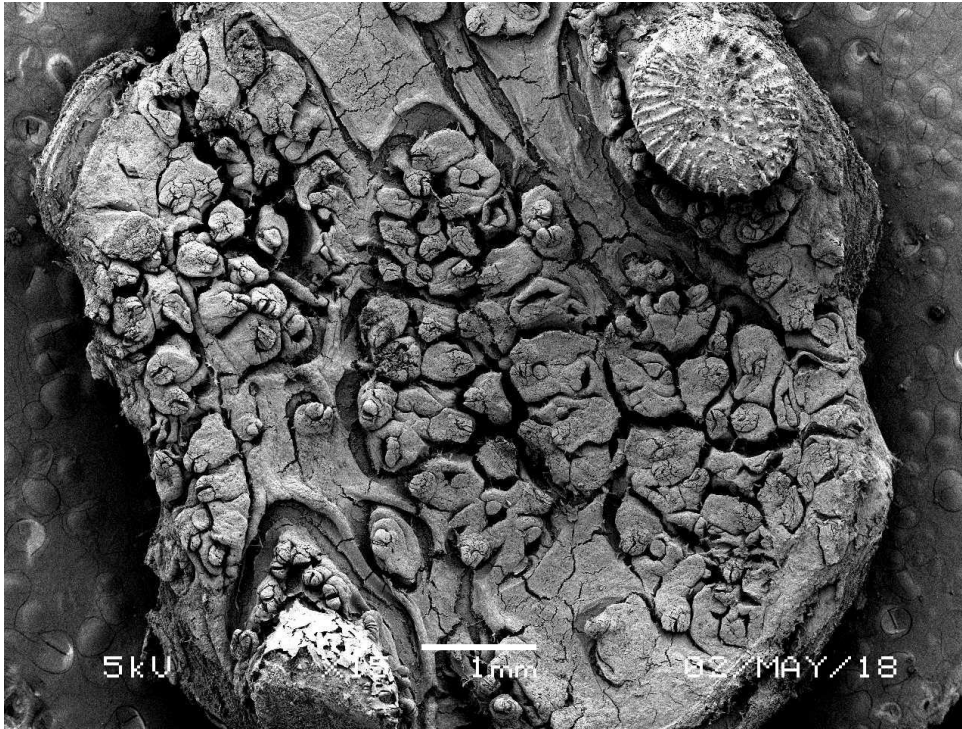


Figure 8. SEM image of *P. ochraceus* tissue, sample 1. Image captured at 35 magnification, with the voltage calibrated to 5 and spot size of 44. The Z distance and working distance were set to 20 mm. Image represents the full aspect of sample 1, the full diameter is approximately 8 mm. The textured region around the sample is the carbon disk the sample is seated atop.

The SEM was able to successfully resolve fine detail represented in the *P. ochraceus* spine. Figure 9 showcases the ridges around the circumference with great detail. The spine appears to have a fine texture similar to pockmark-like circular divots around the surface. A closer look at the spine can be found in Figure 15, where the ridges are easily resolved and showcases the ridge characteristics around the edges of the sample.



Figure 9. The above image is a spine of sample 1. Image captured at 60 magnification, with the voltage calibrated to 5 and spot size of 43. The Z distance and working distance were set to 20, however, the autofocus function automatically reset the working distance to 11 mm. The resolution for this image was so good with this working distance, the modification by the autofocus function was not changed to match the Z distance. Final image captured using auto contrast and brightness with autofocus.

Figures 10 and 11 illustrate the fine features present in tissue structure. The most apparent characteristics are the cracks and fissures clearly present on the surface of the sample. Sample 1 was treated in increasing concentrations of ethanol to three treatments of 100% acetone. Acetone was also used to dry the sample in the Critical Point Dryer, and it is likely these cracks are a result of acetone treatments and CO₂ critical point drying. These cracks are unlikely to be present as a characteristic of sea star wasting disease (Erik Thuesen, personal communication).

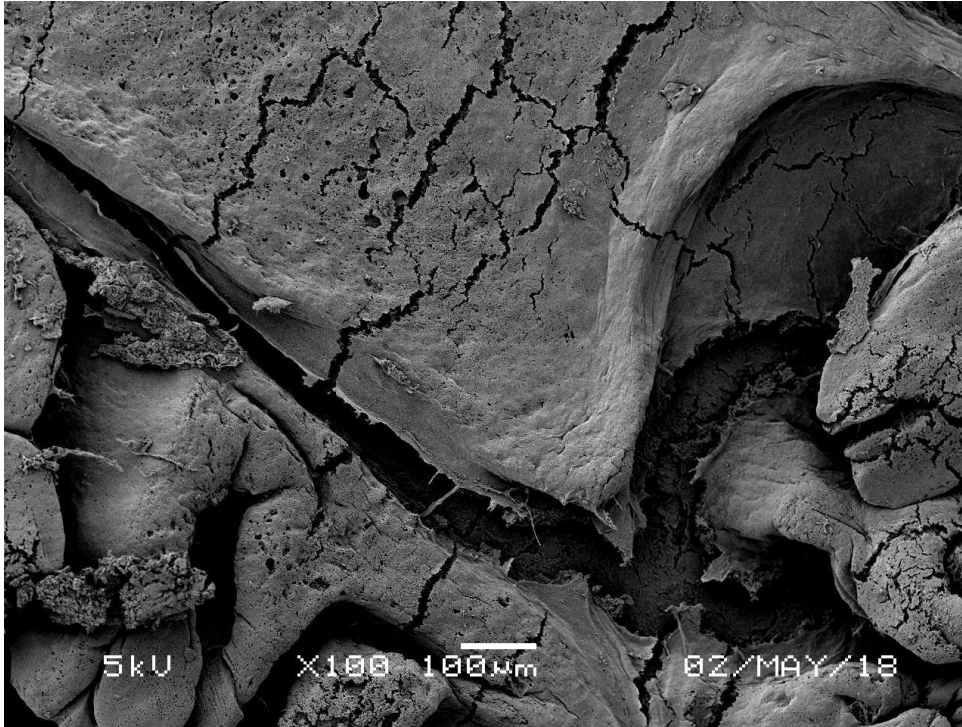


Figure 10. The above image is a mid-section of sample 1 between the two spines captured in this sample. Image captured at 100X magnification, with the voltage calibrated to 5 and spot size of 46. The Z distance and working distance were set to 20, however, the autofocus function automatically reset the working distance to 13 mm. Working distance was not changed to match the Z distance after autofocus modification. Final image captured using auto contrast and brightness with autofocus.

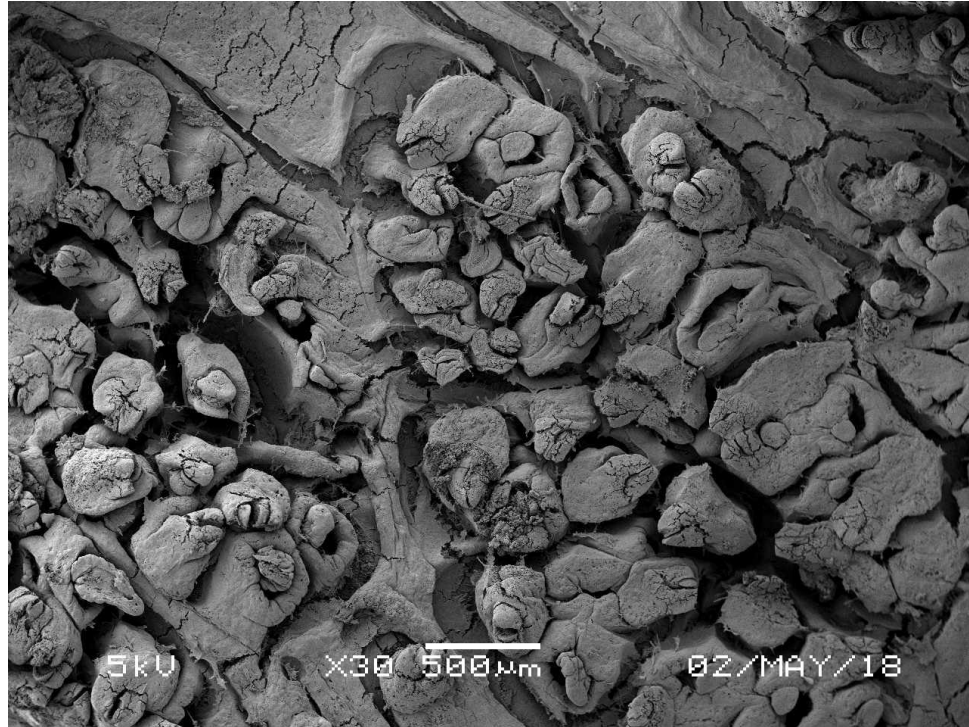


Figure 11. The above image is a larger view of the center of sample 1 between the two spines. Image captured at 30 magnification, with the voltage calibrated to 5 and spot size of 44. The Z distance and working distance were set to 20, however, the autofocus function automatically reset the working distance to 11 mm. The working distance was not changed to match the Z distance.

Figure 12 demonstrates more of the fissures present in the tissue sample and better resolves some of the finer cracks. This image also reveals a texture that appears sponge-like on the surface of the organism. Tissue imaged in Figure 12 reinforces the idea that the cracking is a result of SEM sample preparation methods and this is most clearly illustrated in the bottom left region of this micrograph. Smaller holes in the tissue appear very fine while others are as large as 10 μm across. However, it seems that as the holes increase in size, they begin to form larger cracks, creating the fissures presented in Figure 9.

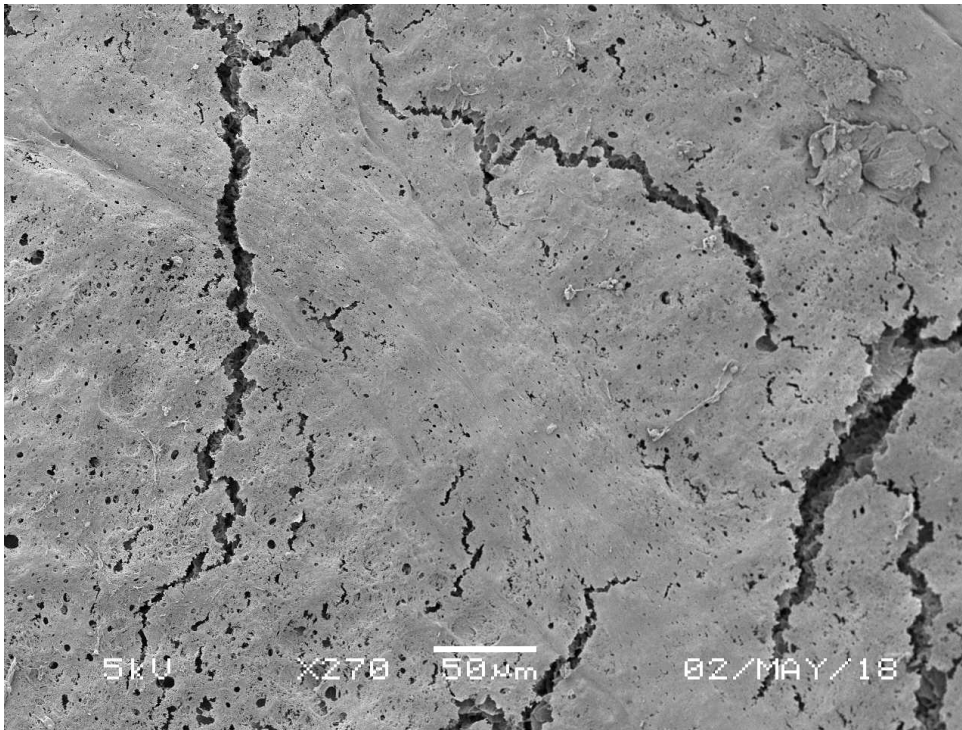


Figure 12. The above image was captured of a more flat surface in sample 1. Image captured at 270 magnification, with the voltage calibrated to 5 and spot size of 43. The Z distance and working distance were set to 20. Autofocus function automatically reset the working distance to 12 mm and this modification was not changed. Final image captured using auto contrast and brightness with autofocus.

Figure 13 is a close-up of one of the rounded nodes seen on the surface of the tissue sample. These details are most curious because the clumps of spongy matter either appear to be coming out of the center from this rounded feature or were once a part of the structure. The texture of this spongy matter is also attached to the side of the top left node so it is challenging to tell from this sample if the sponge-like matter is decimated sea star tissue or other material on the surface of the organism. It is challenging to determine if this sponge-like matter is the same between the two areas or if it is completely different. Figure 14 is a close-up view of Figure 13's node on the left side. It exhibits the porosity of the sea star tissue and presents a finer scale look into the sponge-like material. On the

bottom left of Figure 13 is a side-view of a fissure that opened up in the tissue which occurred during the drying process.

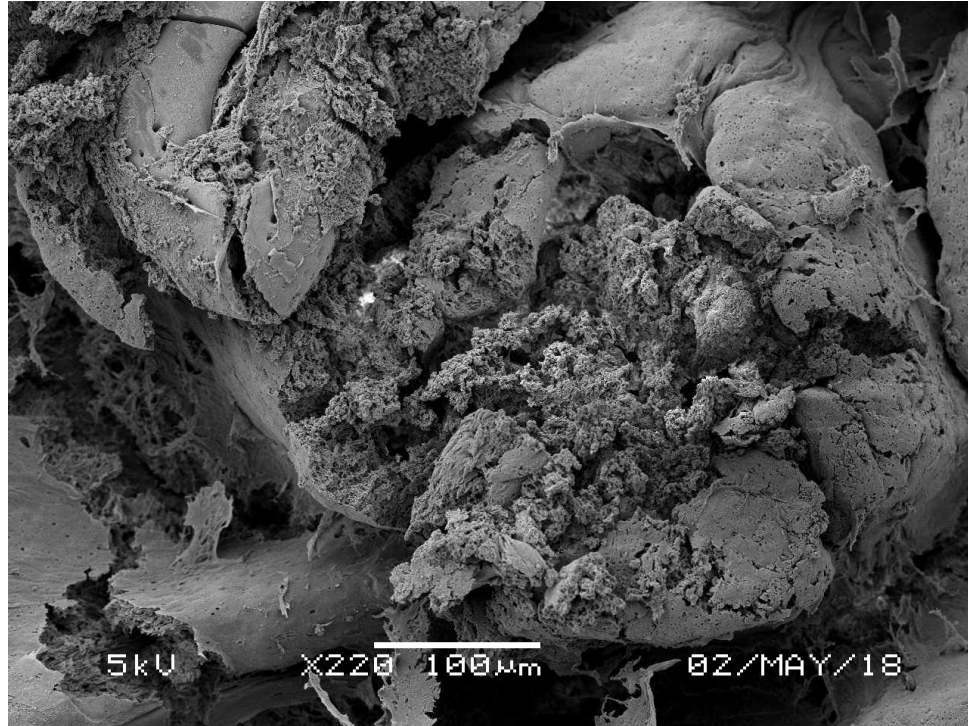


Figure 13. The above image is a region of the spine of sample 1. Image captured at 220 magnification, with the voltage calibrated to 5 and spot size of 41. The Z distance and working distance were set to 20, however, the autofocus function automatically reset the working distance to 11 mm and this was accepted as the working distance for this micrograph. Image was captured by manually blacking out the contrast and brightness then the brightness was increased until a gray screen was just visible. Contrast was increased until fine features could be visualized, then autofocus was initiated to capture this final image.

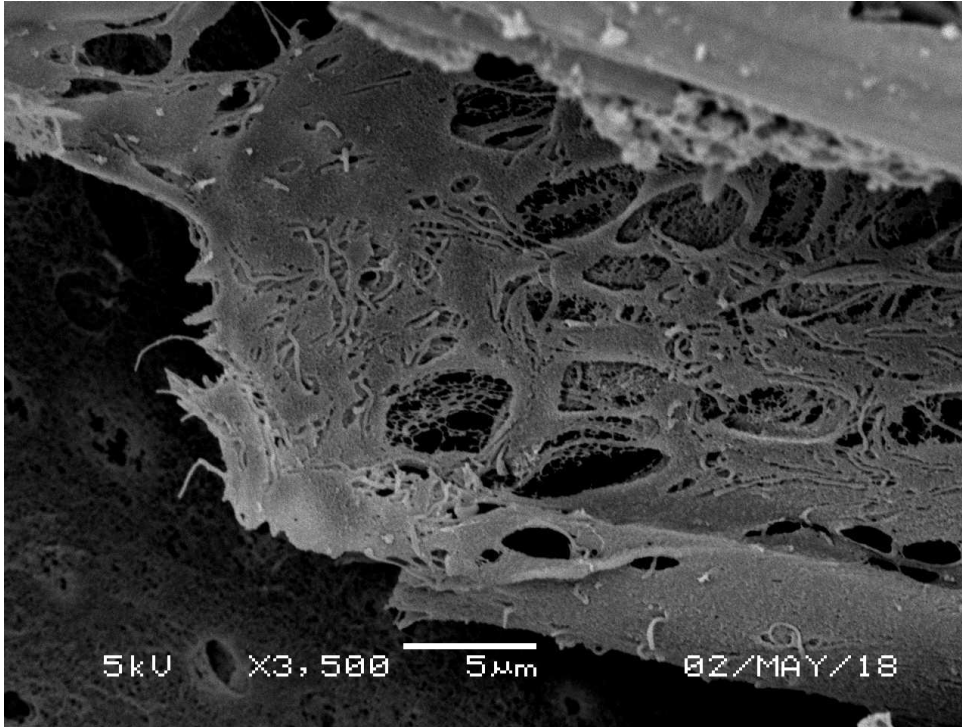


Figure 14. The above image is a close-up image of Figure 10. Image captured at 3500X magnification, with the voltage calibrated to 5 and spot size of 40. The Z distance and working distance were set to 20, and working distance autofocused to 12 mm. Image was calibrated with auto contrast and brightness and autofocus to capture this final image.

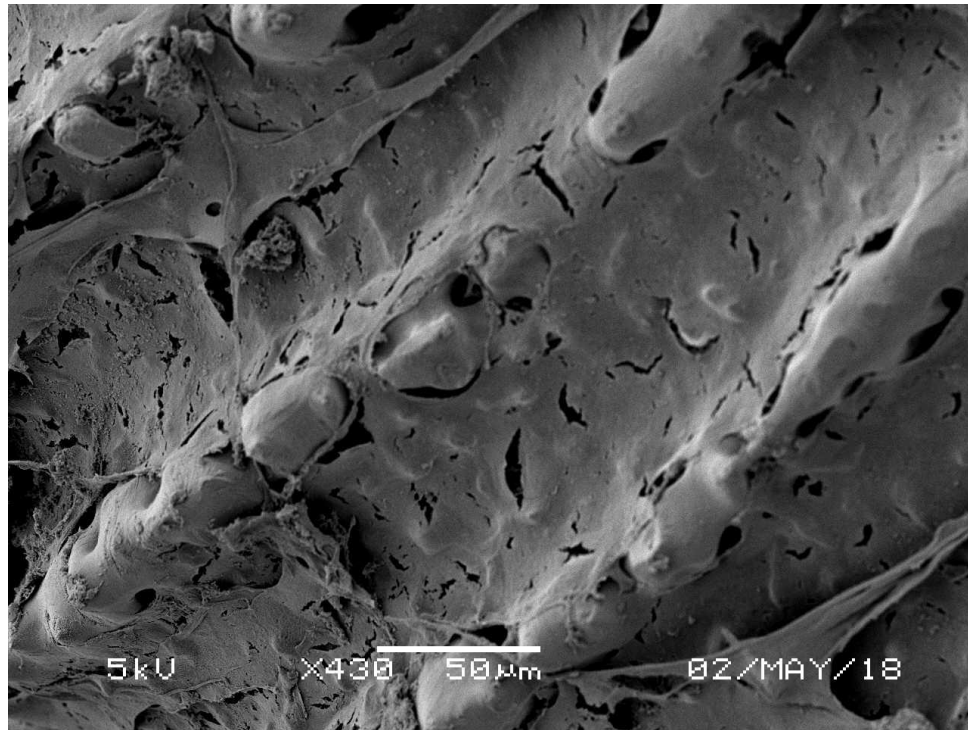


Figure 15. The above image is a closer look at the ridges in the spine of sample 1. Image captured at 430 magnification, with the voltage calibrated to 5 and spot size of 43. The Z distance and working distance were set to 20, however, the autofocus function automatically reset the working distance to 12 mm and this was accepted as the working distance for this micrograph. Image was captured by manually blacking out the contrast and brightness then the brightness was increased until a gray screen was barely visible. Contrast was increased until fine features could be visualized, then focus was adjusted to capture this final image.

The features shown in Figure 16 are replicated in different sponge-like regions throughout Sample 1. They consist of web-like tendrils connected to a center and spread out across the surface. These were mostly found on the nodes and the sponge-like matter within Sample 1. They appear to be features either attached to the surface or protruding from it. It is unclear what they are or if they are even *P. ochraceus* tissue.



Figure 16. Image captured at 7500X magnification, with the voltage calibrated to 5 and spot size of 39. The Z distance was calibrated to 20 and the working distance autofocused to 11 mm. Image was captured by manually blacking out the contrast and brightness then the brightness was increased until a gray screen was just observable. Contrast was increased until fine features could be visualized.

The final three images, Figure 17, Figure 18, and Figure 19 are close ups of a sponge-like region captured with increasing magnifications of 13,000X, 70,000X and 300,000X respectively. Increasing the magnification, decreases the crispness of the images so that less and less fine detail is resolvable. The final image Figure 19, is the most important for this research project. It was taken at the highest magnification the SEM could achieve. A couple items are important to note, firstly the visibility of the image's contents is not at all sharp enough to resolve fine viral material let alone with proper accuracy. Next, the maximum measurement the SEM scale bar is set to at 300,000X magnifications is 50 nanometers. The dengue virus measures at 20-25 nanometers (Hewson et al. 2014), half the size of the scale bar shown in Figure 16. The

SEM is both challenged in its ability to produce crisp and clear images at very high magnification necessary to identify dengue virus. This particular model of SEM at Evergreen cannot also zoom in far enough to see the incredibly small size of dengue virus. Therefore, this project concludes that the SEM model at Evergreen appears to be insufficient for detecting dengue virus in *P. ochraceus* due to the smallness of virus's size.

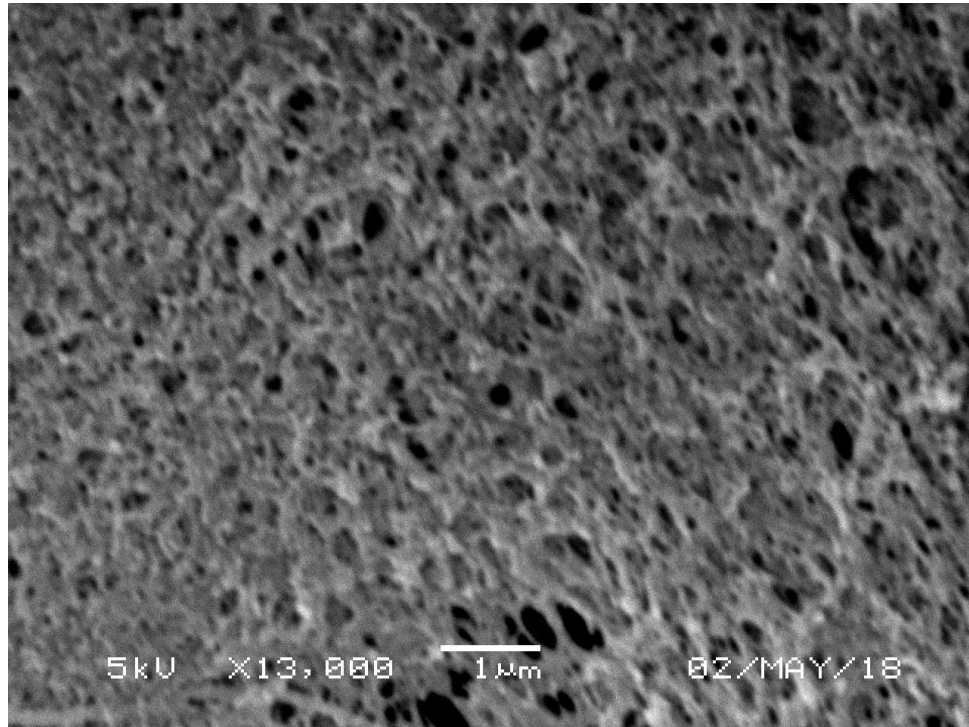


Figure 17. Image captured at 13,000X magnification, with the voltage calibrated to 5 and spot size of 38. The Z distance was adjusted to 20 and the working distance autofocused to 12 mm. Image was captured by manually blacking out the contrast and brightness then the brightness was increased until a gray screen was just visible Contrast was increased until fine features could be pictured.

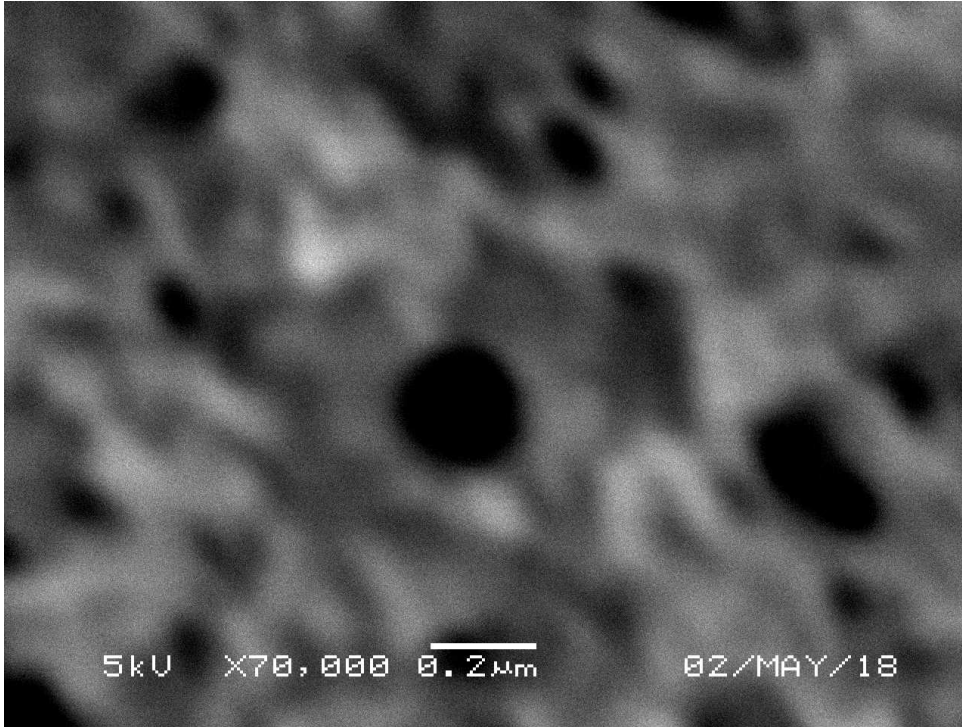


Figure 18. The above image is a close up of Figure 14. Image captured at 13,000X magnification, with the voltage calibrated to 5 and spot size of 37. The Z distance was calibrated to 20 and the working distance autofocused to 20 mm. Image was captured by manually blacking out the contrast and brightness then the brightness was increased until a gray screen was just observable. Contrast was increased until fine features could be visualized.

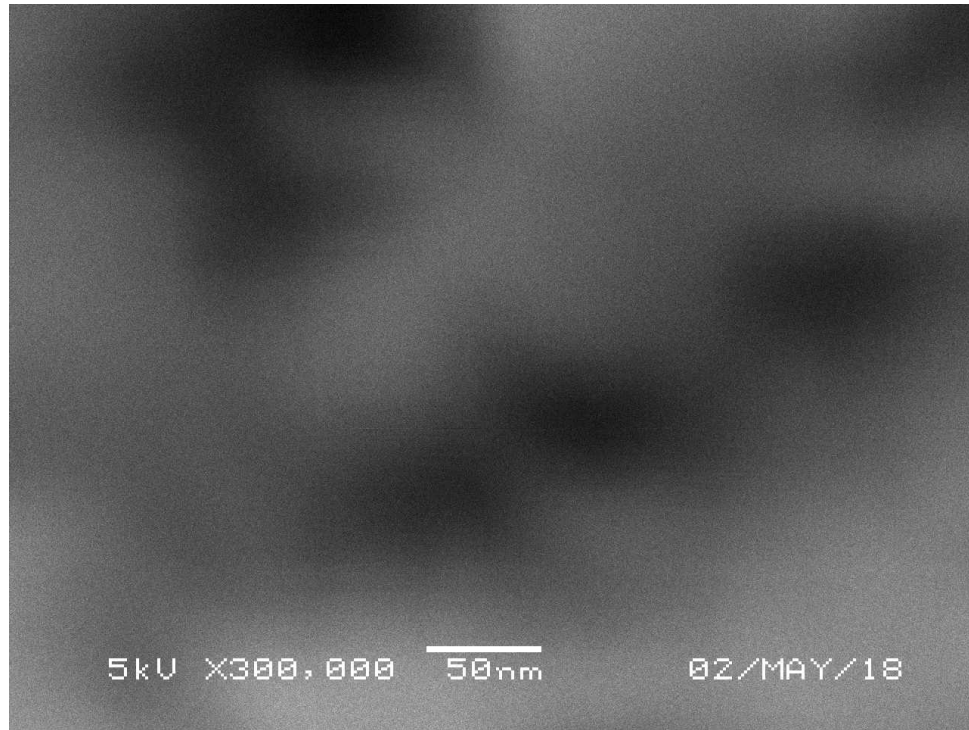


Figure 19. The above image is a close up of Figure 15. Image captured at 300,000X magnification, with the voltage calibrated to 5 and spot size of 34. The Z distance was adjusted to 20 and the working distance to 20 mm. Image was captured by manually blacking out the contrast and brightness then the brightness was increased until a gray screen was just observable. Contrast was increased until fine features could be visualized. This procedure was performed 3 times for this image until the best contrast and brightness was present. Focus was calibrated manually using fine adjustment tool until the above image was resolved.

Sample 2

The first image of Sample 2 is a full view which showcases the variety of features present on the sample (Figure 20). Sample 2 was removed from the top of an adult *P. ochraceus* arm using an 8 mm punch biopsy. The sample is mounted on a carbon disk atop a 10 mm SEM sample stud whose pock-like marks can be seen around the outside of the sample. Figures 21 and 22 are magnified views of the *P. ochraceus* spine, which is located in the middle, at the top of Figure 20. Figure 21 captures clear views of the nodes present in this sample, to the left of the spine; a characteristic that was also seen in

Sample 1.

Sample 2 was also particularly challenging to capture images of, even at lower magnifications. This sample was most challenging when trying to adjust for brightness and contrast. The contrast would be too bright and the brightness would cause the sample to wash out so that no fine features could be visualized. These images of Sample 2 were therefore captured at very low brightness and moderate contrast. These challenges also made it difficult to obtain a sharp focus. It was better overall to adjust the spot size to a higher range to smooth out the surfaces, which made it easier for the SEM to achieve a quality focus on the sample.

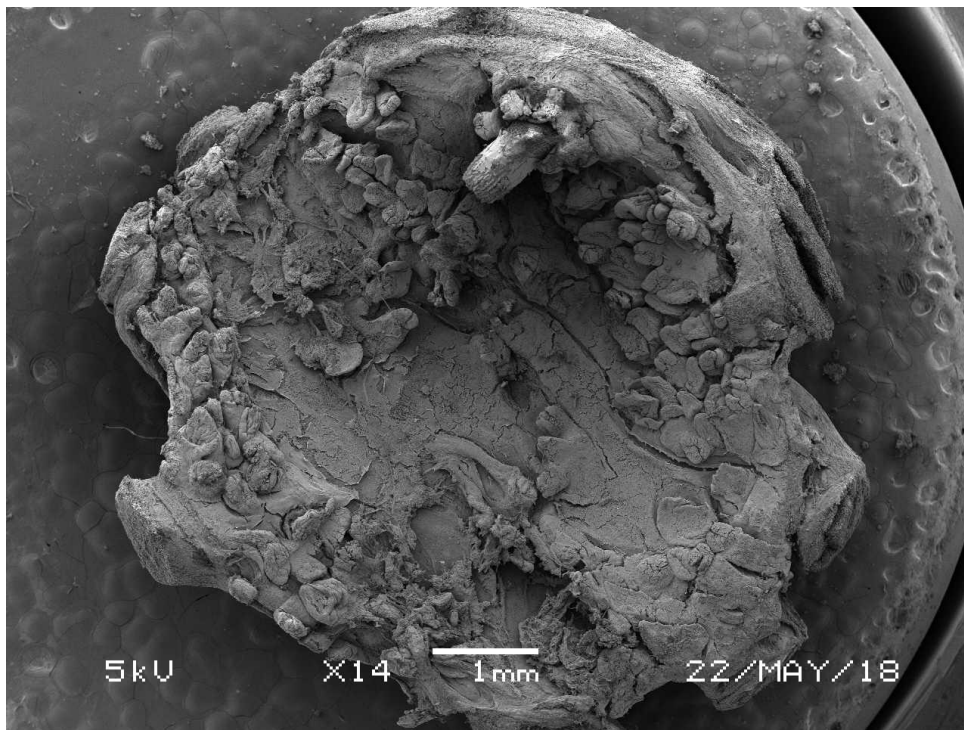


Figure 20. The above image is from diseased *P. ochraceus* tissue. This is a large view image of Sample 2. Image captured at 14 magnification, with the voltage calibrated to 5 and spot size of 45. The Z distance was adjusted to 20 and the working distance to 36 mm.

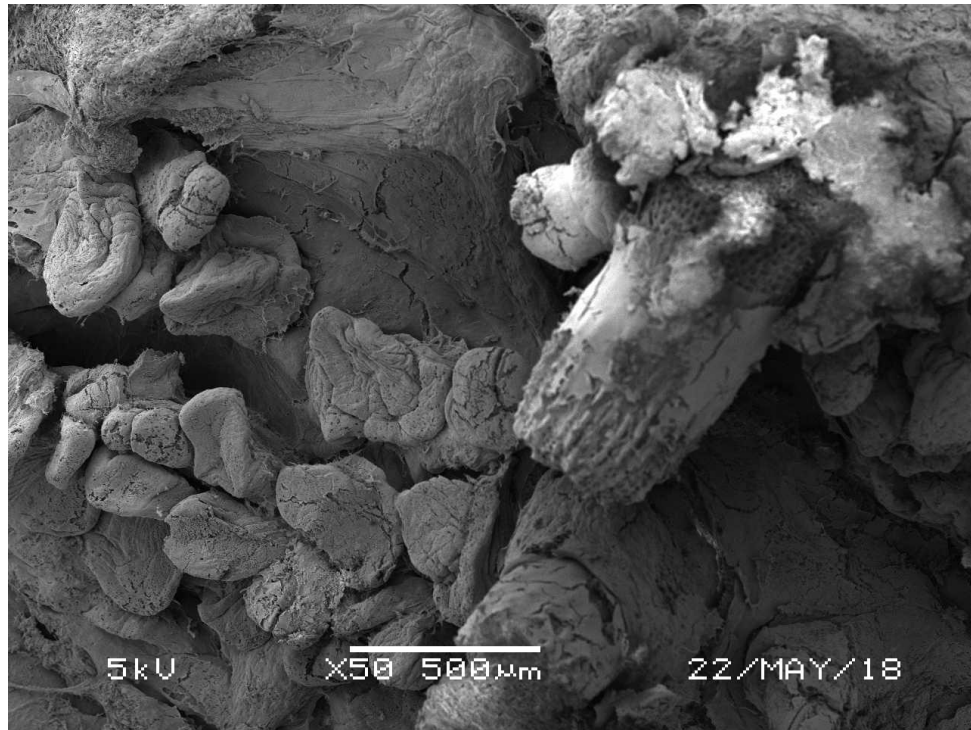


Figure 21. The above image is a close up of a spine in Sample 2, pictured at the top of Figure 17. Image captured at 50 magnification, with the voltage calibrated to 5 and spot size of 43. The Z distance was adjusted to 20 and the working distance to 18 mm.

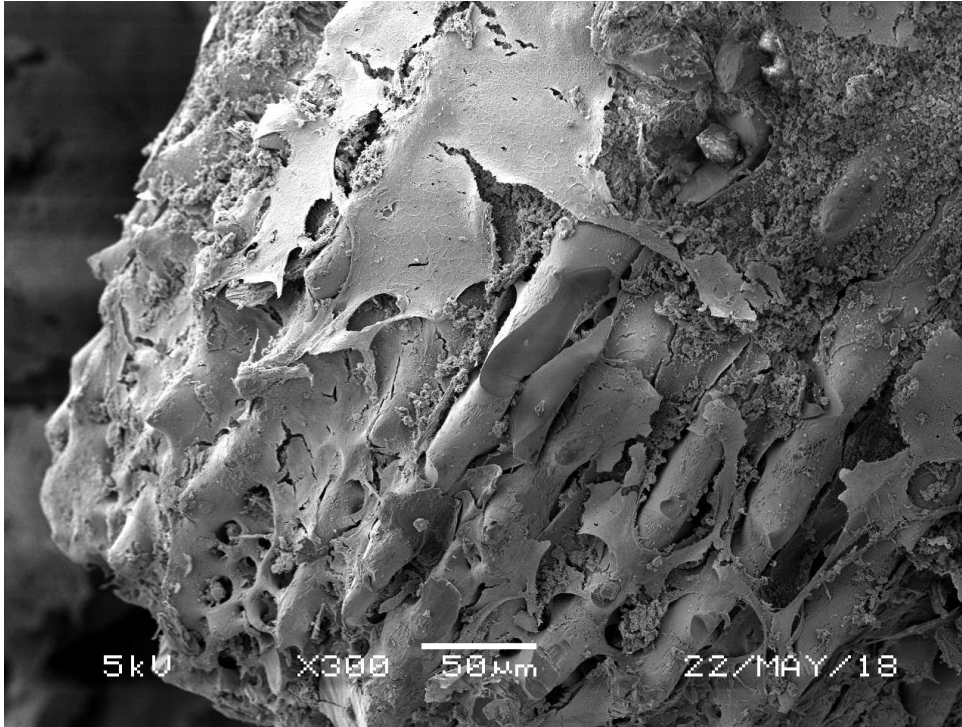


Figure 22. The above image is an even closer look at the spine of Sample 2. Image was captured at 300X magnification, with the voltage calibrated to 5 and spot size of 43. The Z distance was adjusted to 20 and the working distance to 18 mm.

The features present in Figures 23 and 24 illustrate more familiar sample characteristics. On the surface are cracks and fissures from the SEM sample preparation drying process. In Figure 24 the same porosity observed in Sample 1 can also be visualized in this image. The final image captured of Sample 2 (Figure 25), was the highest magnification The Evergreen State College SEM was capable of achieving. This image is a highly magnified region of the features on Figure 24. The white region in the middle of the sample is tissue and the dark regions around it are the cracks which can be seen Figure 24. This image at 300,000X magnification was not captured at as high a quality resolution as Figure 19, but illustrates the limitations of the imaging at such a high magnification.

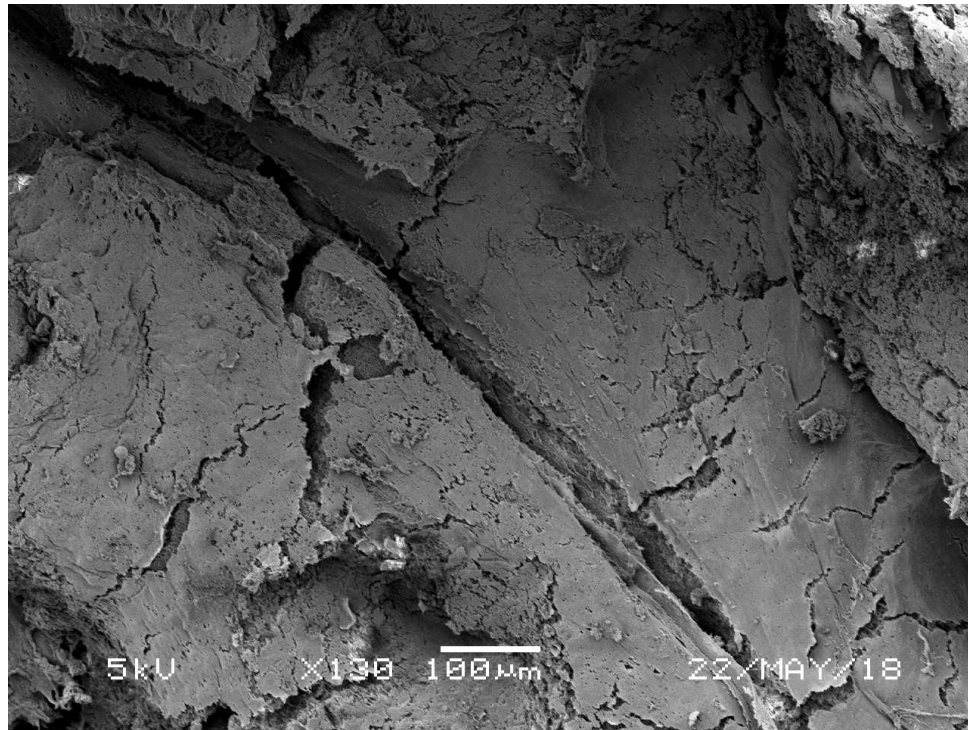


Figure 23. This is an image taken from Sample 2. Image captured at 130 magnification, with the voltage calibrated to 5 and spot size of 45. The Z distance was adjusted to 20 and the working distance to 36 mm.

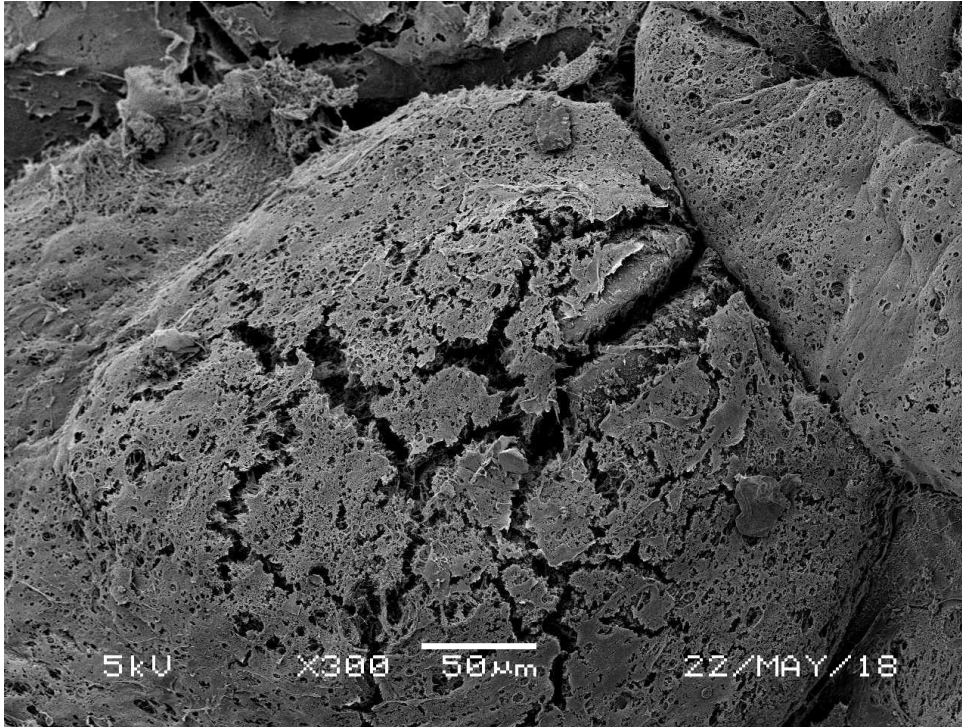


Figure 24. Image captured at 300X magnification, with the voltage calibrated to 5 and spot size of 38. The Z distance was adjusted to 20 and the working distance to 18 mm.

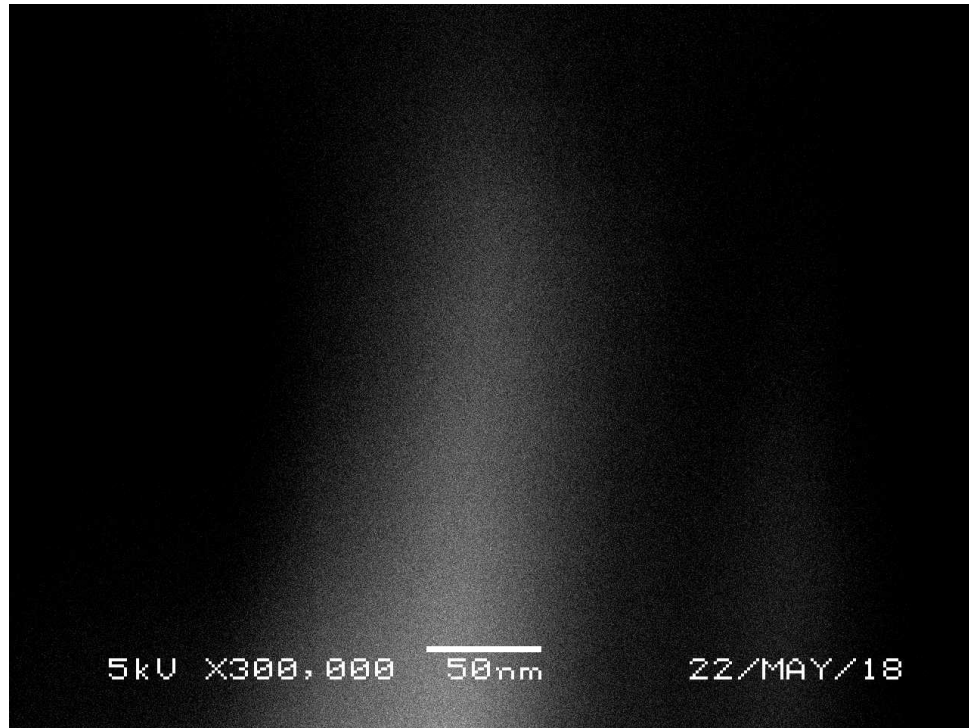


Figure 25. The above image demonstrates the SEM at maximum magnification for Sample 2. Image captured at 300,000X magnification, with the voltage calibrated to 5 and spot size of 28. The Z distance was adjusted to 20 and the working distance to 18 mm.

Sample 3

Sample 3 was taken from the top of an adult *P. ochraceus* arm. Figure 26 is the widest view captured of this sample, in large part because the machine was already calibrated to a Z distance of 20. This was the widest view that could be achieved by the machine at this distance and captures the overall topography of the sample very well. In Figures 26 and 27, the nodes in the *P. ochraceus* tissue are easily observed, however, the nodes appear less well-defined than those in Samples 1 and 2. This may be due to damage to the sample either during the drying process or in transit from the field to the lab. This may also simply be differences in sample features between organisms.

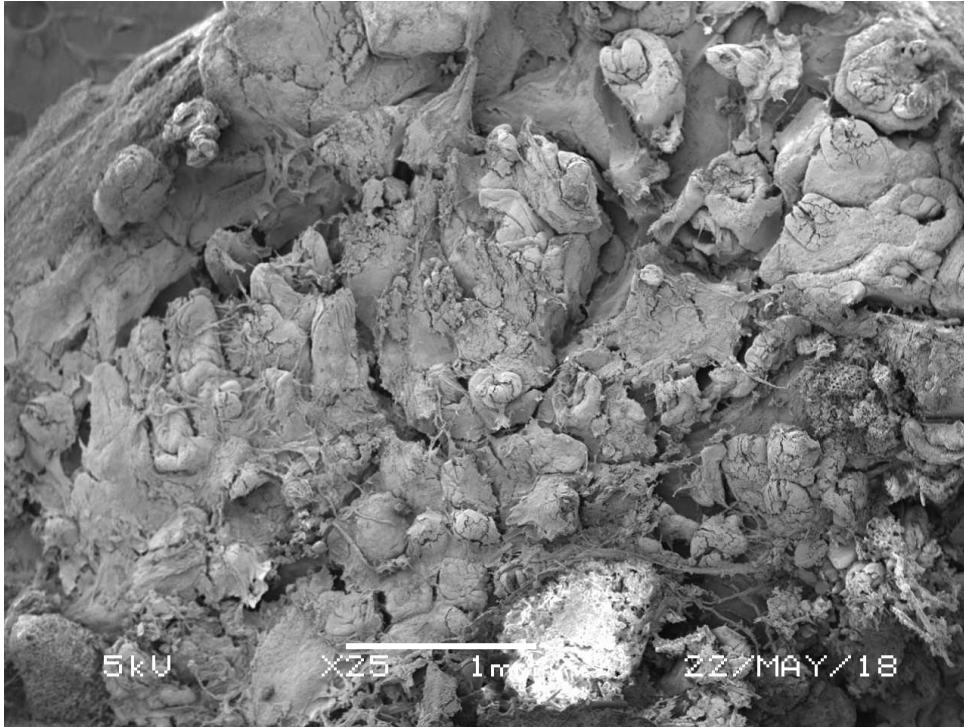


Figure 26. The above image is a wide-view picture of Sample 3. Image captured at 25 magnification, with the voltage calibrated to 5 and spot size of 50. The Z distance was adjusted to 20 and the working distance to 17 mm.

Figure 27 is a magnified image of a region in the left of Figure 26. It illustrates some of the unique webbing present on many tissue sample images, where the web-like structures appear to lie on top of the nodes and stretch out between them. It is unclear if this webbing is a part of the *P. ochraceus* tissue or if it is an anomalous characteristic present on the samples. Sample 3 definitely carries the largest quantity of the web-like matter of all samples scanned under SEM.

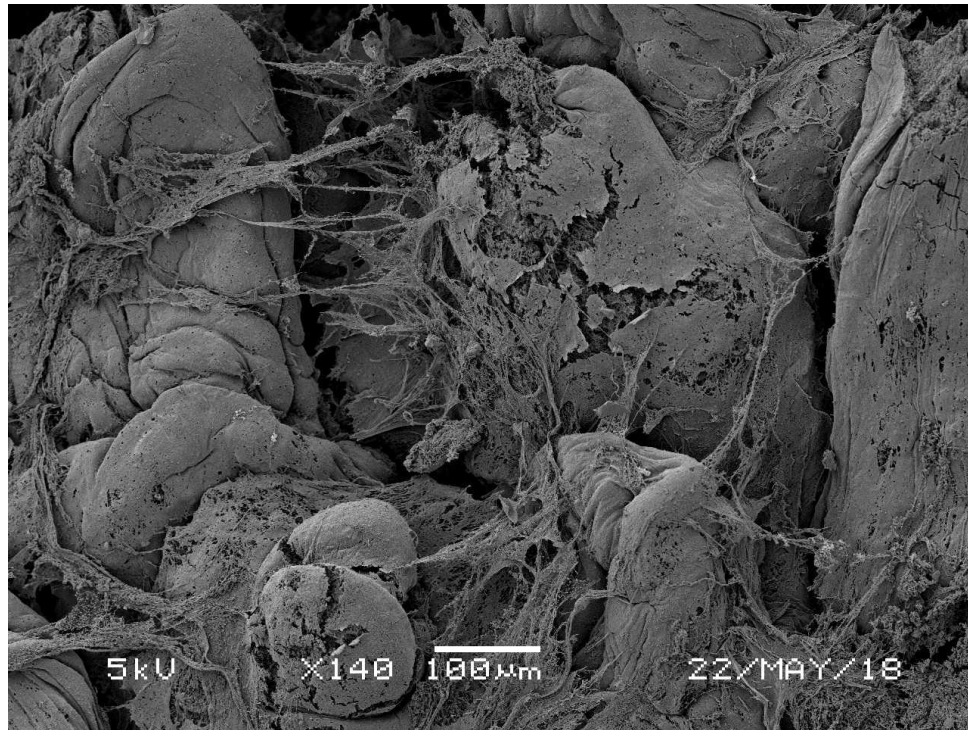


Figure 27. Image captured at 140 magnification, with the voltage calibrated to 5 and spot size of 34. The Z distance was adjusted to 20 and the working distance to 18 mm.

The third image, Figure 28, is a close up of a central region pictured in Figure 27. It is scaled at 160,000X magnification and was calibrated to have very high contrast. This image demonstrates the challenges with achieving a quality image at this scale range. This image was useful in visualizing the tissue with the highest contrast before approaching the final image, Figure 29, at 300,000X magnification. In Figure 29, the white space on the right is *P. ochraceus* tissue and the dark space on the left is a gap around the tissue from the central region of Figure 27. Of the images taken at 300,000X magnification, Figure 29 is the poorest quality and resolution, however, it is the best high magnification image captured for Sample 3.

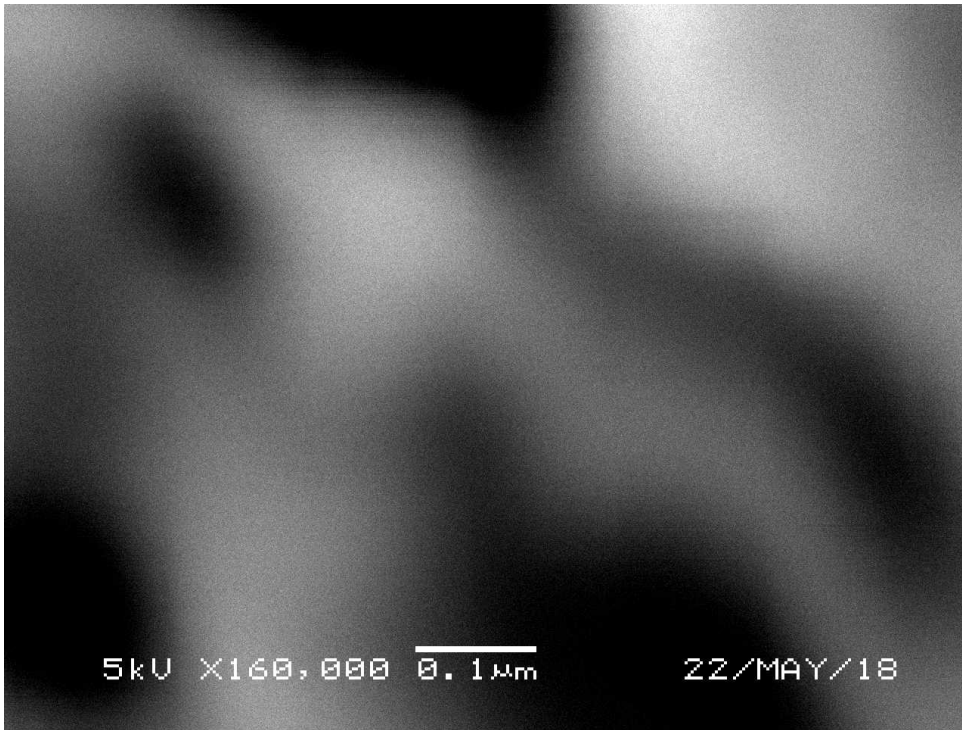


Figure 28. Image captured at 160,000X magnification, with the voltage calibrated to 5 and spot size of 40. The Z distance was adjusted to 20 and the working distance to 18 mm.

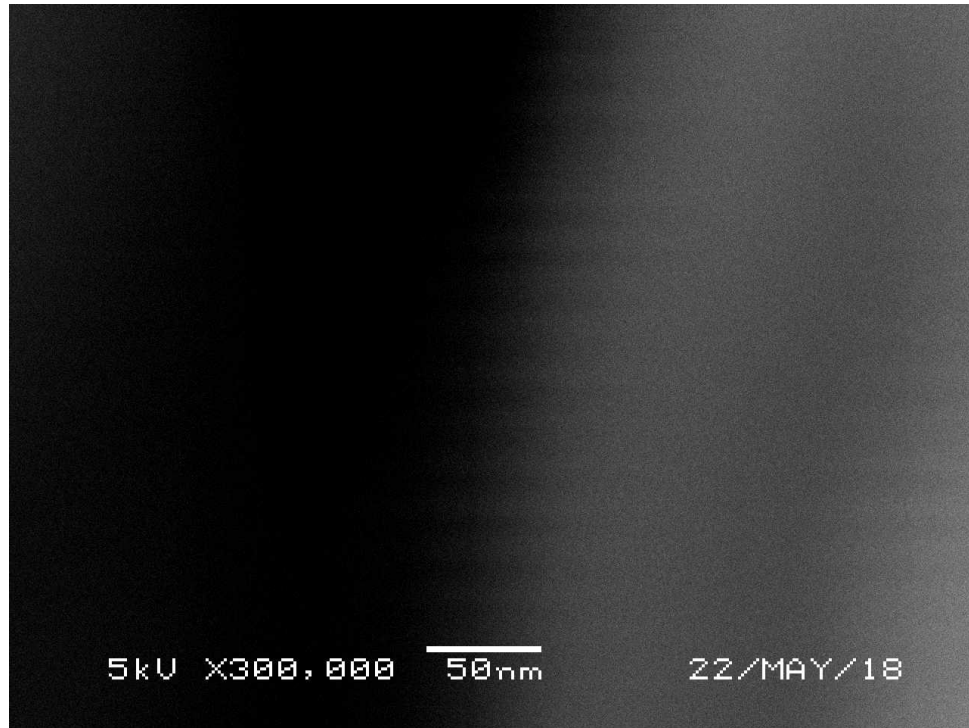


Figure 29. The above image is sample 3 under the SEM at maximum magnification. Image captured at 300,000X magnification, with the voltage calibrated to 5 and spot size of 35. The Z distance was adjusted to 20 and the working distance to 18 mm.

Sample 3.5

A second tissue sample was taken from the third *P. ochraceus* sampled for this project and is thus called Sample 3.5. The tissue was removed not from the wasted region at the top like Sample 3, but from the underside of the organism. An 8 mm punch biopsy was removed from the tube feet of the third *P. ochraceus*; these tube feet were not yet necrotic and still appeared to possess mobility. Figure 30 is a wide-view of Sample 3.5. The tube feet protrude from the base of the sample and curve at an angle, down and to the left. Half of the tube feet are mostly in-tact from the top to the tube feet pictured in the middle in the left. On the right, the tube feet have been slightly damaged either from the punch biopsy, transportation to the lab or during sample preparation.

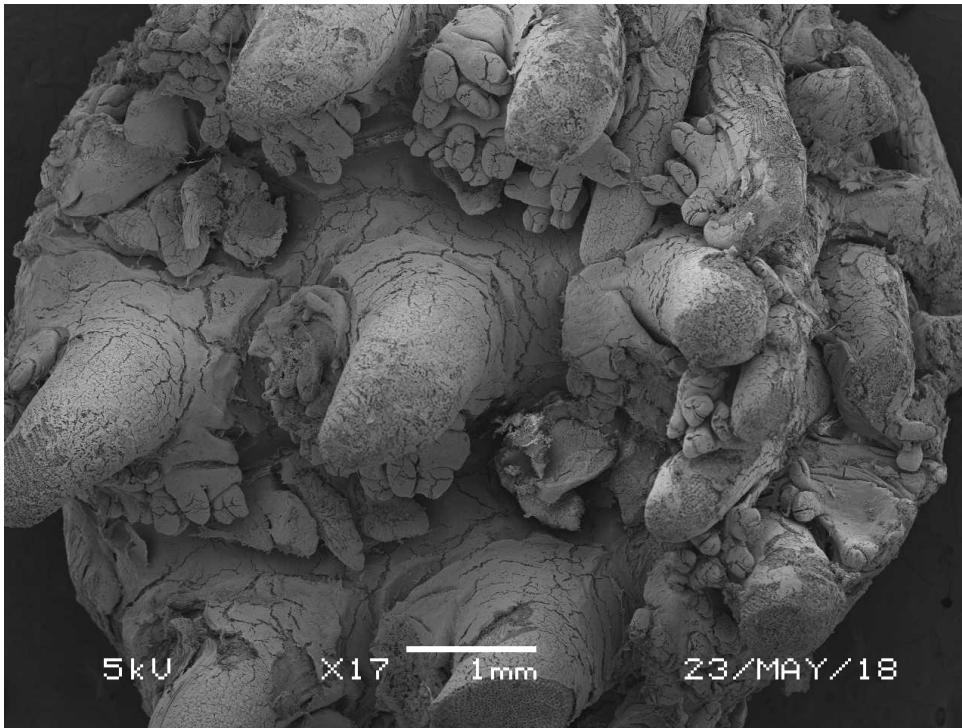


Figure 30. This figure is representative of a second sample taken from the underside of the third *P. ochraceus* sampled for this research. Pictured are the desiccated tube feet from a diseased individual. Image captured at 17 magnification, with the voltage calibrated to 5 and spot size of 45. The Z distance was adjusted to 20 and the working distance to 36 mm.

The nodes which have been visible in Samples 1, 2, and 3, are also present around the base of the tube feet but with longer shape variations. Figure 31 is a closer view of the tube foot at the bottom of Figure 30. This tube foot is interesting because it was sliced in half during biopsy and illustrates a dissected *P. ochraceus* tube foot. The center of this feature appears to have a sponge-like quality a mass of connective tissues riddled with small holes.

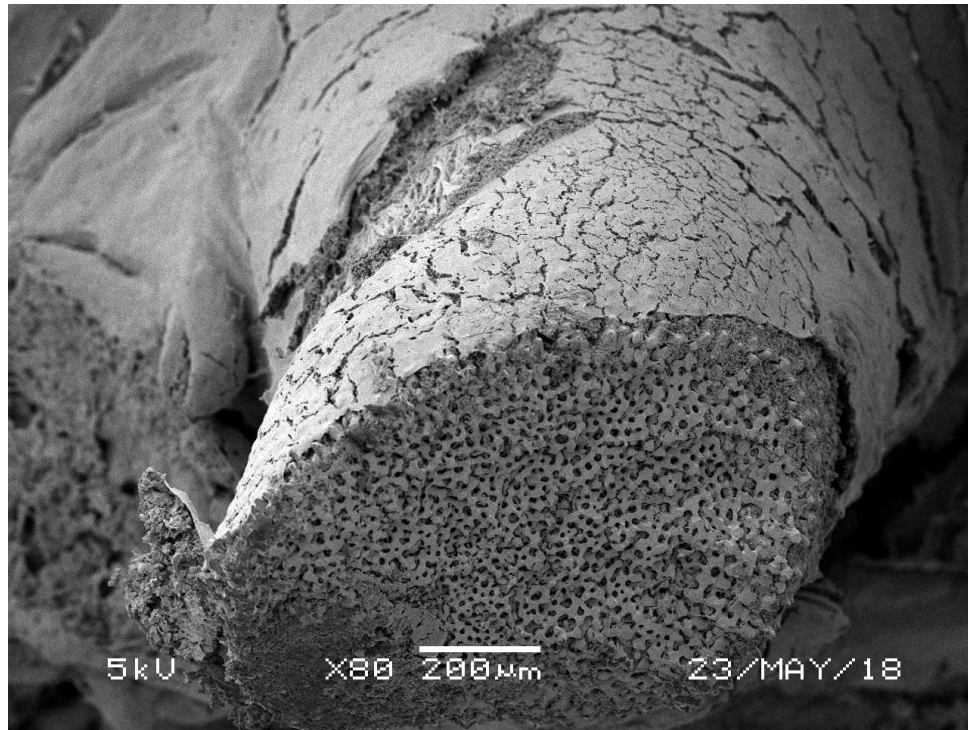


Figure 31. This micrograph demonstrates a tube foot of Sample 3.5 which has been sliced in half. Image captured at 80 magnification, with the voltage calibrated to 5 and spot size of 32. The Z distance was adjusted to 20 and the working distance to 16 mm.

The external texture of the *P. ochraceus* tube feet are evident in Figures 31 and 32. The outside, resembles desert cracks with pieces of the tissue almost lifting off of the surface in a flaking or peeling manner. Figure 33 is a close-up view of tissue between two tube feet imaged in the upper right corner of Figure 30. These features resemble the nodes present in Samples 1-3. However, they appear elongated with a symmetrical arrangement around a center which is not seen in this image but looks to begin at the base of the tube feet.

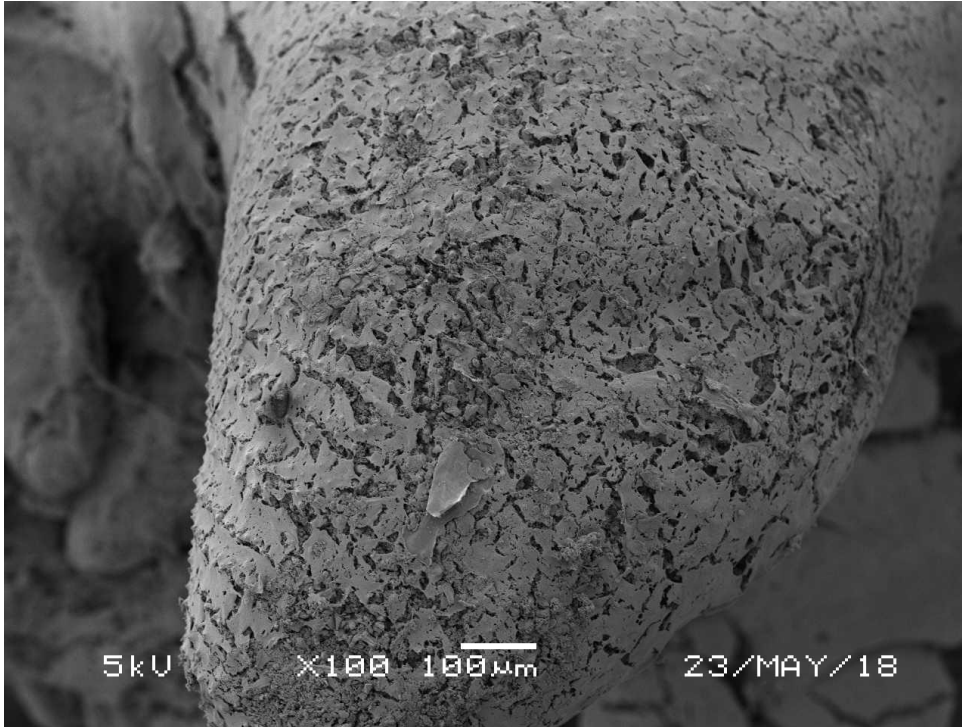


Figure 32. The above image is an intact but desiccated tube foot. Image captured at 100X magnification, with the voltage calibrated to 5 and spot size of 32. The Z distance was adjusted to 20 and the working distance to 18 mm.

A close-up view of Figure 32 can be seen in Figures 34 and 35, where the region in the bottom center of Figure 32 is magnified to reveal the nature of the white matter protruding between the tube feet. Upon closer inspection, the white material in Figure 34, appears to be tattered or shredded looking matter lying on top of the tissue. Within this tattered material, are small rounded ovals pictured in Figure 35. These rounded features do not appear anywhere but the tattered material and give the impression like they're nested within it.

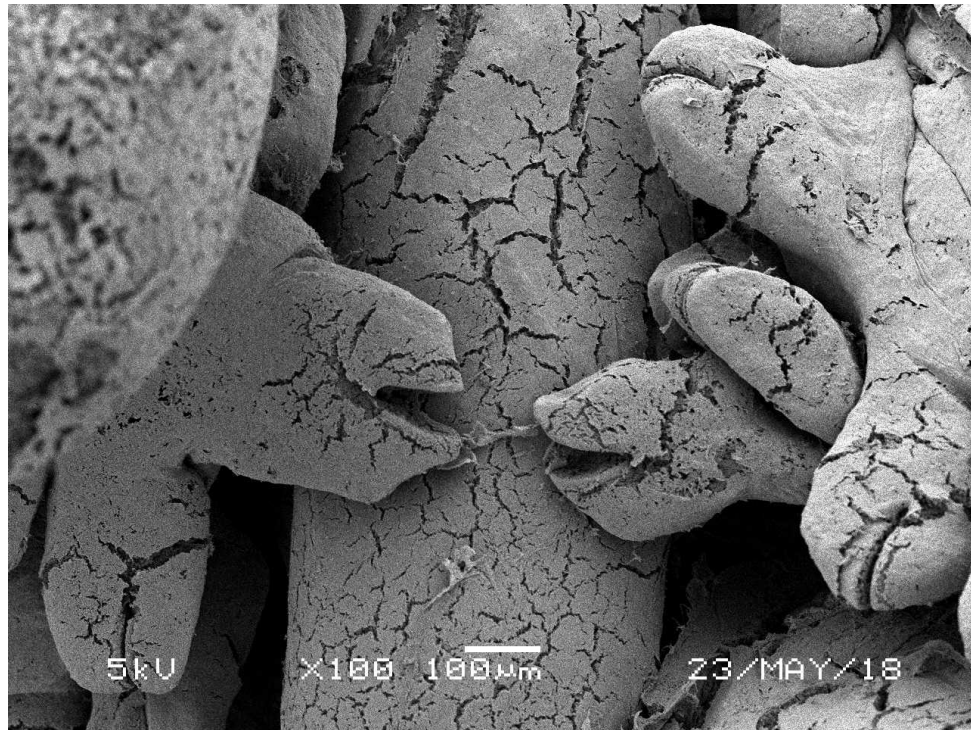


Figure 33. This image is a close up of a region between two tube feet. Image captured at 100X magnification, with the voltage calibrated to 5 and spot size of 18. The Z distance was adjusted to 20 and the working distance to 16 mm.

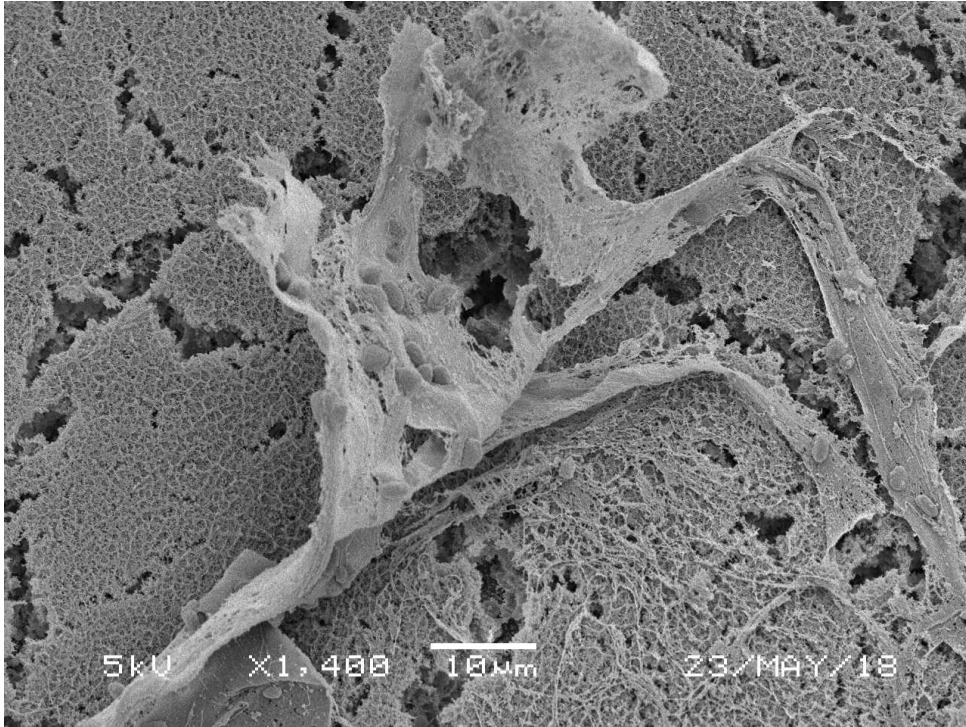


Figure 34. Pictured above is a region of the tube feet. Image captured at 1,400X magnification, with the voltage calibrated to 5 and spot size of 28. The Z distance was adjusted to 20 and the working distance to 15 mm.

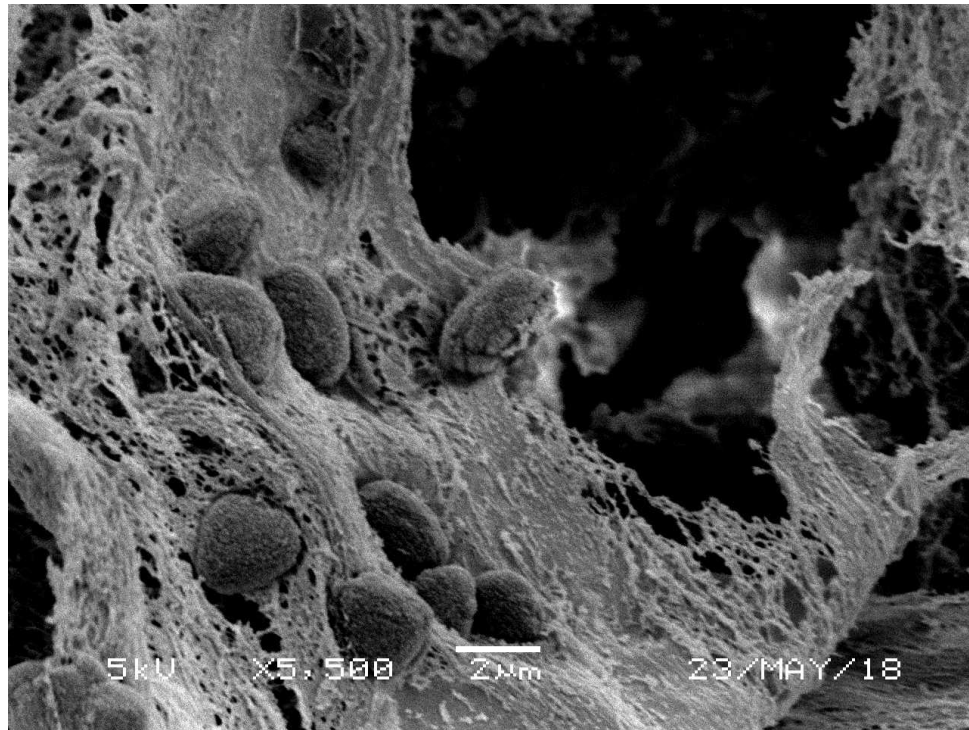


Figure 35. This picture is a close up of the central region of Figure 31. The rounded, oval shapes are characteristically similar in size and feature to bacteria. This image depicts the only example of bacteria-like structures present on any of the samples imaged for this project. However, their legitimacy as bacteria cannot be confirmed without genetic tests. Image captured at 5,500X magnification, with the voltage calibrated to 5 and spot size of 28. The Z distance was adjusted to 20 and the working distance to 16 mm.

The final image of Sample 3.5 (Figure 36) is a high magnification view of Figure 35. The light, white regions are the *P. ochraceus* tissue and the dark regions are the spaces and gaps between the sample. This image is one of the better images captured at 300,000X magnification because it is at least able to resolve some of the variability and shapes in the tissue. This image was challenging to resolve because Sample 3.5 experienced points of high light which is best illustrated in Figure 35 behind the tattered materials and the right-most oval where the light is particularly bright. This is due in large part to SEM electron scatter and the microscope was challenged by its ability to hone in on a region and remain still. The scatter shifted the background of Figures 35 and

36 quite a lot and so capturing these photos involved a great deal of image tinkering and fine adjustment to the wobbler to reduce some of this image shifting.

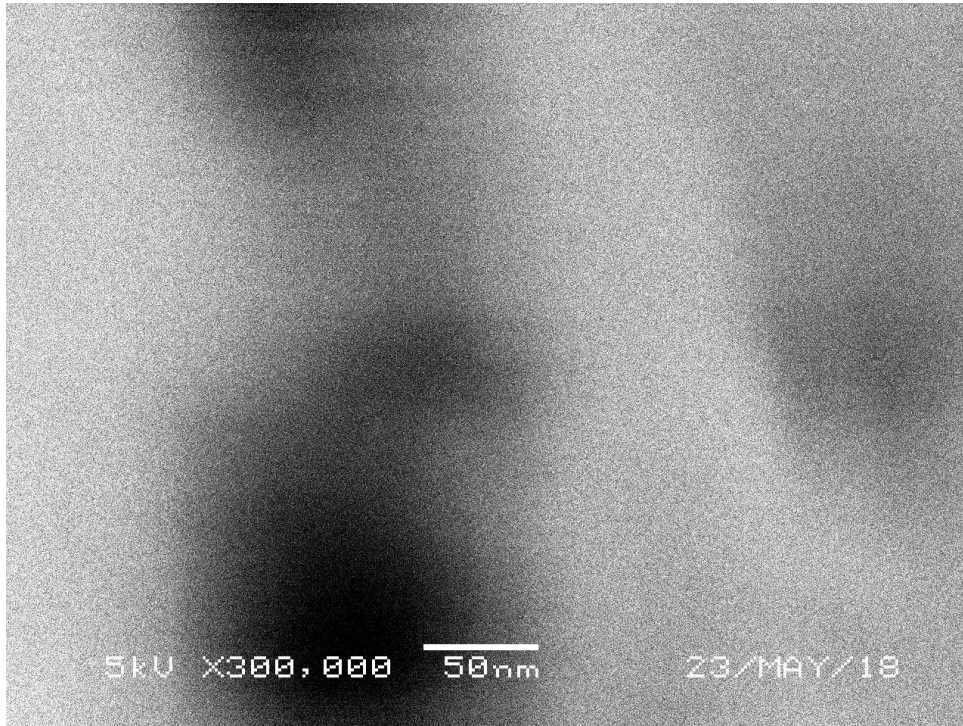


Figure 36. This micrograph is an image of Sample 3.5 at the SEM's highest magnification. Image captured at 300,000X magnification, with the voltage calibrated to 5 and spot size of 10. The Z distance was adjusted to 20 and the working distance to 16 mm.

Sample 4

The first image of Sample 4 (Figure 37) is a wide-view of the fourth *P. ochraceus* sampled for this project. The tissue removed for this sample was necrotic and taken from the top of an adult sea star arm. In the top left region of Figure 37, is another large, rounded spine. Around the spine are more of the nodes which have been seen in the previous samples. The nodes in Sample 4 do not appear to be as pronounced or abundant as those seen in Samples 1, 2, and 3, but are instead spread out across the sample, being flat in topography.

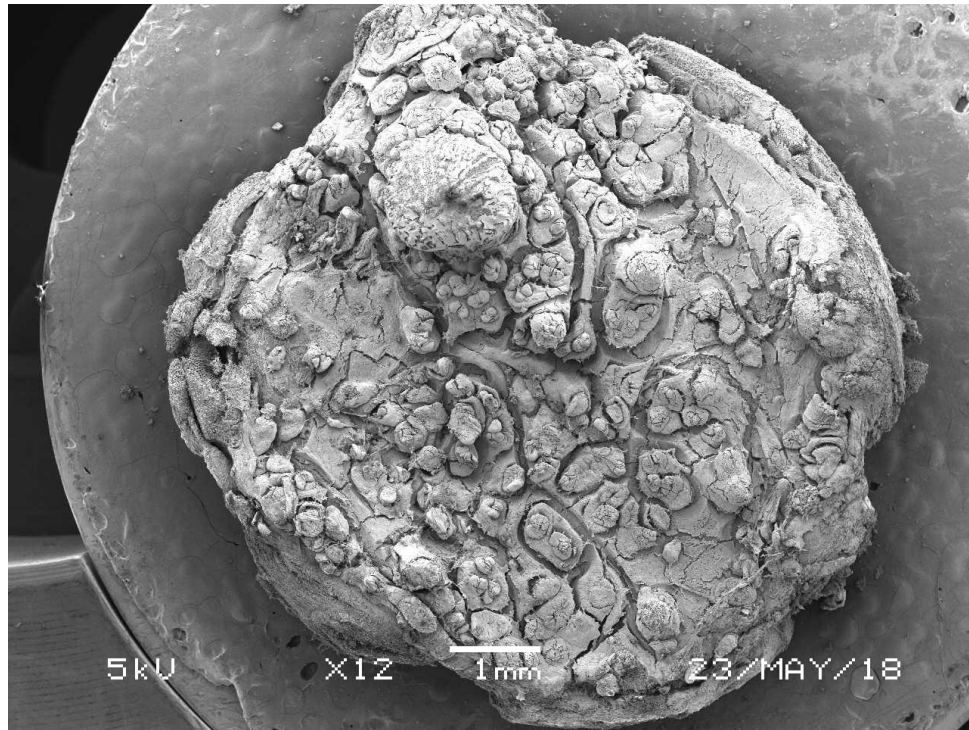


Figure 37. This image is a wide-view of Sample 4. Image captured at 12 magnification, with the voltage calibrated to 5 and spot size of 45. The Z distance was adjusted to 40 and the working distance to 49 mm.

Figure 38 is a closer view of a bottom right protrusion in Figure 37. It seems to be either another rounded protruding feature different than the spines, or may be the early stage of a spine growing from the tissue. To understand this structure, another image was taken of a magnified region of Figure 38 to observe the smaller spines on top of the sample. Figure 39 shows a smaller protrusion rising up from the tissue, ending in a fine point. It may be that this is a microscopic spine on top of an early forming spine. The texture of the spines appear to be porous and cracking, similar to the previous samples observed.

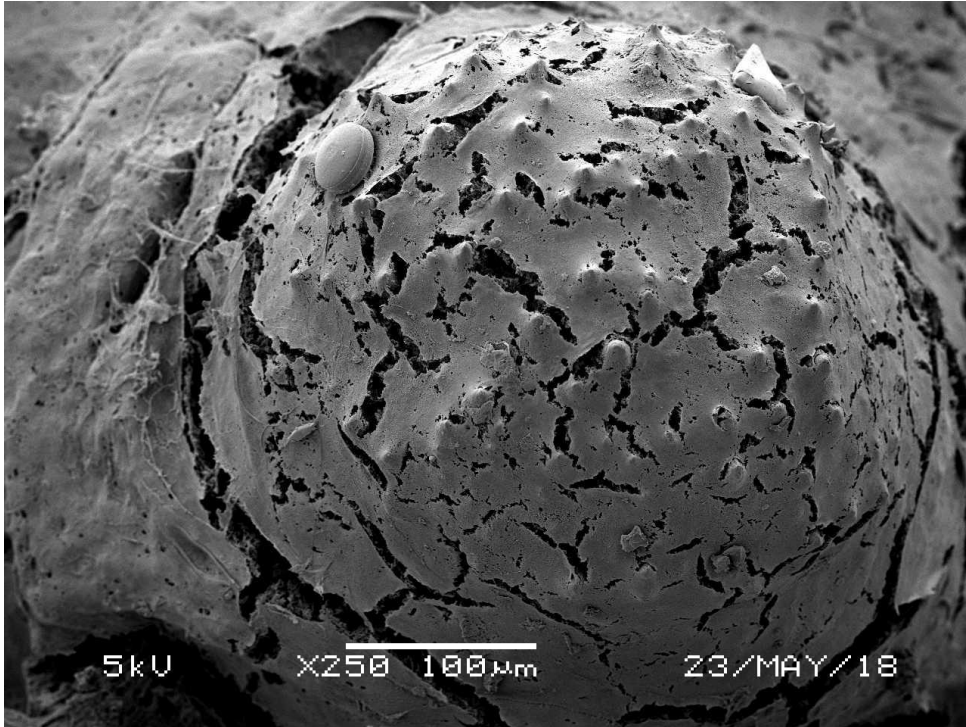


Figure 38. Image captured at 50X magnification, with the voltage calibrated to 5 and spot size of 45. The Z distance was adjusted to 20 and the working distance to 17 mm.

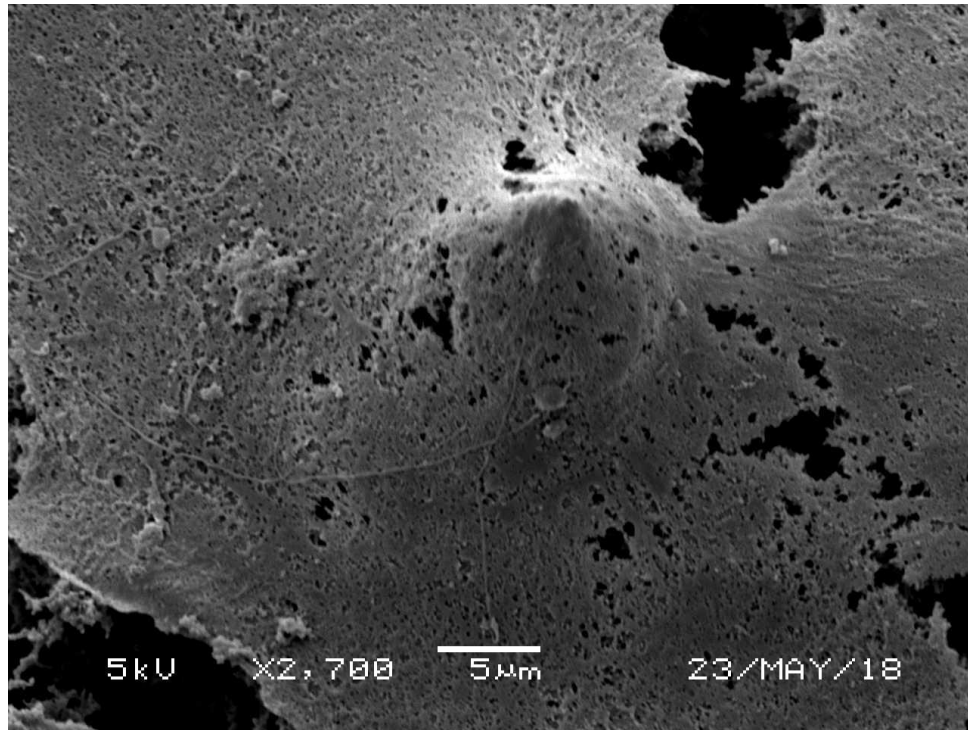


Figure 39. The above image is a close-up of a small spine on Figure 35. Image captured at 2,700X magnification, with the voltage calibrated to 5 and spot size of 45. The Z distance was adjusted to 20 and the working distance to 18 mm.

The final image (Figure 40) is a micrograph of Sample 4 at the highest magnification the SEM is capable of achieving, 300,000X magnification. This image has a smoother texture, especially when compared to Figure 36 because the spot size to capture this image was calibrated to 39. This smooths out the sample features and makes the image appear less grainy. This image further reinforces the challenges with resolving *P. ochraceus* tissue and viral material that may be present, at high magnifications with the SEM.

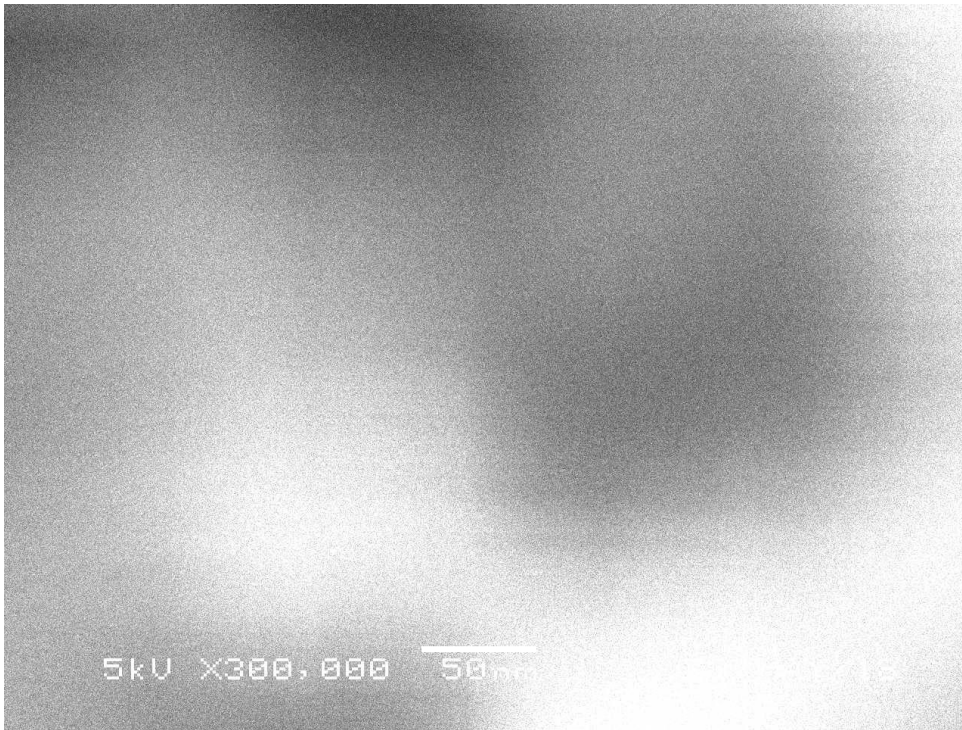


Figure 40. This micrograph demonstrates Sample 4 at the highest magnification achievable by the SEM. Image captured at 300,000X magnification, with the voltage calibrated to 5 and spot size of 39. The Z distance was adjusted to 20 and the working distance to 19 mm.

Sample 4.5

Sample 4.5 was taken from the same organism as Sample 4. The tissue was removed from the underside of an adult *P. ochraceus*, capturing tube feet of the sea star. The tissue on the underside of the *P. ochraceus* did not exhibit signs of wasting disease at the time of removal. The tube feet appear arranged in a similar fashion to those in Sample 3.5. The tissue in Figure 41 appears to have sustained slightly more damage either during biopsy, in transit or through sample preparation than Sample 3.5. The light spaces visible in Figure 41 are potentially a product of the SEM's poor temperament during imaging. A closer view of the tube feet is visible in Figure 42. The same porosity and cracking present in Sample 3.5 is also present in this image, though these tube feet to appear to have fewer smooth surfaces.

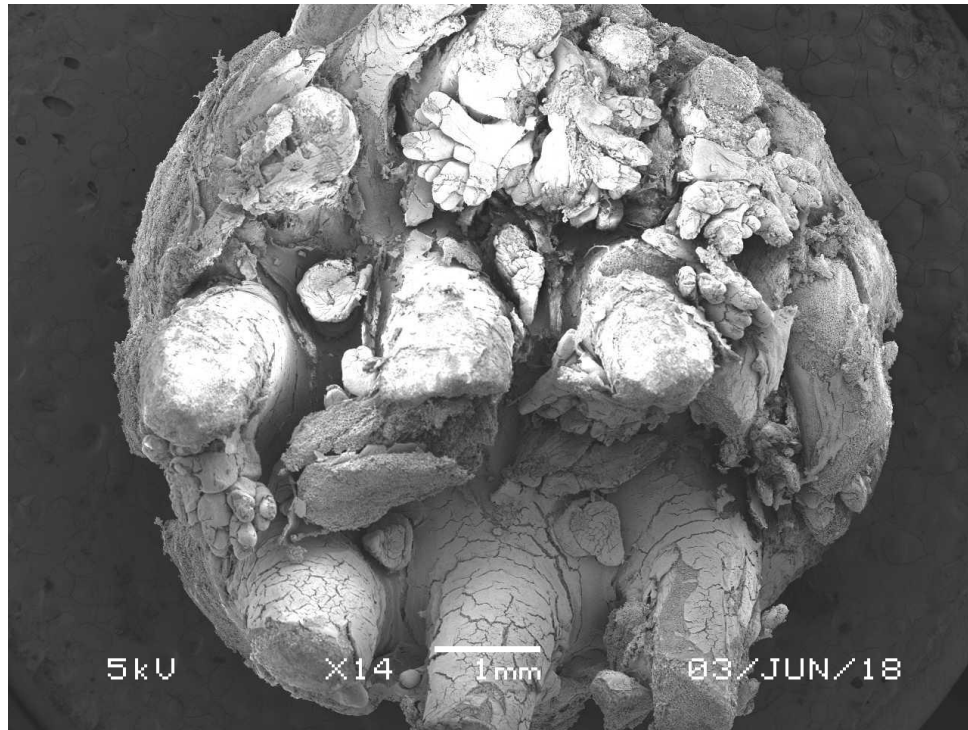


Figure 41. The above image is a wide-view of Sample 4.5. Image captured at 14X magnification, with the voltage calibrated to 5 and spot size of 45. The Z distance was adjusted to 20 and the working distance to 45 mm.

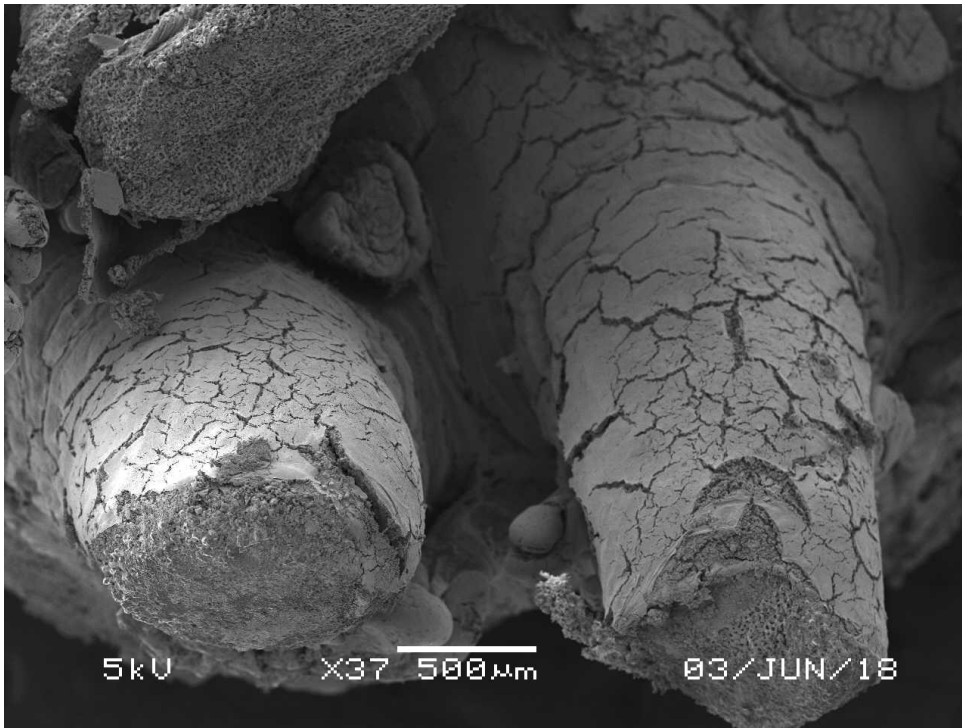


Figure 42. The above image is a close-up of tube feet imaged in Figure 41. Image captured at 37X magnification, with the voltage calibrated to 5 and spot size of 45. The Z distance was adjusted to 20 and the working distance to 16 mm.

Figure 43 demonstrates more of the odd nodes present at the base of the tube feet where the nodes appear to have a center in which they radiate outwards from ending in rounded tips with harsh lines down the center. It is possible these features are present at the base of *P. ochraceus* tube feet as a species. However, too few images were captured of these features to be certain they are a physiological characteristic on the underside of all *P. ochraceus*.

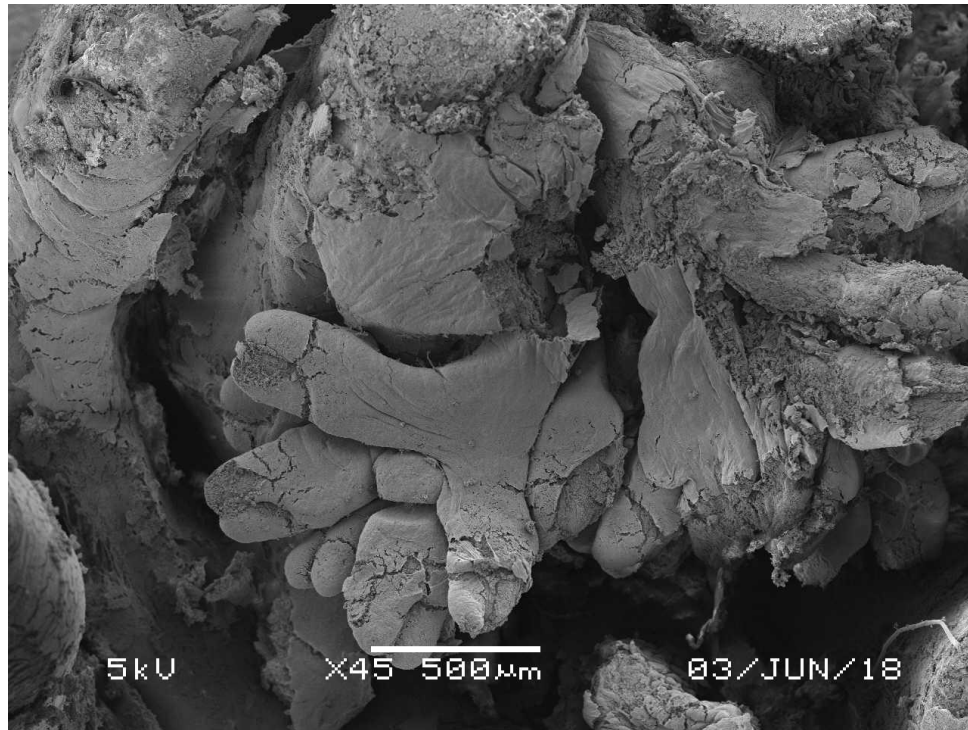


Figure 43. The above image illustrates a region at the base of the tube feet in Sample 4.5. Image captured at 45X magnification, with the voltage calibrated to 5 and spot size of 45. The Z distance was adjusted to 20 and the working distance to 16 mm.

Sample 4.5 was definitely the most challenging to image. Many times, the scanning area appeared much too bright with light hot spots that prevented much of the surface details from being visible. This seemed to come from issues with the SEM which was acting up when the microscope tried to zoom into magnifications greater than 5,000X. Consequently, the highest magnification this Sample 4.5 was imaged at was 190,000X. On the right and left sides of Figure 44, are white spaces with a large dark streak down the center. The lighter spaces are *P. ochraceus* tissue and the dark region in the center represents the gaps in between tissues. The image has a blurry texture characteristic of imaging with electron drift, where the electron beam experiences challenges focusing in on the samples surface and drags the image across the computer

monitor. The image was not stationary as it was being captured and therefore, appears out of focus and mobile.

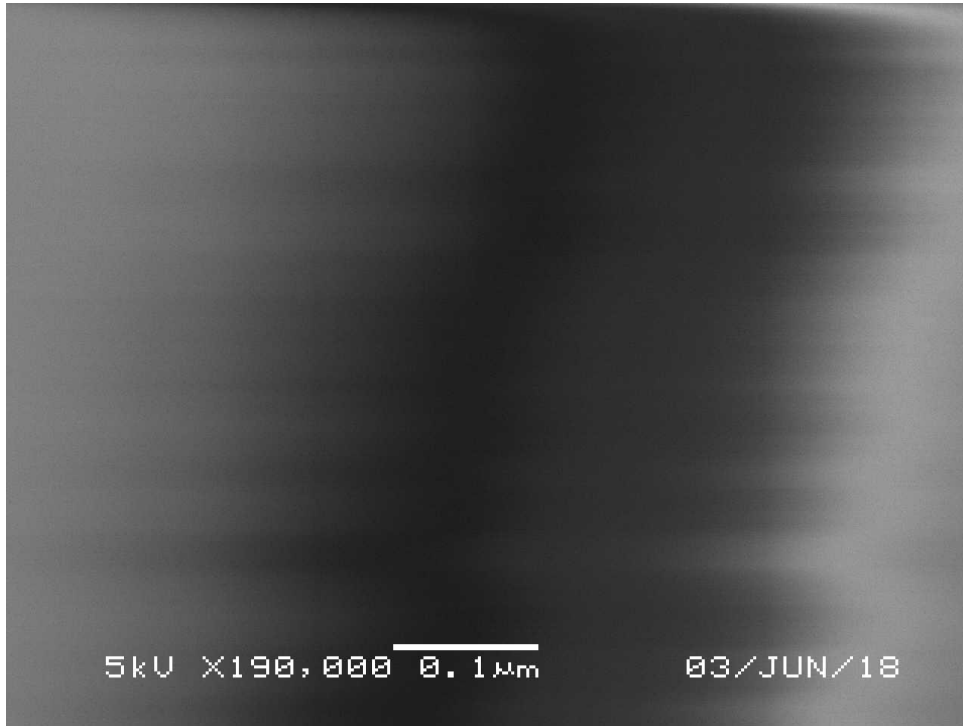


Figure 44. The above image is the highest magnification that could be achieved with Sample 4.5 due to electron drift. Image captured at 190,000X magnification, with the voltage calibrated to 5 and spot size of 45. The Z distance was adjusted to 20 and the working distance to 16 mm.

Sample 5 – Healthy Tissue

A single tissue sample was captured from a healthy, adult *P. ochraceus* to observe the surface characteristics of tissue uninfected with sea star wasting disease. Figure 45 captures the entire surface of the 8mm diameter tissue sample. The tissue was removed from the top of a *P. ochraceus* arm. Figure 45 illustrates the arrangement of sea star spines with nodes dispersed in between them. Sample 5 appears to have less of the sponge-like matter which was present on the top of the sea star spines infected with

wasting disease. The nodes appear fairly intact and snugly fit around the base of each spine.

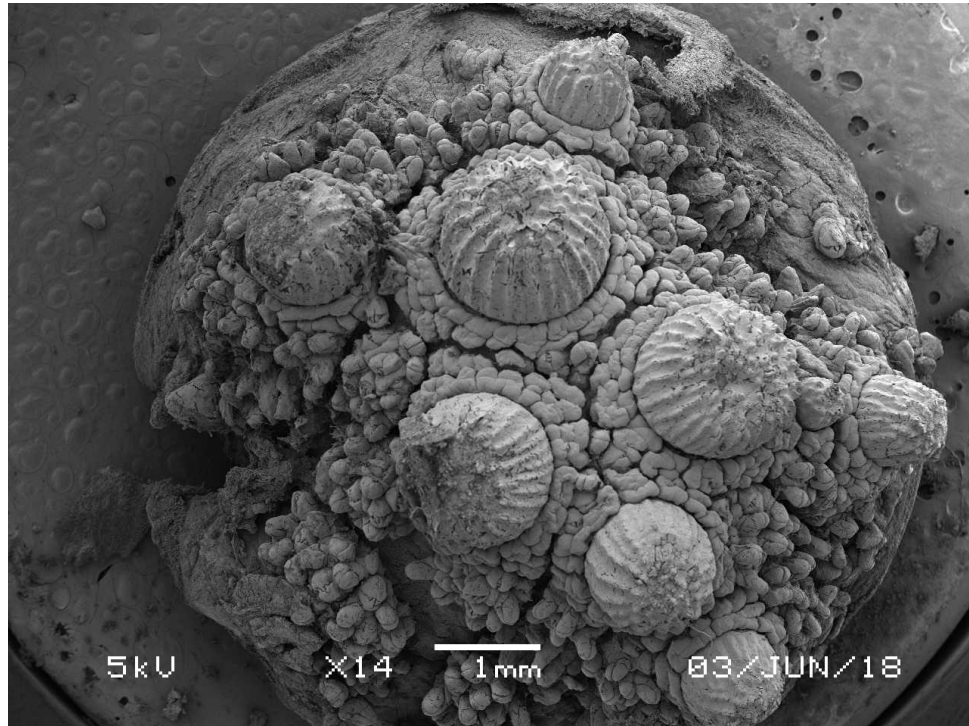


Figure 45. The above image is a wide-view of Sample 5 which is tissue taken from a healthy adult *P. ochraceus*. Image captured at 14X magnification, with the voltage calibrated to 5 and spot size of 45. The Z distance was adjusted to 20 and the working distance to 35 mm.

A closer view of the spines is represented in Figure 46. These spines were arranged on the left side of the tissue imaged in Figure 45 and protrude away from the center. This image demonstrates *P. ochraceus* spines at different levels of development on the top of the body. The left most spine is the largest, with fully developed ridges. The center spine is the smallest and carries visible bumps but no ridges around the outside of the spine. The right most spine is in what appears to be a mid-level developmental stage where the smaller bumps are present on the top and the spine is now beginning to form

ridges around the edges as it expands. Nodes are inset in between the spines in this micrograph.

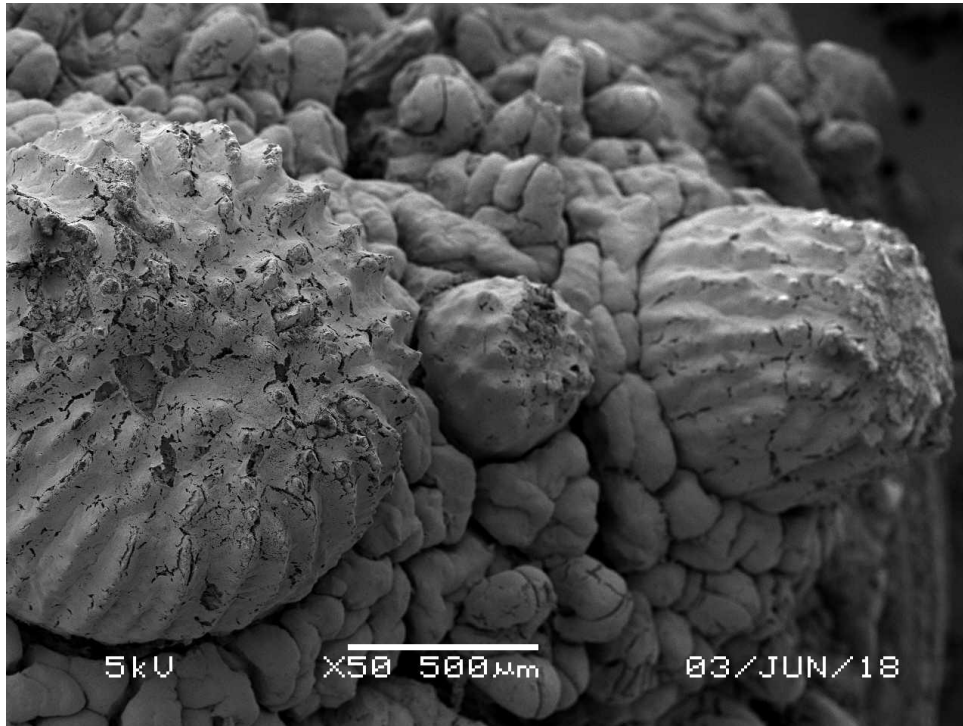


Figure 46. The above image is a closer view of spines and nodes on Sample 5. Image captured at 50X magnification, with the voltage calibrated to 5 and spot size of 42. The Z distance was adjusted to 20 and the working distance to 14 mm.

The nodes in Sample 5 are the most curious feature because they appear very smooth, unlike the nodes present in all necrotic tissue which is usually covered by the sponge-like matter. The nodes in Figure 47 are plump with a soft rolling texture that exhibits the same porosity as all other samples, from the drying process. Nodes appear to wrap around spines and lay against each other in a woven pattern. This structure was not seen in the tissues of diseased individuals due to the large amounts of background noise present in each sample.

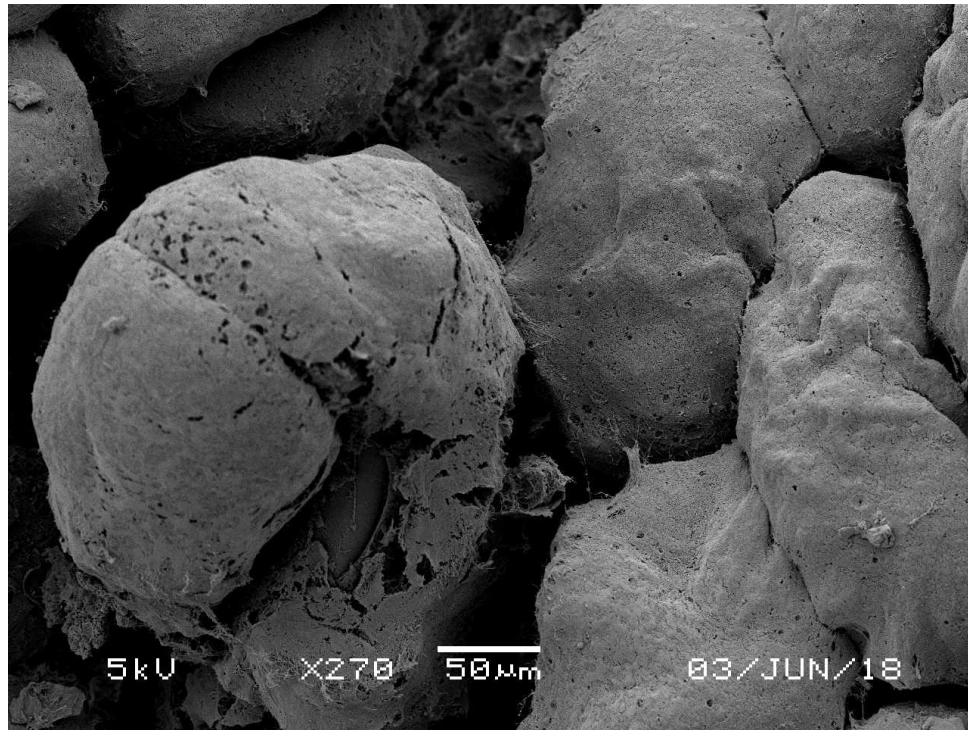


Figure 47. The above image demonstrates the texture of the nodes in Sample 5. Image captured at 270X magnification, with the voltage calibrated to 5 and spot size of 36. The Z distance was adjusted to 20 and the working distance to 14 mm.

The final image of Sample 5 was captured at the highest magnification capable by The Evergreen State College SEM. This image demonstrates a higher quality resolution than most of the images captured at 300,000X magnification. The lighter gray regions are *P. ochraceus* tissue and the dark gray to black areas are space in between the tissue.

Figure 48 demonstrates the closest image of *P. ochraceus* tissue porosity as a result of the drying process necessary for SEM sample preparation.

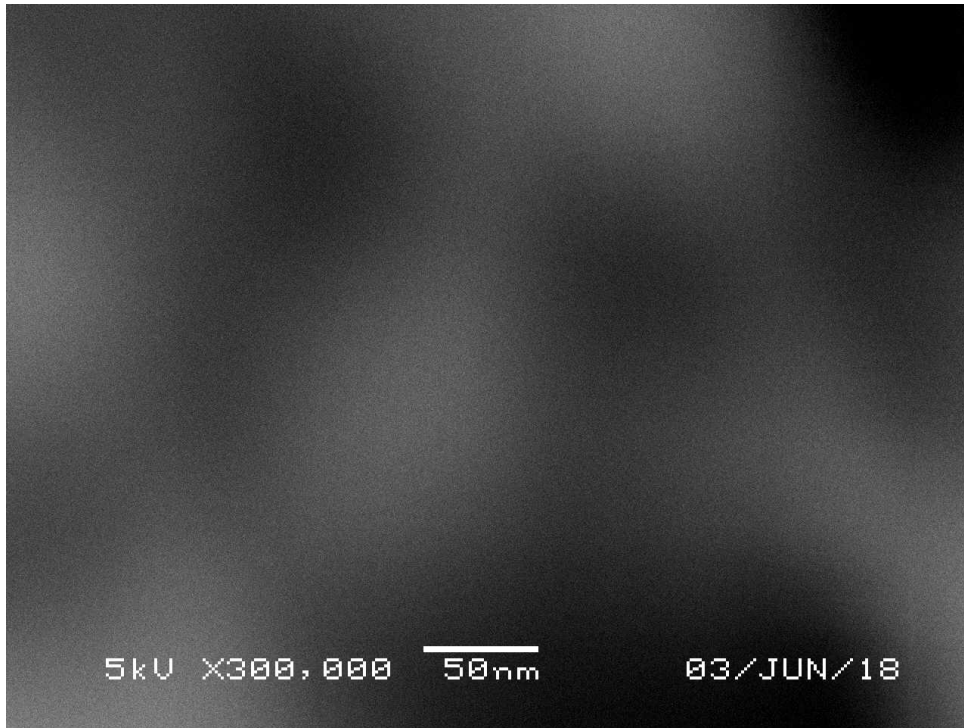


Figure 48. The above image is Sample 5 captured at the highest magnification the SEM was capable of achieving. Image captured at 300,000X magnification, with the voltage calibrated to 5 and spot size of 42. The Z distance was adjusted to 20 and the working distance to 14 mm.

Conclusive Results

Images captured of *P. ochraceus* tissue at the highest magnification achievable by The Evergreen State College's SEM were not successful at producing high resolution images. Fine features in Figures 19, 25, 29, 36, 40, and 48 were not resolvable at the 300,000X magnification. The scale bar at this highest magnification was 50 nm, while the diameter of the densovirus this project attempted to detect were 20-25 nm; half the distance of this scale bar range. It is clear from the images captured at 300,000X magnification that SEM is not strong enough to resolve potential features of densovirus in *P. ochraceus*.

This project also found a lack of abundant or accurately discernable bacterial features. Four of the 5 tissue samples analyzed under the SEM, were removed from necrotic *P. ochraceus* tissue infected with sea star wasting disease. Of these samples, only Sample 4 in a small region pictured in Figure 34, had any discernable rounded bacteria-like structures. However, the ovals may be features contaminating the sample and are not conclusively bacterial in origin (Erik Thuesen, personal communication). Thus, bacteria were not definitively present on necrotic *P. ochraceus* tissue samples analyzed for this project.

In conjunction with the viral and bacterial findings from the SEM analysis, this project also identified successful methods for *P. ochraceus* soft tissue preparation for SEM. One of the methods implemented for this research, involved comparing the difference between *P. ochraceus* tissue sample drying using ethanol versus ethanol and acetone. This project found that samples were fully dried after having been submerged in increasing ethanol concentrations and 3 treatments of 100% acetone. The single experimental drying trial used ethanol exclusively in increasing concentrations and included ethanol in the CO₂ Critical Point Dryer for the final stage of the sample drying process. Upon critical point drying completion, the sample was removed, still wet with ethanol. The ethanol, by itself, was not capable of completely drying the *P. ochraceus* tissue. The Critical Point Dryer was not able to fully bleed off the ethanol and the tissue was warped from this final stage of drying. Therefore, this project found that acetone is a necessary component for effective *P. ochraceus* soft tissue SEM sample preparation.

Discussion

This project attempted to detect the densovirus in *P. ochraceus* tissue infected with sea star wasting disease. The final method implemented, which prepared whole necrotic *P. ochraceus* tissue found that the SEM at The Evergreen State College (JEOL JSM-6480LV) was not strong enough to detect the virus with a diameter of 20-25 nm. Although, magnification has been a critical reference point for this project's analysis, it is only one component of SEM. The most important aspect of quality SEM micrograph imaging, lies in the challenge of attaining high resolution. Resolution deals with the ability to visualize features within an image. This project found it difficult to achieve a high-resolution image above 25,000X magnification.

Resolution is a component of SEM imaging that is essential for achieving quality micrographs. Scanning at high magnification, places stress on the user's ability to also obtain high quality resolution. For successful densovirus identification, it was necessary to achieve both high magnification and quality resolution so that viral characteristics could be visualized and used as a tool for identification. At the magnification necessary to visualize densovirus (300,000X), excellent resolution is incredibly challenging to achieve, especially for a new user. A more advanced user with an abundance of experience scanning at high magnification, may have more skills in their ability to generate high quality micrographs at high magnification.

The other challenge this research encountered was that the SEM at Evergreen was temperamental; the machine was broken for two months and repaired half-way through the data collection process for this project. This presented a new set of challenges, since Evergreen's SEM had already experienced technical difficulties prior to this episode.

Issues such as electron drift were frequent, especially at high magnification, where electrons were unstable and the electron beam was unable to focus on a specified region causing the image to shift and blur. It is possible that an advanced SEM user with a more reliable microscope could achieve higher resolution images at very high magnification. However, there is little evidence in the literature to suggest that high quality resolution at 300,000X magnification is regularly accomplished (Wells 1974). Thus, this thesis does not recommend this project's methods, as an avenue to resolve densovirus in *P. ochraceus* infected with sea star wasting disease.

One method this project had originally been inspired to attempt was to use ionic suspension fluid in the SEM sample chamber for analysis. This was a method utilized by Golding et al. (2016) which was effective at resolving quality images of Ebola virus compared to traditional methods of drying and sputter coating. An issue Golding et al. (2016) reconciles in their research is the sample coverage sputter coating imposes to create conductivity in the sample. Sputter coating can coat fine details such as viruses that may be present in the sample and reduce the resolvability of microscopic structures. Ionic suspension fluid was a method Golding et al. (2016) applied to avoid these challenges with virus resolution under SEM. However, this project was not able to include ionic suspension fluid in this method development because the solution is too dangerous to use. Ionic suspension fluid has the unfortunate quality of degrading into hydrofluoric acid, an extremely toxic substance harmful to humans. Handling this solution would require full personal protective equipment.

The primary concern with using ionic suspension fluid, was the already temperamental nature of The Evergreen State College's SEM. The microscope had

experienced mechanical challenges in recent years; it was decided that this project would not attempt ionic suspension fluid out of fear it could damage the machine. In the future, it would be interesting to see if a virus as small as densovirus, could be successfully resolved using ionic suspension fluid in a SEM.

A brief and limited comparison of necrotic *P. ochraceus* tissue to a single healthy tissue sample was executed by this project. Major deductions cannot be made from these few images, but the distinct lack of sponge-like matter in Sample 5 is highly intriguing. Most of the wasted *P. ochraceus* tissue samples which exhibited definitive signs of sea star wasting disease in the field, appeared to have large masses on top of the nodes which lie in between the sea star spines. In the healthy *P. ochraceus* tissue, only nodes were present and the tissue appeared smoother in Sample 5 than in Samples 1, 2, 3, or 4. It is challenging to know if these differences in *P. ochraceus* tissue characteristics are a product of sea star wasting disease. With only visual observations, there does appear to be a perceptible difference between tissues collected from diseased individuals and the single healthy *P. ochraceus* tissue sample. More research and images of the physical changes *P. ochraceus* tissue experiences at the microscopic level from wasting disease is needed. Visualizing tissue decay and comparing it further to healthy organisms, may elucidate the nature of diseased tissues and help researchers understand what wasting looks like and how it behaves microscopically.

Although this project was unsuccessful at developing a new method for viral identification in *P. ochraceus*, more research into viral host interactions in sea stars and echinoderms as a whole, is crucial. At present, our knowledge of existing viral-host relationships in the rocky intertidal zone is severely limited. The sea star-associated

densovirus (SSaDV) was the first pathogen to exhibit a strong correlation with sea star wasting disease (Hewson et al. 2014). However, the inadequate baseline knowledge of viruses in echinoderms, undermines SSaDV as a conclusive disease-causing pathogen, raising more questions than answers as to the source behind sea star wasting disease.

The ambiguity of sea star wasting, and the nature of viral detection in asteroids, makes studying this phenomena complicated and frustrating. There still exists a need to understand the mass wasting event from 2013-2015, how it impacted Northeast Pacific asteroid populations, and how it will continue to affect the coastlines. The future of sea star wasting disease is uncertain with its continued presence in sea stars and an incomplete knowledge of its cause. For a time, the long-term influences of this disease on *P. ochraceus* was also unclear as their populations experienced dramatic decreases especially during the sea star wasting event. Today, populations of *P. ochraceus* do appear to be rebounding on the coastline, reclaiming their place in intertidal ecosystems as keystone predators (Moritsch & Raimondi 2018, Miner et al 2018). With time, there is hope *P. ochraceus* can create the same predation pressure on mussels, and maintain intertidal species biodiversity, as they did prior to the 2013 sea star wasting outbreak.

Conclusion

This project set out to develop an accessible method which would allow others the opportunity to contribute to sea star wasting disease research. Originally, it was thought that the key to answering this question would lie in developing a successful filtration method that would simultaneously isolate densovirus from the host tissue and prepare the sample for SEM analysis. The challenges faced in developing a successful filtration method were unanticipated. However, failure did not deter this project which turned to preserving and preparing whole *P. ochraceus* tissue for SEM analysis. The images captured of necrotic and healthy *P. ochraceus* tissue were examined for this research. None of the images demonstrated incontrovertible presence of bacterial assemblages, further reinforcing that sea star wasting disease is not caused by a bacterial pathogen. At the highest magnification of 300,000X, the SEM was not capable of producing a high magnification image at a high-quality resolution. This project concludes that the methods implemented for this research were insufficient to identify densovirus in *P. ochraceus* infected with sea star wasting disease.

Bibliography

- Bates, A.E., B.J. Hilton, C.D.G. Harley, 2009, Effects of Temperature, season and locality on wasting disease in the keystone predatory sea star *Pisaster ochraceus*. *Diseases of Aquatic Organisms*, Vol. 86, pp245-251.
- Becker, P., Gillan, D., Lanterbecq, D., Jangoux, M., Rasolofonirina, R., Rakotovao, J., and Eeckhaut, I, 2004. The skin ulceration disease in cultivated juveniles of *Holothuria scabra* (Holothuroidea, Echinodermata). *Aquaculture* 242: 13-30
- Bochow, S., Condon, K., Elliman, J., & Owens, L. (2015). First complete genome of an Ambidensovirus; *Cherax quadricarinatus* densovirus, from freshwater crayfish *Cherax quadricarinatus*. *Marine genomics*, 24, 305-312.
- Bonaviri, C., Graham, M., Gianguzza, P., & Shears, N. T. (2017). Warmer temperatures reduce the influence of an important keystone predator. *Journal of Animal Ecology*.
- Bruemmer, A., Scholari, F., Lopez-Ferber, M., Conway, J. F., & Hewat, E. A. (2005). Structure of an insect parvovirus (*Junonia coenia* Densovirus) determined by cryo-electron microscopy. *Journal of molecular biology*, 347(4), 791-801.

- Bucci, C., Francoeur, M., McGreal, J., Smolowitz, R., Zazueta-Novoa, V., Wessel, G. M., & Gomez-Chiarri, M. (2017). Sea Star Wasting Disease in *Asterias forbesi* along the Atlantic Coast of North America. *PloS one*, *12*(12), e0188523.
- Buck, J. C., & Ripple, W. J. (2017). Infectious Agents Trigger Trophic Cascades. *Trends in Ecology & Evolution*, *32*(9), 681-694.
- Chandler, V. K., & Wares, J. P. (2017). RNA expression and disease tolerance are associated with a “keystone mutation” in the ochre sea star *Pisaster ochraceus*. *PeerJ*, *5*, e3696.
- Cotmore, S. F., Agbandje-McKenna, M., Chiorini, J. A., Mukha, D. V., Pintel, D. J., Qiu, J., ... & Davison, A. J. (2014). The family parvoviridae. *Archives of virology*, *159*(5), 1239-1247.
- Eisenlord, M. E., Groner, M. L., Yoshioka, R. M., Elliott, J., Maynard, J., Fradkin, S., ... & Harvell, C. D. (2016). Ochre star mortality during the 2014 wasting disease epizootic: role of population size structure and temperature. *Phil. Trans. R. Soc. B*, *371*(1689), 20150212.
- Evans, A. S. (1976). Causation and disease: the Henle-Koch postulates revisited. *The Yale journal of biology and medicine*, *49*(2), 175.

- Fahsbender, E., Hewson, I., Rosario, K., Tuttle, A. D., Varsani, A., & Breitbart, M. (2015). Discovery of a novel circular DNA virus in the Forbes sea star, *Asterias forbesi*. *Archives of virology*, *160*(9), 2349-2351.
- François, S., Filloux, D., Roumagnac, P., Bigot, D., Gayral, P., Martin, D. P., ... & Ogliastro, M. (2016). Discovery of parvovirus-related sequences in an unexpected broad range of animals. *Scientific Reports*, *6*.
- François, S., Bernardo, P., Filloux, D., Roumagnac, P., Yaverkovski, N., Froissart, R., & Ogliastro, M. (2014). A novel itera-like densovirus isolated by viral metagenomics from the sea barley *Hordeum marinum*. *Genome announcements*, *2*(6), e01196-14.
- Fuess, L. E., Eisenlord, M. E., Closek, C. J., Tracy, A. M., Mauntz, R., Gignoux-Wolfsohn, S., ... & Friedman, C. S. (2015). Up in arms: immune and nervous system response to sea star wasting disease. *PLoS One*, *10*(7), e0133053.
- Gale, A. S. (1987). Phylogeny and classification of the Asteroidea (Echinodermata). *Zoological Journal of the Linnean Society*, *89*(2), 107-132.
- Golding, C. G., Lamboo, L. L., Beniac, D. R., & Booth, T. F. (2016). The scanning electron microscope in microbiology and diagnosis of infectious disease. *Scientific reports*, *6*, 26516.

- Gudenkauf, B. M., & Hewson, I. (2016). Comparative metagenomics of viral assemblages inhabiting four phyla of marine invertebrates. *Frontiers in Marine Science*, 3, 23.
- Gudenkauf, B. M., Eaglesham, J. B., Aragundi, W. M., & Hewson, I. (2014). Discovery of urchin associated densovirus (family Parvoviridae) in coastal waters of the Big Island, Hawaii. *Journal of General Virology*, 95(3), 652-658.
- Gudenkauf, B. M., & Hewson, I. (2015). Metatranscriptomic analysis of Pycnopodia helianthoides (Asteroidea) affected by sea star wasting disease. *PloS one*, 10(5), e0128150.
- Hajibagheri, M. N. (Ed.). (1999). *Electron Microscopy: Methods and Protocols*. Springer Science & Business Media.
- Hayat, M.A. (1974). *Principles and Techniques of Scanning Electron Microscopy*. Van Nostrand Reinhold Company.
- Heywood, V.H. (1971). *Scanning Electron Microscopy*. London: Academic Press.

Hewson, I., Button, J. B., Gudenkauf, B. M., Miner, B., Newton, A. L., Gaydos, J. K., ... & Fradkin, S. (2014). Densovirus associated with sea-star wasting disease and mass mortality. *Proceedings of the National Academy of Sciences*, *111*(48), 17278-17283.

Jackson, E. W. (2016). The diversity and community composition of microorganisms associated with echinoderms (Doctoral dissertation, Cornell University).

Jackson, E. W., Bistolas, K. S., Button, J. B., & Hewson, I. (2016). Novel Circular Single Stranded DNA Viruses among an Asteroid, Echinoid and Holothurian (Phylum: Echinodermata). *PloS one*, *11*(11), e0166093.

Kang, Y. J., Huang, W., Zhao, A. L., Lai, D. D., Shao, L., Shen, Y. Q., ... & Zhang, W. (2017). Densoviruses in oyster *Crassostrea ariakensis*. *Archives of Virology*, 1-5.

Kessel, R. G., & Shih, C. Y. (2012). *Scanning Electron Microscopy in BIOLOGY: A Students' Atlas on Biological Organization*. Springer Science & Business Media.

Kohl, W. T., McClure, T. I., & Miner, B. G. (2016). Decreased temperature facilitates short-term sea star wasting disease survival in the keystone intertidal sea star *Pisaster ochraceus*. *PloS one*, *11*(4), e0153670.

Lawrence, J. M. (2013). *Starfish: biology and ecology of the Asteroidea*. JHU Press.

- Menge, B. A., Cerny-Chipman, E. B., Johnson, A., Sullivan, J., Gravem, S., & Chan, F. (2016) Sea star wasting disease in the keystone predator *Pisaster ochraceus* in Oregon: insights into differential population impacts, recovery, predation rate, and temperature effects from long-term research. *PloS one*, *11*(5), e0153994.
- Miner, C. M., Burnaford, J. L., Ambrose, R. F., Antrim, L., Bohlmann, H., Blanchette, C. A., ... & Miner, B. G. (2018). Large-scale impacts of sea star wasting disease (SSWD) on intertidal sea stars and implications for recovery. *PloS one*, *13*(3), e0192870.
- Montecino-Latorre, D., Eisenlord, M. E., Turner, M., Yoshioka, R., Harvell, C. D., Pattengill Semmens, C. V., ... & Gaydos, J. K. (2016). Devastating Transboundary Impacts of Sea Star Wasting Disease on Subtidal Asteroids. *PloS one*, *11*(10), e0163190.
- Moritsch, M. M., & Raimondi, P. T. (2018). Reduction and recovery of keystone predation pressure after disease-related mass mortality. *Ecology and Evolution*.
- Mothersill, C., & Austin, B. (2000). *Aquatic invertebrate cell culture*. Berlin: Springer.
- Paine, R. T. (1969). The *Pisaster*-*Tegula* Interaction: Prey Patches, Predator Food Preference, and Intertidal Community Structure. *Ecology*, *50*(6), 950-961.

- Paine, R.T. (1995). "A Conversation on Refining the Concept of Keystone Species".
Conservation Biology. **9** (4): 962–964.
- Pankey, M. S., & Wares, J. P. (2009). Overdominant maintenance of diversity in the sea star *Pisaster ochraceus*. *Journal of evolutionary biology*, *22*(1), 80-87.
- Scanning Electron Microscope A To Z. (2009). JEOL Ltd. <http://www.jeol.com/>.
- Smith, A. (2017). The Impact of the Mass Mortality of Ochre Stars (*Pisaster ochraceus*) and Sunflower Stars (*Pycnopodia helianthoides*) on Intertidal and Subtidal Communities in Puget Sound (Doctoral dissertation).
- Stahli, Annette, Schaerer, Rolf, Hoelzle, Katharina, Ribl, Georrg, 2009. Temperature induced disease in the starfish *Astropecten jonstoni*. *Marine Diversity Records* 2: 1-5.
- Suttle, C. A. (2005). Viruses in the sea. *Nature*, *437*(7057), 356-361. van Oers, M. M., Bateman, K. S., & Stentiford, G. D. (2017). Viruses of invertebrates related to the food chain.
- Tijssen, P., Péntzes, J. J., Yu, Q., Pham, H. T., & Bergoin, M. (2016). Diversity of small, single stranded DNA viruses of invertebrates and their chaotic evolutionary past. *Journal of invertebrate pathology*, *140*, 83-96.

Wells, O.C. (1974). Scanning Electron Microscopy. New York: McGraw-Hill Book Company.

Xie, R., Chu, L. Y., Chen, W. M., Xiao, W., Wang, H. D., & Qu, J. B. (2005).

Characterization of microstructure of poly (N-isopropylacrylamide)-grafted polycarbonate track-etched membranes prepared by plasma-graft pore-filling polymerization. *Journal of Membrane Science*, 258(1-2), 157-166.

Yang, W. T., Shi, S. H., Jiang, Y. L., Zhao, L., Chen, H. L., Huang, K. Y., ... & Wang, C.

F. (2016). Genetic characterization of a densovirus isolated from great tit (*Parus major*) in China. *Infection, Genetics and Evolution*, 41, 107-112.

Appendices

Appendix A

Sample 1

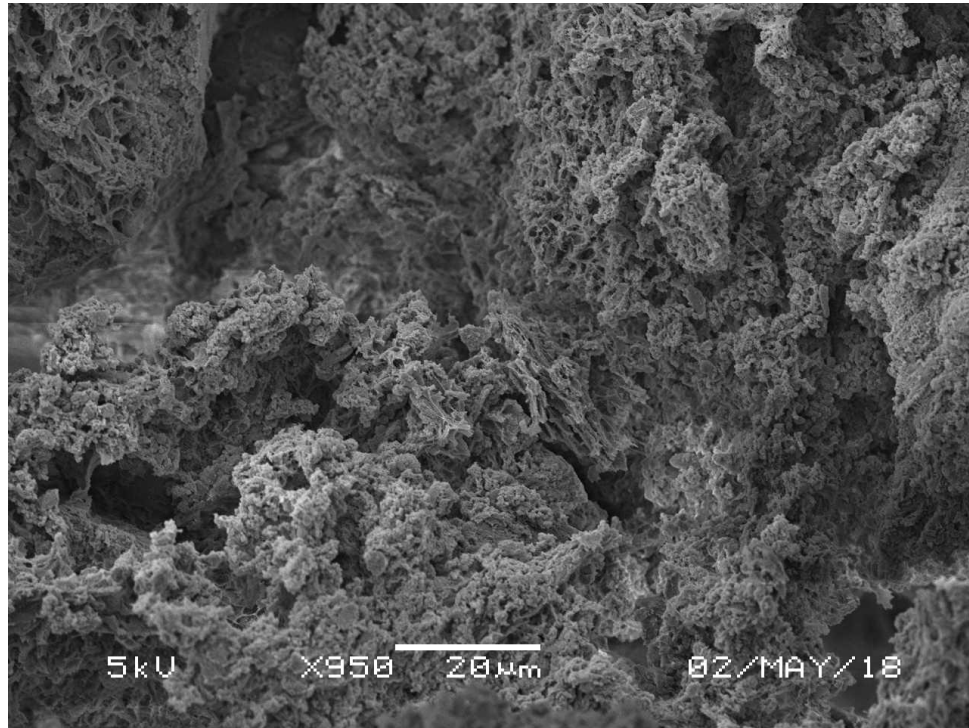


Figure 49. Necrotic *P. ochraceus* tissue captured at 950X magnification. Voltage is 5kv, spot size of 42, Z distance is 20 and working distance is 12 mm.

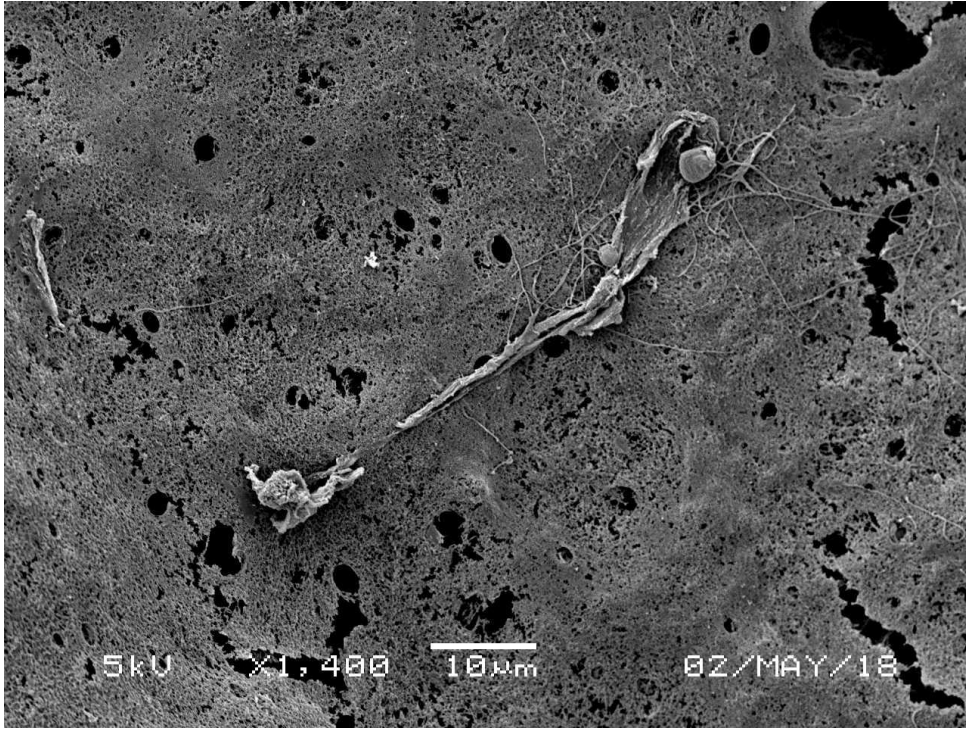


Figure 50. Necrotic *P. ochraceus* tissue captured at 1,400X magnification. Voltage is 5kv, spot size of 41, Z distance is 20 and working distance is 15 mm.

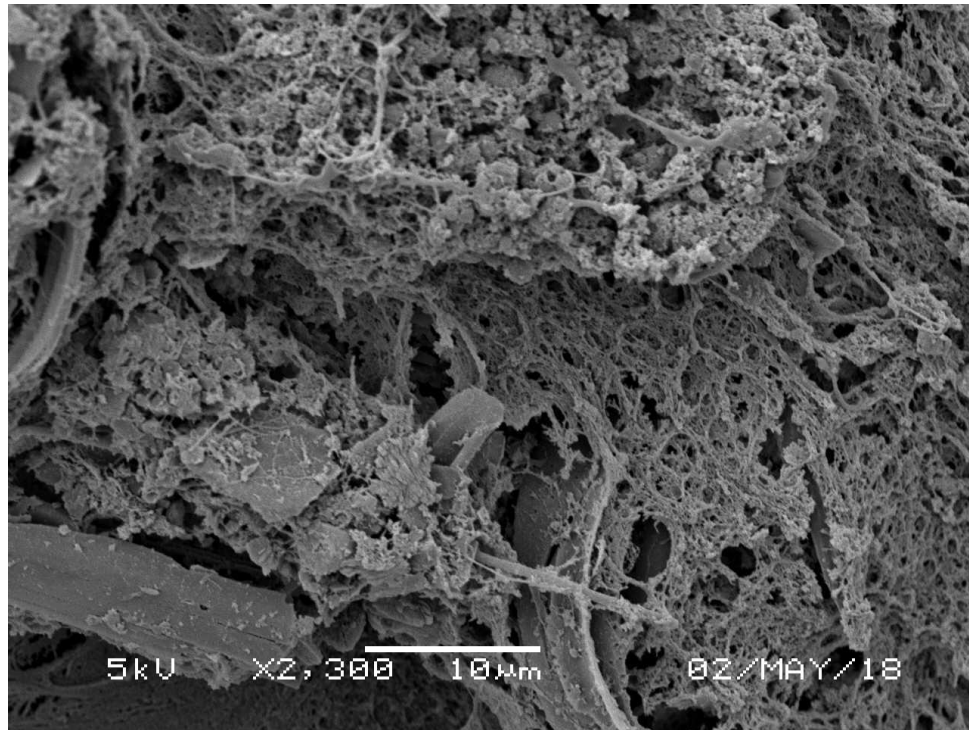


Figure 51. Necrotic *P. ochraceus* tissue captured at 2,300X magnification. Voltage is 5kv, spot size of 42, Z distance is 20 and working distance is 12 mm.

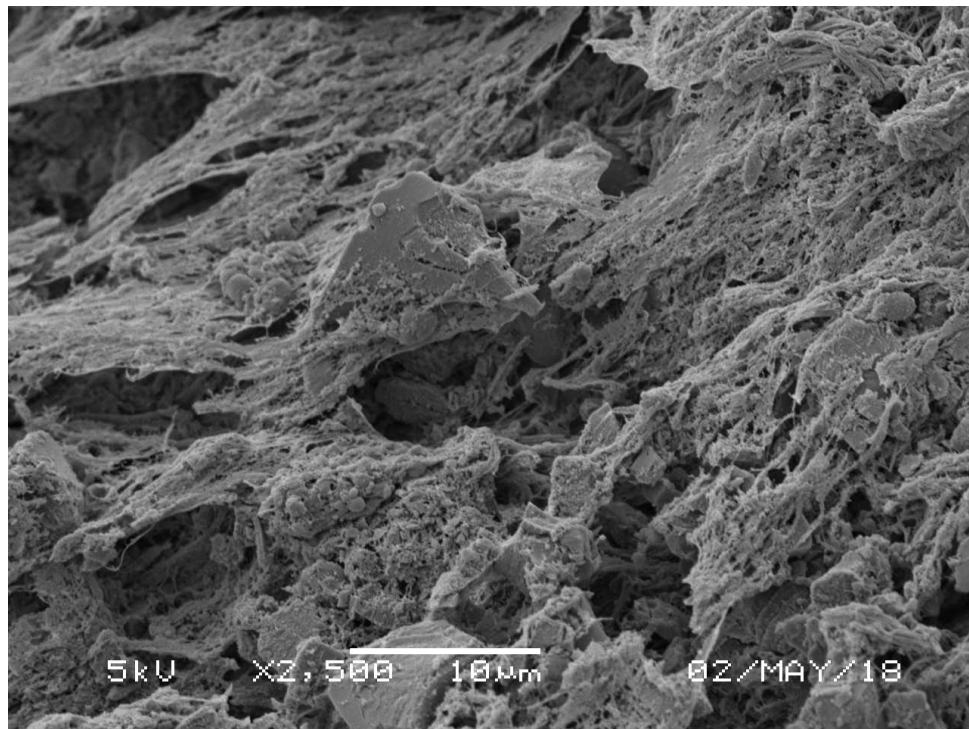


Figure 52. Necrotic *P. ochraceus* tissue captured at 2,500X magnification. Voltage is 5kv, spot size of 42, Z distance is 20 and working distance is 20 mm.

Sample 3

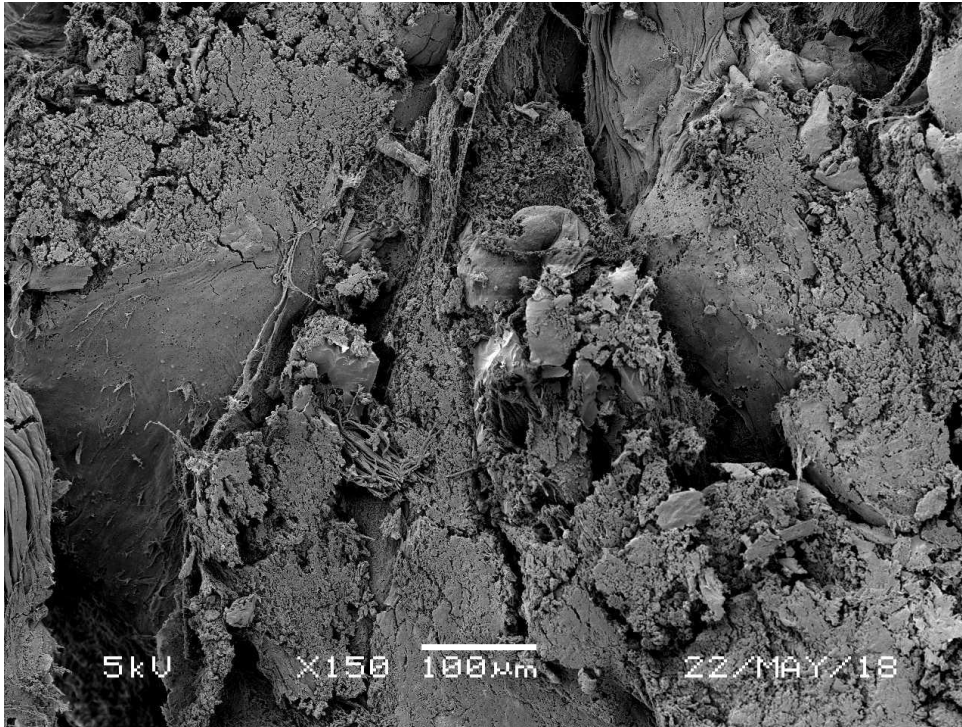


Figure 53. Tissue from the tube feet of Sample 3, captured at 150X magnification. Voltage is 5kv, spot size of 50, Z distance is 20 and working distance is 18 mm.

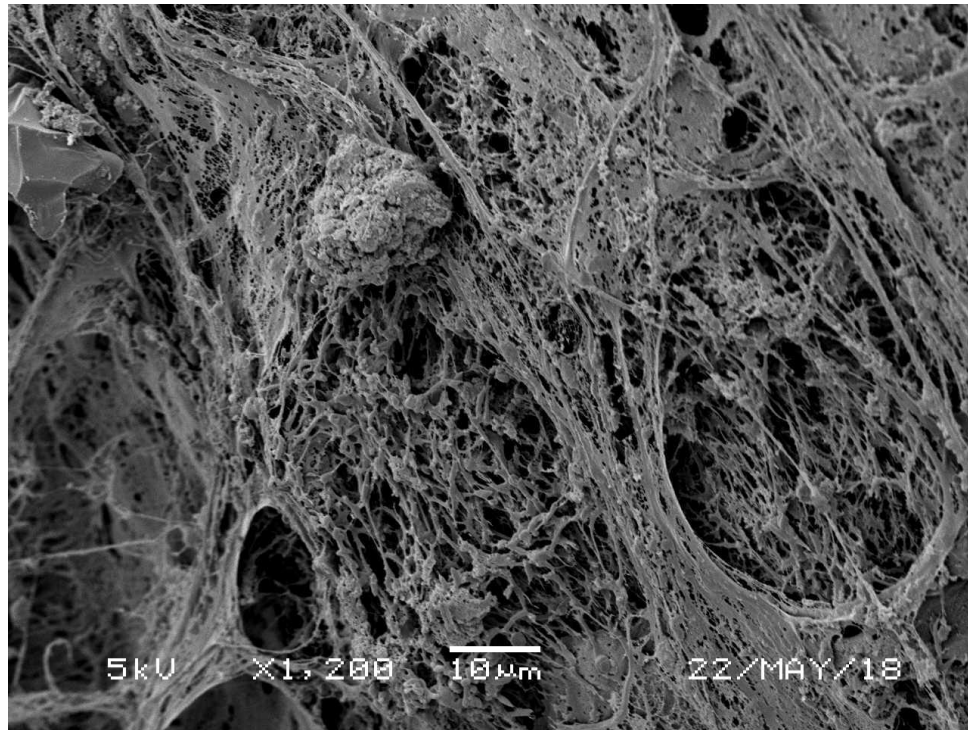


Figure 54. *P. ochraceus* tissue from the tube feet of Sample 3 captured at 1,200X magnification. Voltage is 5kv, spot size of 40, Z distance is 20 and working distance is 18 mm.

Sample 3.5

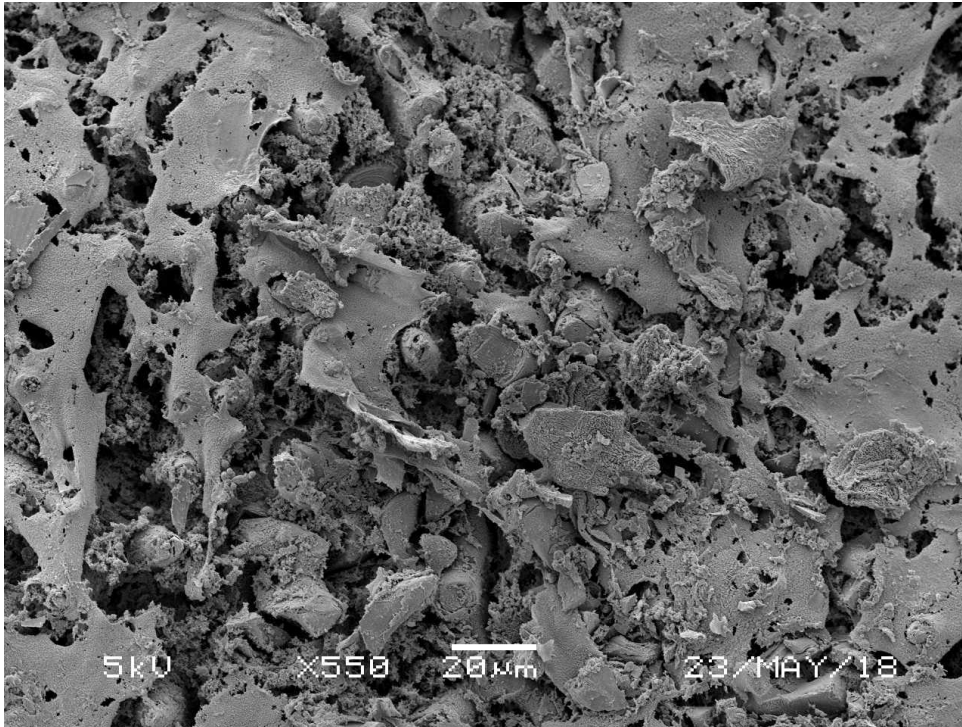


Figure 55. Tissue from the tube feet of Sample 3 captured at 550X magnification. Voltage is 5kv, spot size of 45, Z distance is 20 and working distance is 15 mm.

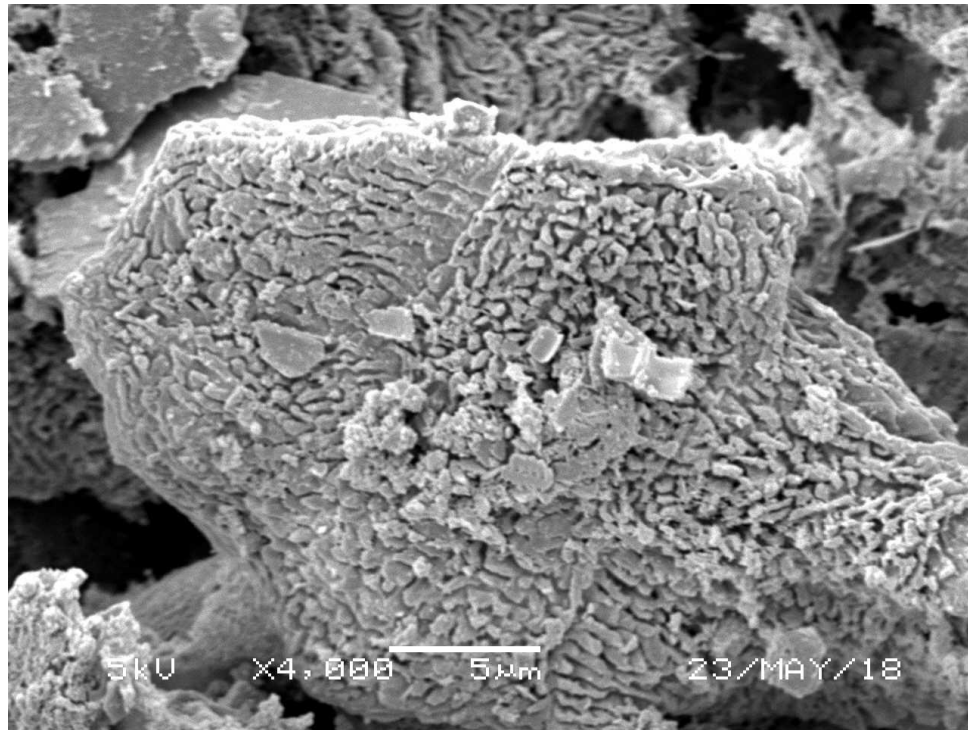


Figure 56. *P. ochraceus* tissue from the underside of the organism captured at 4,000X magnification. Voltage is 5kv, spot size of 41, Z distance is 20 and working distance is 15 mm.

Sample 4

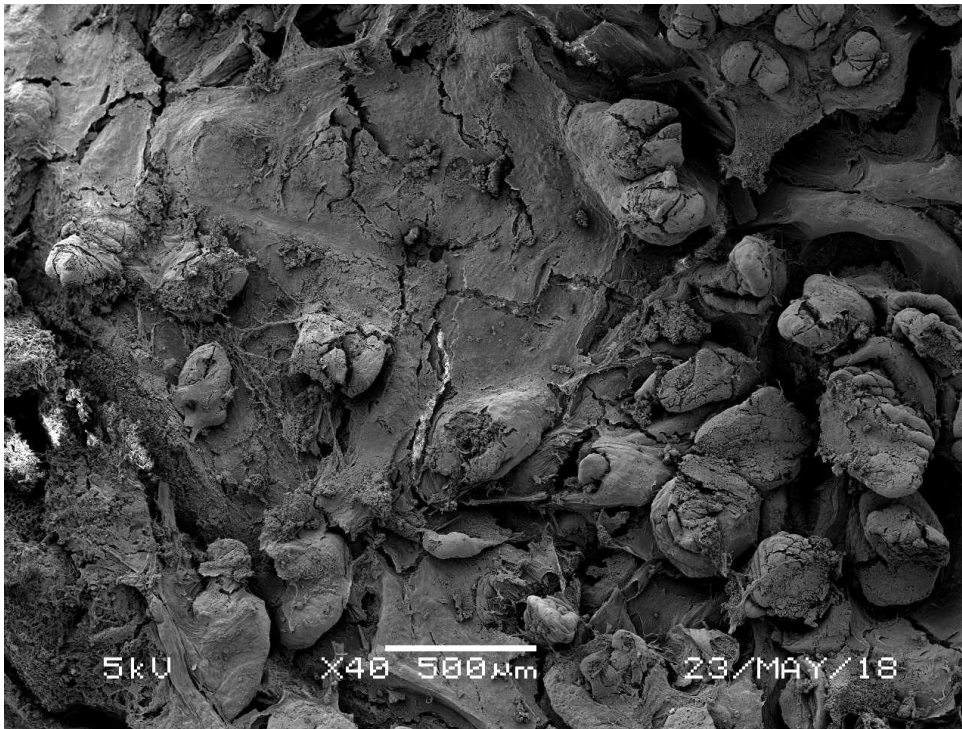


Figure 57. Necrotic *P. ochraceus* tissue captured at 40X magnification. Voltage is 5kv, spot size of 45, Z distance is 20 and working distance is 18 mm.

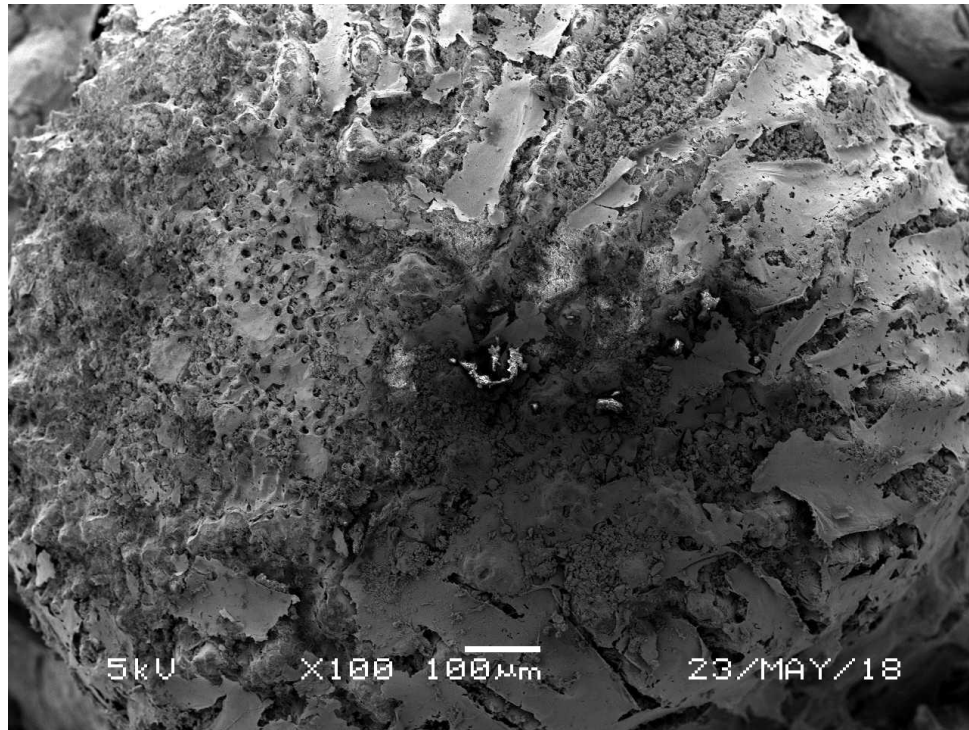


Figure 58. Necrotic *P. ochraceus* tissue captured at 100X magnification. Voltage is 5kv, spot size of 45, Z distance is 20 and working distance is 17 mm.

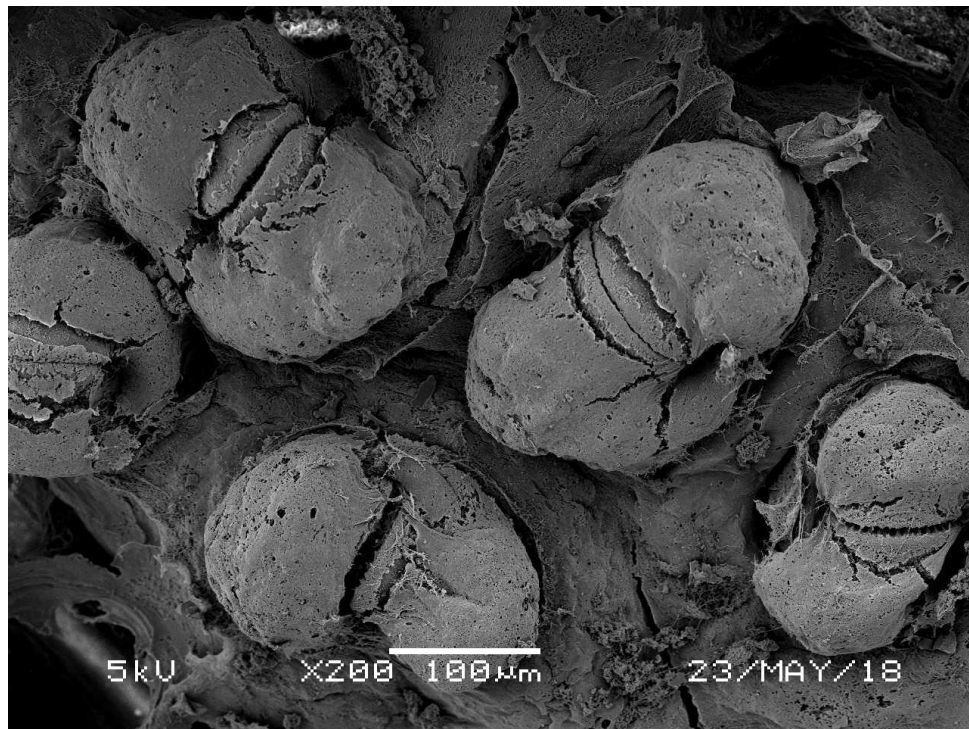


Figure 59. Necrotic *P. ochraceus* tissue captured at 200X magnification. Voltage is 5kv, spot size of 45, Z distance is 20 and working distance is 19 mm.

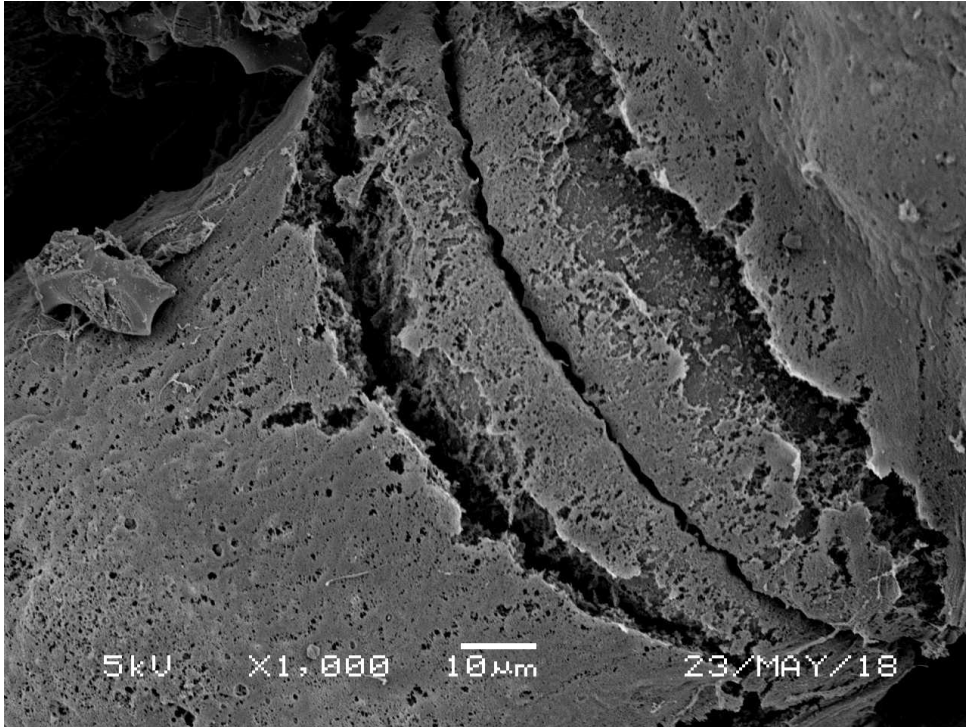


Figure 60. Necrotic *P. ochraceus* tissue captured at 1,000X magnification. Voltage is 5kv, spot size of 45, Z distance is 20 and working distance is 19 mm.

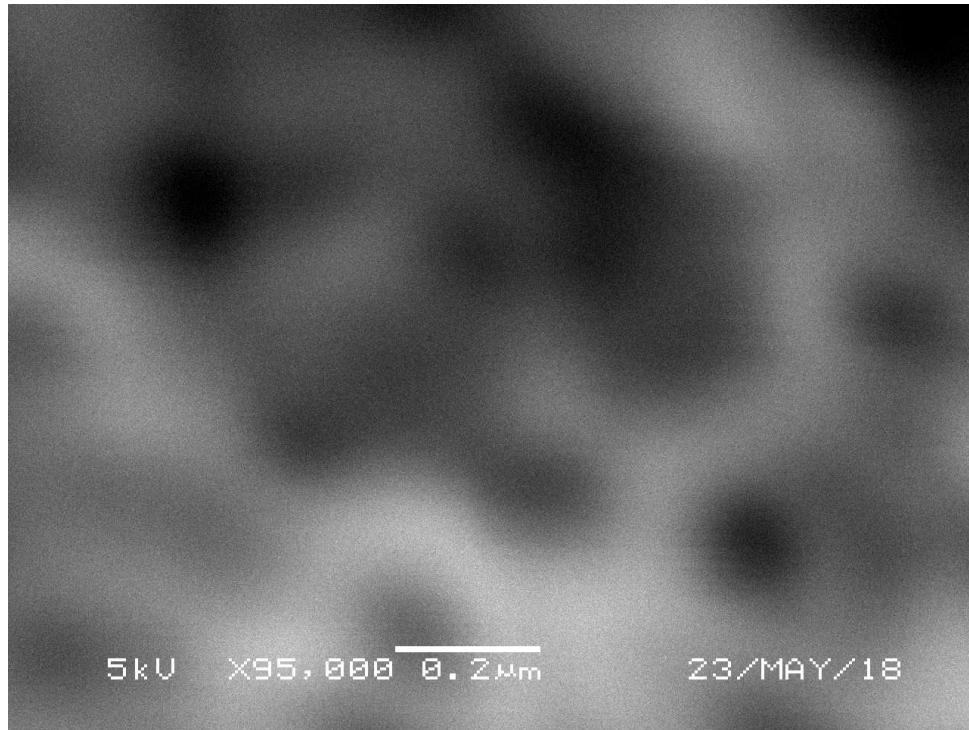


Figure 61. Necrotic *P. ochraceus* tissue captured at 95,000X magnification. Voltage is 5kv, spot size of 45, Z distance is 20 and working distance is 19 mm.

Sample 4.5

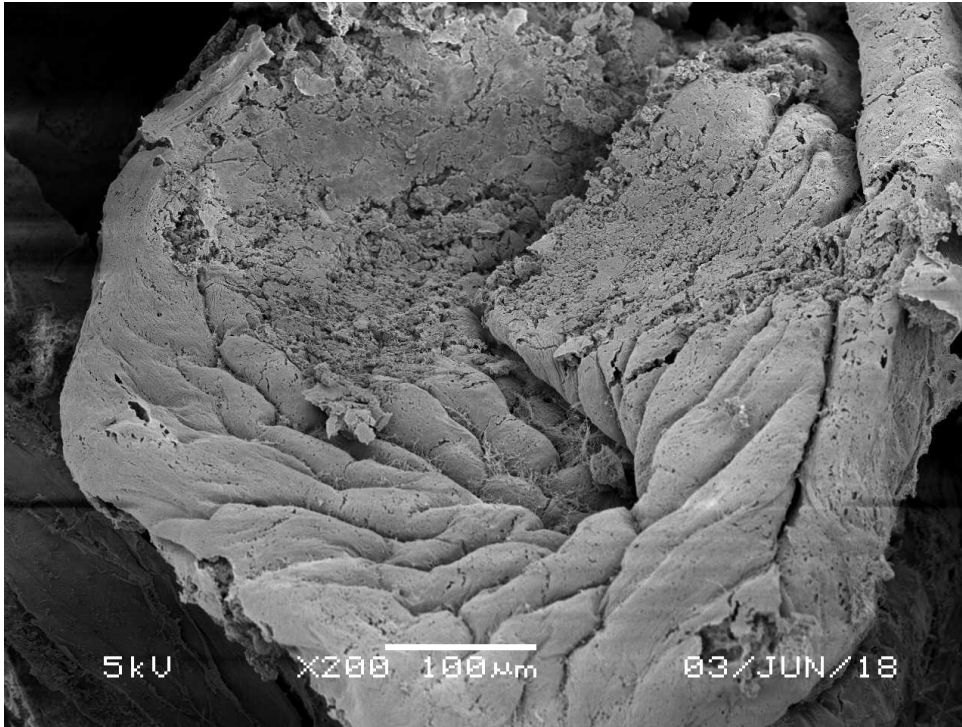


Figure 62. Necrotic *P. ochraceus* tissue captured at 200X magnification. Voltage is 5kv, spot size of 45, Z distance is 20 and working distance is 16 mm.

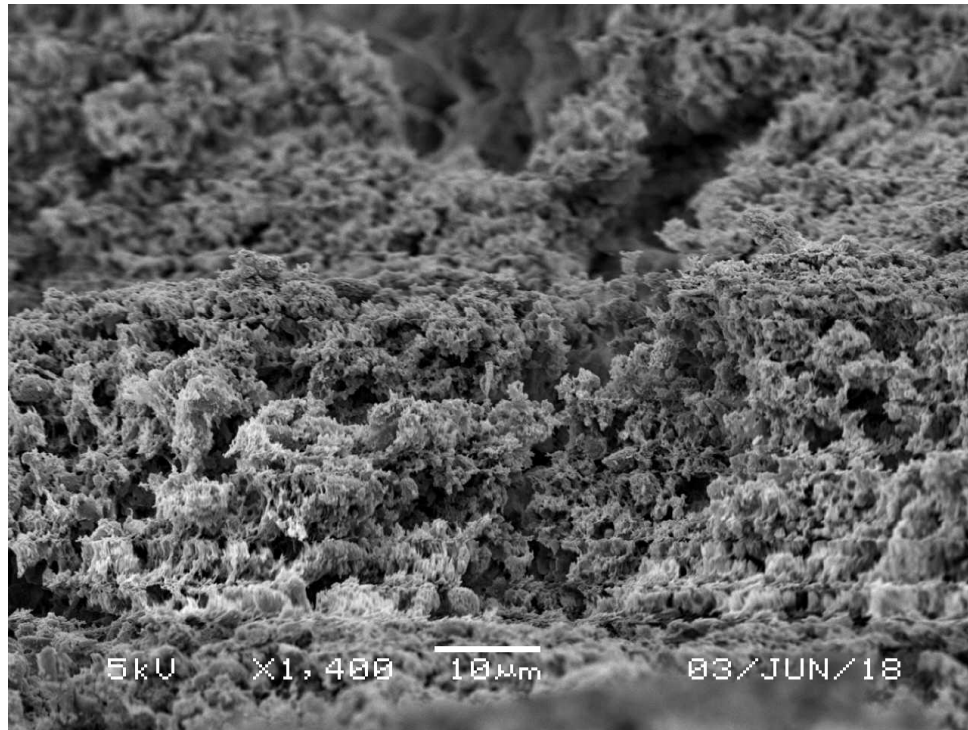


Figure 63. Necrotic *P. ochraceus* tissue captured at 1,400X magnification. Voltage is 5kv, spot size of 45, Z distance is 20 and working distance is 16 mm.

Sample 5—Healthy Tissue

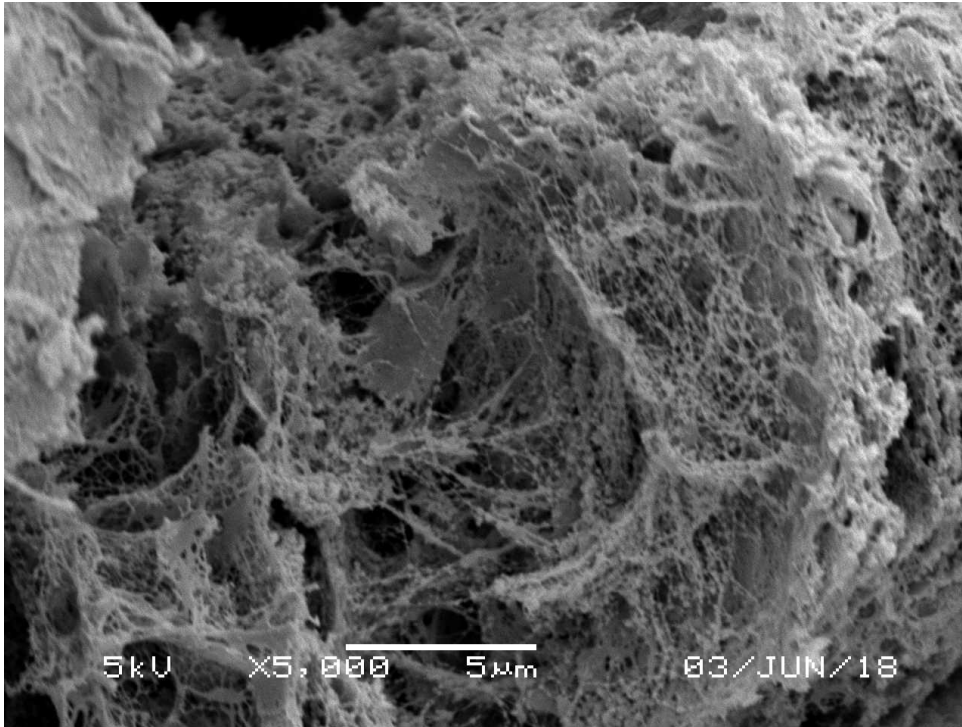


Figure 64. Healthy *P. ochraceus* tissue captured at 5,000X magnification. Voltage is 5kv, spot size of 39, Z distance is 20 and working distance is 14 mm.

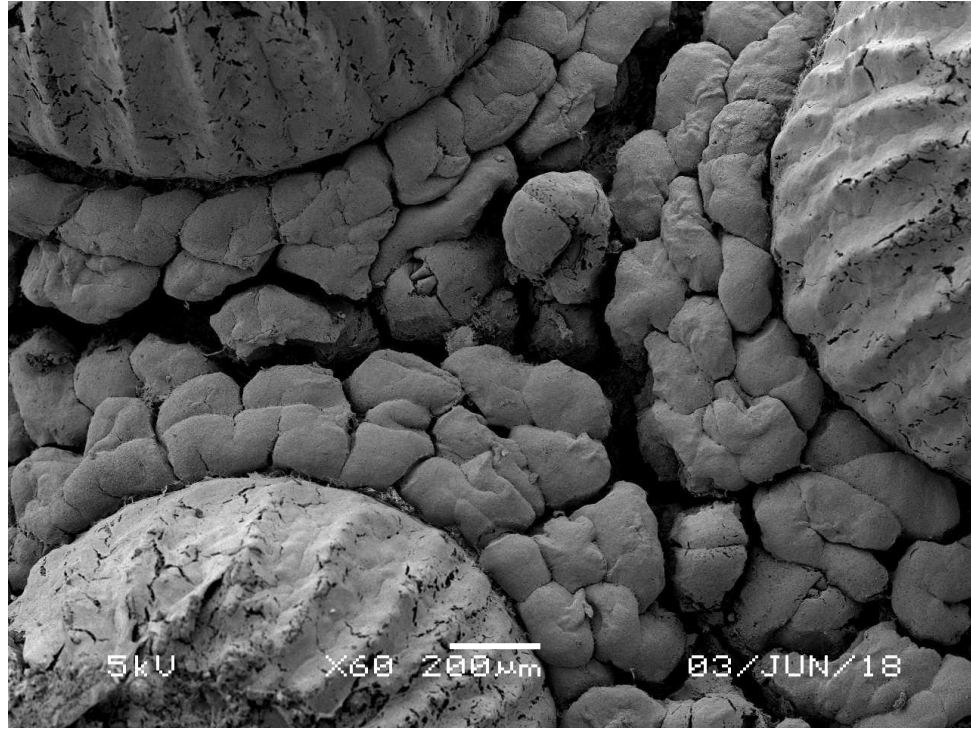


Figure 65. Healthy *P. ochraceus* tissue captured at 60X magnification. Voltage is 5kv, spot size of 39, Z distance is 20 and working distance is 14 mm.